Universidade Estadual de Campinas
Faculdade de Engenharia Elétrica e de Computação

Uiara Celine de Moura

Cognitive Methodology for Optical Amplifier Gain Adjustment in Dynamic Networks

Metodologia Cognitiva para Ajuste do Ganho de Amplificadores Ópticos em Redes Dinâmicas

Campinas

2017

Uiara Celine de Moura

Cognitive Methodology for Optical Amplifier Gain Adjustment in Dynamic Networks

Metodologia Cognitiva para Ajuste do Ganho de Amplificadores Ópticos em Redes Dinâmicas

Thesis presented to the School of Electrical and Computer Engineering of the State University of Campinas in partial fulfillment of the requirements to obtain the degree of Doctor in Electrical Engineering in the area of Telecommunication and Telematics.

Tese de Doutorado apresentada à Faculdade de Engenharia Elétrica e de Computação da Universidade Estadual de Campinas como parte dos requisitos para obtenção do título de Doutora em Engenharia Elétrica na área de Telecomunicações e Telemática.

Advisor/*Orientador*: *Prof. Dr. Evandro Conforti*

Co-advisor/*Co-orientador*: *Dr. Juliano Rodrigues Fernandes de Oliveira*

Este exemplar corresponde à versão final da tese defendida pela aluna Uiara Celine de Moura, e orientada pelo Prof. Dr. Evandro Conforti

Campinas

2017

Agência(s) de fomento e nº(s) de processo(s): Não se aplica.
ORCID: http://orcid.org/0000-0002-8820-0597

Ficha catalográfica
Universidade Estadual de Campinas
Biblioteca da Área de Engenharia e Arquitetura
Luciana Pietrosanto Milla - CRB 8/8129

	Moura, Uiara Celine de, 1983-
M865c	Cognitive methodology for optical amplifier gain adjustment in dynamic networks / Uiara Celine de Moura. – Campinas, SP : [s.n.], 2017.
	Orientador: Evandro Conforti. Coorientador: Juliano Rodrigues Fernandes de Oliveira. Tese (doutorado) – Universidade Estadual de Campinas, Faculdade de Engenharia Elétrica e de Computação.
	1. Amplificadores ópticos. 2. Raciocínio baseado em casos. 3. Redes ópticas. 4. Aprendizado de máquina. I. Conforti, Evandro,1947-. II. Oliveira, Juliano Rodrigues Fernandes de. III. Universidade Estadual de Campinas. Faculdade de Engenharia Elétrica e de Computação. IV. Título.

Informações para Biblioteca Digital

Título em outro idioma: Metodologia cognitiva para ajuste do ganho de amplificadores ópticos em redes dinâmicas
Palavras-chave em inglês:
Optical amplifiers
Case-based reasoning
Optical networks
Machine learning
Área de concentração: Telecomunicações e Telemática
Titulação: Doutora em Engenharia Elétrica
Banca examinadora:
Evandro Conforti [Orientador]
Joaquim Ferreira Martins Filho
Mônica de Lacerda Rocha
Dalton Soares Arantes
Darli Augusto de Arruda Mello
Data de defesa: 31-07-2017
Programa de Pós-Graduação: Engenharia Elétrica

JUDGING COMMITTEE - DOCTORAL THESIS
(COMISSÃO JULGADORA - TESE DE DOUTORADO)

Candidate (Candidata): Uiara Celine de Moura RA: 140242
Defense date (Data da defesa): 31 de julho de 2017

Thesis title: "Cognitive Methodology for Optical Amplifier Gain Adjustment in Dynamic Networks"
Título da tese: "Metodologia Cognitiva para Ajuste do Ganho de Amplificadores Ópticos em Redes Dinâmicas"

Prof. Dr. Evandro Conforti (Presidente, FEEC/UNICAMP)
Prof. Dr. Joaquim Ferreira Martins Filho (UFPE)
Profa. Dra. Mônica de Lacerda Rocha (EESC/USP-São Carlos)
Prof. Dr. Dalton Soares Arantes (FEEC/UNICAMP)
Prof. Dr. Darli Augusto de Arruda Mello (FEEC/UNICAMP)

The Attestation of Defense, with the respective signatures of the Judging Committee, can be found in the student's academic life file.
A Ata de Defesa, com as respectivas assinaturas dos membros da Comissão Julgadora, encontra-se no processo de vida acadêmica da aluna.

Acknowledgements

First of all, I would like to thank my advisor, Prof. Evandro Conforti, for his patient guidance, wisdom and support throughout this work. Thanks to my co-advisor Juliano Oliveira and Miquel Garrich, for all the support and friendship. A special thank to Prof. Amílcar Careli César, for keeping in touch and providing fruitful contributions to this work.

I would like to thank the committee members, for their helpful comments and suggestions that undoubtedly improve this thesis.

I must express my gratitude to my parents, Nadja and Valter, and my sister, Maiara, for their unconditional love and encouragement; to my husband Sérgio, for his patience, love and help; to all my family (from Recife-PE to São José do Rio Preto-SP) and to Romeu S2.

Many thanks to Rafael Figueiredo and Tiago Sutili, for their help in many ways; and to Noemia and Camila, for all the administrative support at FEEC/Unicamp.

Thanks to all my colleagues and friends from CPqD (so many that there is no place to name all here), for sharing their expertise and providing a pleasant environment. In particular to Eduardo Rosa and Giovanni Farias, for releasing some hours of work to conclude this thesis.

Thanks also to my childhood friends Fernanda, Renata and Thaysa; and to my new friends from Fofoletes group and from Jazz/Ballet, for their companionship.

Finally, I would like to thank to CNPq and Funttel/Finep for the financial support.

Abstract

The ability of optical amplifiers to simultaneously amplify multiple channels with transparency to both modulation format and bit rate has been crucial for the current optical networks revolution. However, this amplification on the optical domain introduces noise, which degrades the optical signal quality. Since the noise addition depends on the amplifier's operating point, it is expected that there would be an optimal gain combination for an amplifier cascade, which is associated to the lowest signal degradation. Aiming at searching for this optimal gain combination, this work proposes a methodology based on a cognitive process to adjust the amplifier gains along an optical lightpath. Applied together with the routing and wavelength assignment (RWA) processes, this Cognitive Methodology uses case-based reasoning (CBR) to propose new gains using the performance of past connections. The Cognitive Methodology is evaluated experimentally and in simulation, considering different scenarios and comparing it with different gain conditions. The obtained results present a cognitive behavior, i.e., an optical performance improvement over time, for most of the evaluated scenarios, associated to a significant increase in execution time. The Cognitive Methodology limitations regarding the execution time and optical performance convergence are presented and discussed. In addition, an upgrade on the Cognitive Methodology, with the purpose to reduce the execution time and guarantee the optical performance, is also proposed and evaluated, presenting considerable time reduction and maintaining (or improving) the optical performance achieved by the original Methodology.

Keywords: Case-based reasoning, cognitive networks, dynamic optical networks, optical amplifiers.

Resumo

A utilização de amplificadores ópticos tem contribuído para revolucionar as redes ópticas devido à sua capacidade de amplificar vários canais simultaneamente, transparentes ao formato de modulação e à taxa de transmissão. Porém, essa amplificação no domínio óptico é acompanhada da introdução de ruído, que degrada a qualidade do sinal óptico. Como a adição de ruído depende do ponto de operação do amplificador, é possível prever a existência de uma combinação de ganhos ótima para uma cascata de amplificadores, associada à menor degradação do sinal. Em busca dessa combinação ótima, este trabalho propõe uma metodologia baseada em processos cognitivos para ajuste dos ganhos dos amplificadores ao longo de um caminho óptico. Aplicada em conjunto com o roteamento e atribuição de comprimento de onda (RWA), esta Metodologia utiliza raciocínio baseado em casos (CBR) para propor novos ganhos a partir do desempenho de conexões passadas. Tal Metodologia é avaliada experimentalmente e em simulações considerando diferentes cenários e comparando-a a diferentes formas de ajuste de ganho. Os resultados obtidos apresentam um comportamento cognitivo (melhora do desempenho óptico com o tempo) para a maioria dos cenários avaliados, associado a um aumento significativo no tempo de processamento. São apresentadas as limitações e vantagens da Metodologia com relação ao tempo de processamento e convergência do desempenho óptico. Adicionalmente, uma evolução da Metodologia, com a finalidade de reduzir o tempo de processamento e garantir o desempenho óptico, também é proposta e avaliada, apresentando reduções significativas no tempo de processamento e mantendo (ou melhorando) o desempenho óptico obtido pela Metodologia original.

Palavras chave: Amplificadores ópticos, raciocínio baseado em casos, redes cognitivas, redes ópticas dinâmicas.

List of Figures

List of Tables

Acronyms

AcCBR amplifier cognitive CBR

AdGA adaptive gain adjustment

AGC automatic gain control

AN Autonomous Network

ASE amplified spontaneous emission

B&S broadcast-and-select

BDFA bismuth-doped fiber amplifier

BER bit error rate

CBR case-based reasoning

CHRON Cognitive Heterogeneous Reconfigurable Optical Network

DB database

DP-QPSK dual polarization-quadrature phase shift keying

DRA distributed Raman amplifier

DRB double Rayleigh backscattering

DSP digital-signal processing

EDF erbium-doped fiber

EDFA erbium-doped fiber amplifier

fAcCBR fast AcCBR

fAcCBR-MLn fast AcCBR-maximum link n

FEC forward error correction

FG fixed gain

GB Gigabyte

GFF gain flattening filter

IoT Internet of Things

LCoS Liquid Crystal on Silicon

LED light emitting diode

LP lightpath

MEMS microelectromechanical system

OSA optical spectrum analyzer

OSC optical supervisory channel

OSNR optical signal-to-noise ratio

PD photodetector

PON passive optical network

QAM quadrature amplitude modulation

QoS Quality of Service

QoT Quality of Transmission

ROADM reconfigurable optical add-drop multiplexer

ROPA remote optically-pumped amplifier

RWA routing and wavelength assignment

SDM space-division multiplexing

SNR signal-to-noise ratio

SOA semiconductor optical amplifier

SOD supervisory optical demultiplexer

SOM supervisory optical multiplexer

SRS stimulated Raman scattering

SSMF standard single-mode fiber

WDM wavelength division multiplexing

WSS wavelength selective switch

Symbols

h *Planck constant*

NF *Noise figure*

GF *Gain flatness*

ν Light frequency

Er^{3+} *Ionized erbium atom*

En *Energy level n*

Nn *Population of the energy level En*

SNR_{in} *SNR at the optical amplifier's input*

SNR_{out} *SNR at the optical amplifier's output*

G *Optical amplifier gain*

G^{CH} *Optical amplifier channel gain*

n_{sp} *Spontaneous emission factor*

P_{ASE} *ASE power*

$\Delta\nu$ *Optical bandwidth*

NF^{CH} *Channel noise figure*

P_{ASE}^{CH} *Channel ASE power*

ν^{CH} *Channel frequency*

$\Delta\nu^{CH}$ *Channel bandwidth*

λ *Optical channel wavelength*

$\Delta\lambda$ *OSA resolution*

c *Light speed*

ν_P *Signal frequency*

ν_S *Pump frequency*

α *Fiber attenuation*

L *Fiber length or link/span distance*

NF_R *Noise figure of the distributed Raman amplifier*

$NFeq$ *Equivalent noise figure*

NF_{sys} *System noise figure*

G_{new} *New gain vector*

β^{Pin} *Margin considered to retrieve Pin*

$\beta^{\alpha L}$ *Margin considered to retrieve* αL

κ *Percentage of gain in* G_{new} *randomly adjusted by AcCBR*

γ *Probability to alter a gain in* G_{new} *with a null variance*

μ *Probability to alter a gain in* G_{new} *with a non-null variance*

υ *Probability to do not alter a gain in* G_{new}

$OSNR^{CH}$ *Channel OSNR*

G_H *Gain vector of the similar case in DB with the higher OSNR*

G_L *Gain vector of the similar case in DB with the lower OSNR*

$G^{CH,LP}$ *Lightpath channel gain*

$P^{CH,LP}$ *Lightpath channel input power*

$NF^{CH,LP}$ *Lightpath channel noise figure*

$NF_k^{CH,i}$ *Channel noise figure of the* k-th *amplifier at the* i-th *link*

$G_k^{CH,i}$ *Channel gain of the* k-th *amplifier at the* i-th *link*

$Lo_k^{CH,i}$ *Channel fiber loss of the* k-th *span at the* i-th *link*

$Lo_{ROADM}^{CH,i}$ *Channel ROADM loss at the end of the* i-th *link*

$NF^{CH,i}$ *Channel noise figure of the* i-th *link*

$G^{CH,i}$ *Channel gain of the* i-th *link*

t_g *Time interval between connections*

C_d *Connections' duration*

m *Service rate*

l *Connections arrival rate*

Er *Traffic load*

T *Connections duration mean*

Contents

Chapter 1

Introduction

The Internet traffic experienced a dramatic growth on the past two decades, as illustrated in Figure 1.1. In the nineties, it increased from around 100 Gigabyte (GB) per day in 1992 to 100 GB per hour in 1997. Five years latter, in 2002, the traffic reached 100 GB per second (GB/s). It is estimated that by 2020, the gigabyte equivalent of all movies ever made on history will cross the global Internet every two minutes [1].

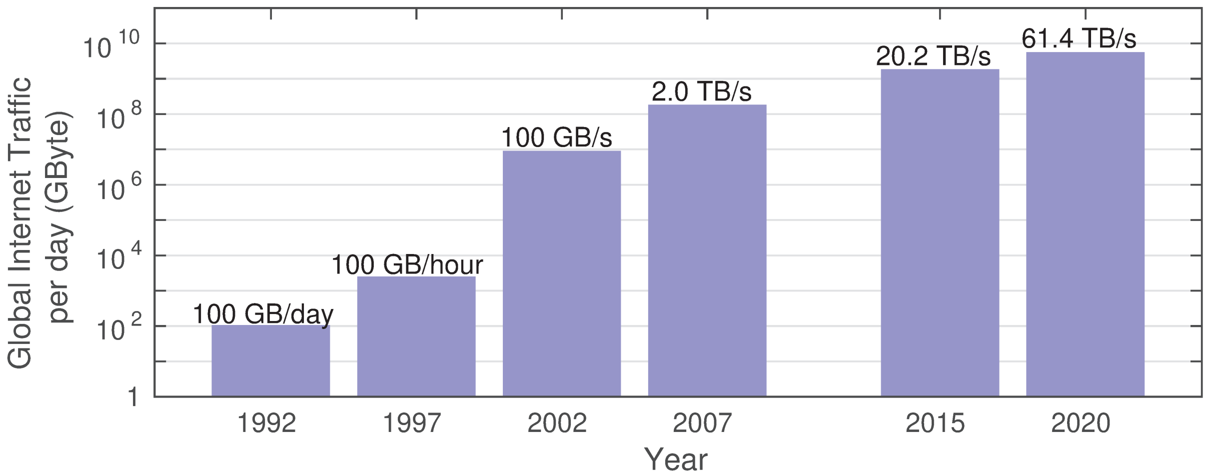

Figure 1.1: Year global Internet traffic per day and corresponding data rate in GB/day, GB/hour, and GB/s [1].

Being deployed worldwide since 1980 [2], optical communication systems based on optical fibers play an important role on the Internet traffic increase shown in Figure 1.1. Chraplyvy divides fiber telecommunications history into three technological eras [3]. The first era is associated to directed-detection and regenerated systems and lasts from 1977 to around 1993. Some events of this era include the transition from multimode fiber at 850 nm wavelengths to monomode at 1300 nm and the first submarine fiber installation. The second era is characterized by dispersion management in wavelength division multiplexing (WDM) systems. It was boosted by the development of practical erbium-doped fiber amplifiers (EDFA) at the end of the 1980s. Finally, the third (and current) era begins in around 2009 and is associated to advanced modulation formats, coherent detection and digital-signal processing (DSP) in WDM systems, with fiber linear and nonlinear penalties mitigated on electronic domain.

Currently, fiber-optic communications are facing the directed-detection return with advanced modulation schemes to attend to the growing demand for broadband services in short-reach transmissions [4]; the elastic optical networks becoming a reality as many network operators are migrating to spectrum selective switches based on the flexgrid technology [5]; and the intensive research on space-division multiplexing (SDM) approaches using multicore and multimode fibers to increase the system capacity [6]. Maybe it is a sign of a new era, characterized by a mixture of coherent and direct detection in flexgrid WDM and SDM systems. However, it is too soon to define it.

After this brief overview on fiber-optic communications history, the remainder of this Chapter is organized as follows. Section 1.1 focus on recent research on the main topics covered on this thesis. Section 1.2 presents the thesis objective. Finally, Section 1.3 describes the thesis structure.

1.1 State-of-the-art

Optical communication is a diverse and rapidly changing field [3]. New emerging services and applications, such as mobile Internet, high-resolution videos, cloud-based services, and the Internet of Things (IoT) increase traffic heterogeneity and require high-bandwidth [7]. To account for these ever-increasing demands for higher capacity, the current transparent and dynamic optical network is evolving towards a reconfigurable and flexible optical layer, enabling the transmission of different data rates and modulation formats [8]. However, such traffic and network heterogeneity poses additional requirements and challenges at the control and management plane [7], demanding improvements to guarantee an acceptable Quality of Service (QoS) and Quality of Transmission (QoT) in dynamic optical networks. Some examples of these requirements and challenges are a higher optical signal-to-noise ratio (OSNR) for advanced modulation formats and spectral fragmentation mitigation in flexgrid scenarios.

An important concept in dynamic optical networks is the wavelength-routed WDM. In such networks, given a set of connections, the problem of setting up lightpaths by routing and assigning a wavelength to each connection is called routing and wavelength assignment (RWA) [9]. The RWA problem is more challenging in current transparent optical networks, without optical-electronic-optical conversions to regenerate the signal and convert the wavelength, if needed. In transparent networks, the optical signal remains on the optical domain from source to destination, being more affected by noise addition, filtering penalties, and chromatic dispersion. Moreover, high-order modulation formats require a higher OSNR, which needs a higher signal power launched at the optical fiber, achieving the limit of nonlinearities. Thus, RWA approaches must consider physical layer impairments and wavelength continuity constraint in transparent optical networks. A detailed review of such approaches can be found in [10]. Recent works on RWA include an adaptive-alternative routing algorithm for all-optical networks that selects the route considering OSNR restrictions [11]; an ant colony optimization approach to solve the grooming, routing, and wavelength assignment problem considering mixed line rate and physical impairments [12]; and an adaptive approach to choose the most efficient forward error correction (FEC) for different lightpaths based on their individual OSNRs [13].

In transparent optical networks, a reconfigurable and flexible optical layer has contributions on edge and core optical devices [14]. Edge devices are basically transmitter and receivers, while core devices are mainly optical amplifiers, optical fibers and optical routers (that, beyond being routing devices, operate as add and drop filters). Focusing on performance-adaptive applied to edge devices, recent research includes a dynamic rerouting demonstration with bit-rate or modulation format adaptation aiming at minimize the spectrum utilization [15]; a flexible transmitter/receiver architecture that adapts its modulation format and symbol rate according to the bit error rate (BER) information [16]; a spectral efficiency-adaptive optical transmission using time domain hybrid quadrature amplitude modulation (QAM) considering a trade-off between spectral efficiency and achievable distance [17, 18]; a method for optical link survivability by acting on the transmitter launch power and bit-rate, and on the receiver DSP for linear/nonlinear impairments compensation, based on the status of the OSNR and the BER [19]; and an optical spectral shaping optimization based on genetic algorithm for fiber nonlinearities mitigation in high baud-rate transmission systems [20] and in unrepeated links [21].

On the other hand, there are two main reconfigurable core devices: optical routers and optical amplifiers. They are also key elements because they provide routing and amplification, respectively, directly on the optical domain. Recent proposals of enhanced controls for these devices include wavelength selective switch (WSS) configuration using global equalization strategies to improve network performance [22]; power budget strategies that combine the control of amplifiers and WSSs jointly with RWA obtaining OSNR improvements in meshed network scenarios [23]; a dynamic gain equalization using WSSs [24]; and a local adaptive gain control technique for optical amplifiers based on their individual performance, demonstrating an end-to-end performance improvement [25] and reducing the blocking probability in a physical layer impairment aware RWA [26]. Additionally, a self-adaptive amplifier based on machine learning and considering the performance of the entire amplifier cascade is proposed [27] and evaluated considering nonlinear effects [28]. Finally, new local and global approaches for optical amplifiers are proposed and evaluated, demonstrating a performance improvement when compared with previous approaches [29].

All these strategies apply adaptive schemes to maintain performance and service continuity under dynamic scenarios. The next step toward a self-reconfigurable optical layer is the addition of learning capability on these strategies, so that they can make use of their experience in future actions. In this way, cognitive approaches and machine learning techniques, successfully applied in radio and wireless technologies [30], can be applied in optical network scenarios to address the increasing variety of technologies and proposals that enable flexible networking [31]. A cognitive network perceives current conditions, plans, decides, acts, and learns from these adaptations to use them in future decisions, considering end-to-end goals [32]. In this context, the European project Cognitive Heterogeneous Reconfigurable Optical Network (CHRON) has made remarkable contributions by addressing the challenge of controlling and managing the next generation of heterogeneous optical networks, supporting the Future Internet [33]. Besides, it introduces the technologies and techniques that will enable a cognitive optical network to observe, act, learn and optimize its performance [34].

Some studies related with CHRON that use cognitive techniques in optical networks include cognitive applications to reduce the connection blocking probability by improving the performance of route and wavelength selection to lightpahs [35, 36] or by using reactive and proactive lightpath restoration techniques [37]; a failure restoration time improvement by dynamically adjusting the modulation formats to satisfy QoT requirements [38]; a method that automatically learns and predicts the traffic behavior to save energy [39]; and cognitive mechanisms to reconfigure/design virtual topologies [40, 41, 42, 43, 44]. In addition, [45] presents a control plane structure to coordinate the cognitive optical network elements.

Additional examples of cognition applied to optical networks are a cognitive control and management system with an architecture on demand scheme to minimize complexity and to better handle environmental unpredictability [46]; a software defined network based failure recovery solution including failure detection scheme, dynamic routing algorithm and failure recovery application [47, 48]; a cognitive power management technique that enhances the decision making with traffic prediction [49]; and a Fuzzy controller applied to cognitive optical networks that defines new routes based on new connections demand considering physical layer penalties [50, 51].

Therefore, cognitive approaches and techniques applied to optical networks are viable candidates to manage complexity and to permit efficient utilization of available resources [30]. There are different models used to accomplish machine learning processes, such as decision trees, genetic algorithms, artificial neural networks, and case-based reasoning [52]. The technique chosen in this work is the case-based reasoning (CBR), a problem solver approach that uses old experience to understand and solve new problems [53]. It is a versatile and mature approach that has been successfully applied to many fields (beyond machine learning), including health science, industry, enterprise systems, business and engineering [54, 55, 56, 57]. Some examples of recent studies are a framework for mapping the monthly average daily solar radiation for help to select a suitable location for the photovoltaic system installation [58]; an automatic method to detect landslides using CBR and genetic algorithm [59]; a telemedicine framework for health care information exchange [60]; the prediction of the hourly electricity consumption of an institutional building, combining CBR with artificial neural networks techniques [61]; a learning diagnostic system to give the learners feedback and suggestion in real time [62]; the design of processes for gold extraction [63]; and the insulin calculators enhancement that assist people with diabetes to estimate the amount of insulin required for meals [64].

Examples of CBR applied to optical networks are a quality of transmission estimator for classifying lightpaths [65, 66, 67, 68, 69, 70]; and in a cognitive RWA approach aiming to reduce the computational time and the blocking probability [71]. The last stores previous connections solutions (in terms of nodes) and considers this information in future connections, not changing devices along the lightpath. This cognitive RWA is extended in [72] to consider the transmission impairments, estimating the OSNR and blocking the connection if it is bellow a defined threshold.

Up to now, it was presented an overall network scenario and the new research exploring techniques and applications to provide flexibility and self-knowledge in fiber-optic communications. However, there are studies focusing on optical devices, such as flexible, colorless, contentionless, and directionless WSSs; multicore, multimode, and ultra-low-loss optical fibers; and low noise and broadband optical amplifiers; also contributing to overcome the increasing demand. Optical amplifiers, mainly based on erbium-doped fiber and Raman scattering, were responsible to transparent transmission and to extend the usable fiber bandwidth in the past. However, they are currently viewed as a bottleneck for capacity increase as they limit the accessible optical spectrum [73]. There are three approaches to accomplish a high capacity system: expanding the optical bandwidth to increase the number of WDM channels; using the available bandwidth more effectively, applying advanced modulation formats; and exploring SDM. These three approaches challenge the optical amplifier project, as following detailed.

The first approach needs amplifiers with extended bandwidth. Research in this theme explores new architectures and new materials. Examples are an EDFA with 70-nm continuous amplified bandwidth (C and L bands) for submarine application using three erbium-doped fiber stages and two gain flattening filters in a series configuration [74]; the first bismuth-doped fiber amplifier (BDFA) for a bandwidth ranging from 1640 to 1770 nm [75]; a bismuth/erbium co-doped fiber for amplifiers with the gain bandwidth ranging from 1530 to 1770 nm [76]; a thulium-doped fiber amplifier operating at 1650-

2050 nm waveband and presenting a high gain and a low noise figure [77].

On the other hand, increasing the demand by using spectrally efficient modulation formats requires a higher OSNR to achieve a suitable BER. Thus, optical amplifiers need to be designed to introduce less noise. New studies on low noise amplifications combine distributed Raman amplifier with EDFA in hybrid configurations, allowing also to extend the operational bandwidth beyond the C-band [78]. Additionally, an experimental study on hybrid optical amplifiers topologies based on first order Raman and EDFA to enable the repeaterless transmission of 40x112 Gbps dual polarization-quadrature phase shift keying (DP-QPSK) over 302 km with standard single-mode fiber (SSMF) [79]; the evaluation of Raman+EDFA and EDFA+Raman hybrid amplifiers configurations in terms of global gain, ripple, and noise figure [80]; and the combination of hybrid Raman-EDFA amplifiers with low loss and high effective area optical fibers to provide low noise optical fiber transmission [81].

Recent studies exploring SDM in optical amplifiers are an absorption-enhanced 7-core erbium-doped fiber showing a low core-to-core crosstalk [82]; a 6-mode fiber amplifier with large erbium-doped area to minimize the gain difference between modes [83]; a 10-mode EDFA with step and ring erbium concentration profiles also to equalize modal gains and reduce the noise figures [84]; a double-cladding multicore fiber for amplifier applications improving the pump efficiency, total gain and noise figure [85]; and the first second-order few-mode distributed Raman amplifier [86].

1.2 Objective

In the context of meshed networks with dynamic and heterogeneous traffic, the main objective of this work is to propose a self-reconfigurable optical layer by acting on the optical amplifiers. These actions must be performed by a centralized controller, and should be based on past experience, in terms of previous adjustments and their consequences on the connections' performance, in a cognitive approach. The learning capability, with optical performance improvements along the time, must be the main contribution of this work.

1.3 Thesis structure

The current Chapter presents the state-of-the-art and outlines the objective of the work. The remaining Chapters are organized as follows:

- **Chapter 2** summarizes the fundamental concepts of the main topics covered on this thesis, which are: optical networks, RWA, optical amplifiers, and CBR.
- **Chapter 3** introduces the proposed Cognitive Methodology and the proposed modification to reduce the execution time.
- **Chapter 4** shows the results for the experimental validation in a single network.
- **Chapter 5** presents the simulation results for the Cognitive Methodology for different networks.
- **Chapter 6** outlines the conclusions and publications, suggesting future works.

Chapter 2

Theoretical background

Important concepts on optical networks, devices, and a computational algorithm based on learning process to solve extensive problems are explored in this work. Overall, the theoretical background to understand the proposed methodology is presented in this Chapter. Section 2.1 overviews the fundamental concepts regarding optical WDM networks; Section 2.2 presents some general concepts regarding RWA; Section 2.3 reviews the main optical amplifier technologies used in long-haul systems; and Section 2.4 details how CBR works, a classical approach used to solve problems.

2.1 Optical networks

An optical network provides a common infrastructure over which a variety of services can be delivered [87]. It can be deployed mainly using four topologies: bus, star, ring, and meshed, as illustrated in Figure 2.1. In many cases, a meshed network is implemented in the form of interconnected rings [87] and it is the main topology used in this work.

In terms of architecture, optical networks are divided into three main categories, depending on the area they cover. Transport, core or long-haul networks cover

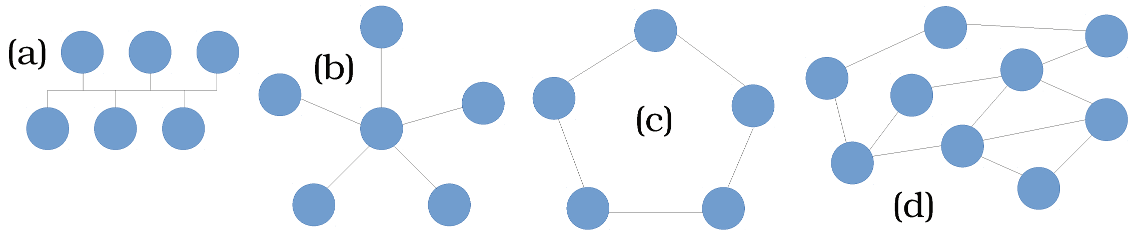

Figure 2.1: Some examples of possible network topologies. (a) bus, (b) star, (c) ring, and (d) mesh.

a country or continent geography usually in a meshed topology and transferring a huge amount of data. Metropolitan networks, or simply metro networks, cover a medium area, comprising some cities, usually in a ring topology to provide protection against failures, and transferring a medium data volume. Access networks cover a small area and are the access point for end-to-end users with a small amount of data when compared with core and metro networks. Their common topologies are bus, ring and star [88]. Moreover, in the era of cloud-computing services, warehouse-scale computers (placed on datacenters) are needed to process user data that do not reside anymore at a local personal computer, but "in the cloud". Since optical technologies are penetrating this field, a new group of optical networks dedicated to intra- and inter-datacenter communications recently emerged as datacenter networks. The main characteristics of these networks are the huge amount of traffic in short distances (< 100 km) [3]. This work is restricted to metro and long-haul networks.

Furthermore, optical WDM networks can be classified into opaque, transparent or partially transparent [89]. Each node in Figure 2.1 is responsible to route and additionally, add, drop, or regenerate the optical signal passing through it. If all nodes utilize conversions to electronic domain to perform these actions, the network becomes opaque. On the other hand, if no opto-electronic conversion is utilized, it is a transparent or all-optical network. Between these two extremes, the network is partially transparent [89]. The routing procedure at each node has being done electronically even in 2004 [88]. Currently, the node comprises mostly optical routing, largely focused on reconfigurable optical add-drop multiplexer (ROADM) based on WSSs [3]. Increased wavelength flexibility and need for faster provisioning have led to recent ROADM architecture developments, adding features on the add/drop side, such as colorless (any wavelength can be added/dropped to/from any port), directionless (any transponder can connect to any direction) and contentionless (no blocking in the wavelengths that can be simultaneously dropped to a node from different directions) [3]. Optical regeneration is mainly performed by optical amplifiers, detailed in Section 2.3. This work considers transparent optical networks.

Like switching in the electrical domain, there are two main methods of optical switching: optical circuit switching and optical packet switching [89]. In optical circuit switching, a guaranteed amount of bandwidth is allocated to each connection and is available to the connection all the time, once the connection is set up [87]. The problem with circuit switching is that it is not efficient at handling bursty data traffic, such as the Internet data. In this scenario, optical packet switching has emerged to transport bursty data traffic efficiently. In optical packet switching networks, the data stream is broken up into small packets that are multiplexed together with packets from other data streams. These packets are routed inside the network based on their destination [87]. However, this work considers only optical circuit switching networks.

In meshed-network architectures, only some nodes are connected directly by point-to-point links (a link comprises optical fiber spans and amplifiers). For this reason, the creation of a virtual circuit between two arbitrary nodes requires switching at one or more intermediate nodes [88]. This virtual circuit, that provides an end-to-end optical connection between two nodes, is defined as lightpath. In other words, lightpaths are optical connections carried end-to-end from source to destination nodes over a wavelength on each intermediate link. At intermediate nodes in the network, the lightpaths are routed from one link to another. Lightpaths may have their wavelengths converted along their route considering electronic conversion facilities. Different lightpaths in a wavelength-routing network can use the same wavelength as long as they do not share any common links. This allows the same wavelength to be reused spatially in different parts of the network [87].

Summarizing, this work considers transparent and meshed optical networks in long-haul and metro architectures, with optical circuit switching and no wavelength conversion. The problem of calculating routes and assigning wavelengths to lightpaths in such networks is following detailed in Section 2.2.

2.2 Routing and wavelength assignment (RWA)

This Section gives a brief overview on the RWA problem in optical circuit switching networks. Given a network topology and a set of demands, the RWA determines a route and assigns wavelength(s) along the lightpath in such a way to minimize resources, such as number of wavelengths and number of links [9]. The set of demands (traffic matrix) is the list of all connection that must be established on the network. Thus, each single demand corresponds to an individual connection request, and can be static or dynamic. Static demands refer to permanent connections, with an infinite timelife. On the other hand, dynamic demands have a finite duration. Among the dynamic demands, there are also the scheduled and the ad hoc demands. Schedule dynamic demands have their start time and duration known "a priori" because they are planed. In this case, the network has been already prepared for them. Ad hoc dynamic demands, on the other hand, have their start time and duration unknown. Such parameters are generally modeled by random processes [90].

RWA is an NP-complete problem [9], i.e., in which an optimal solution can not be found in polynomial time using known algorithms (NP stands for "nondeterministic, polynomial time"). Normally, the RWA problem is divided into two subproblems: the routing subproblem and the wavelength assignment subproblem. This separation, although does not guarantee an optical solution, reduces the algorithm execution time [90].

The routing subproblem is responsible to find the shortest path from source to destination nodes. Some classic algorithms, such as Bellman-Ford [91] and Dijkstra [92], are normally used. They consider a cost to each link, associated to the distance, fiber loss, or number of wavelengths already used, and the routing problem is reduced to find the path with the minimum cost.

The wavelength assignment subproblem is normally solved by randomly assigning an available wavelength, by choosing the first non-occupied wavelength (first-fit), or by assigning the less or the must used wavelength [9]. In any case, the wavelength assignment problem must obey the following constraints. Two lightpaths must not be assigned the same wavelength on a given link. If no wavelength conversion is available in the network, then a lightpath must be assigned with the same wavelength all along its route. This situation is referred as the wavelength-continuity constraint [87].

However, as already mentioned in the Introduction, the RWA problem is more challenging in transparent optical networks, in which the optical signal remains on the optical domain for a longer distance, being more affected by physical layer impairments, such as amplifier noise, filtering, chromatic dispersion, polarization dependent loss/dispersion, and nonlinearities. In this scenario, RWA algorithms must consider physical layer impairments besides wavelength-continuity constraint. These impairments can be modeled analytically or by simulations. Moreover, monitoring techniques are also applied, either on the impairment level or at overall performance level [90].

In some practical situations, the RWA must consider traffic grooming, in which high-bandwidth channels are filled up by low-speed traffic streams. It is important that traffic be aggregated appropriately to avoid wasting resources, improving the components and bandwidth usage [88, 93].

The performance of RWA algorithms in circuit-switched networks can be measured by some metrics, such as the blocking probability, the amount of resources (wavelengths, links, nodes) used to perform the lightpaths, or the algorithm execution time [90].

2.3 Optical amplifiers

Optical amplifiers have become essential components in high-performance optical communication systems [87] and have contributed to the success of optical data transport together with low loss transmission fibers, compact laser diodes, and high speed photodiodes [3]. They are responsible to increase the transmission distance by optically amplifying the signal after attenuations caused by optical fibers and passive components, such as multiplexers and couplers. Before using optical amplifiers, the regeneration was performed on the electronic domain, channel by channel, using optoelectronic repeaters. These repeaters converted the optical signal into an electric current and then regenerate it before transmission [2]. Thus, an optoelectronic repeater is needed for each channel and it is dependent on the modulation format and bit rate.

The main advantage of optical amplifiers over optoelectronic regenerators is that they can amplify several channels simultaneously, regardless of modulation format and bit rate. However, differently from optoelectronic regenerators, the process of optical amplification adds noise to the signal, limiting the maximum transparent transmission distance. The origin of amplifier noise and its consequences on the optical signal will be explored further up, when detailing each amplifier technology. Due to the high cost and power consumption of optoelectronic regenerators, they are only used in large scale continental networks, when transmission lengths exceed the maximum transparent reach [3].

According to their application, optical amplifiers are classified into *booster*, *line* and *preamplifier*. These three applications are illustrated in Figure 2.2. Booster amplifiers are placed right after the optical transmitter to boost the signal at the optical fiber input. They need to be designed to handle high input and output powers. Noise is not critical because of the high signal power. Line amplifiers are used in long-haul transmission systems, where the signal needs to be amplified along the link to arrive at the receiver with reliable chances to be detected. They typically operate with moderate low power input signals. Preamplifiers are placed before an optical receiver to improve its sensitivity. They work with low input signals, thus, it must be designed to produce low noise [2, 94].

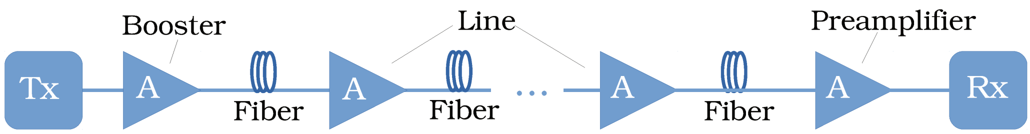

Figure 2.2: Optical amplifier applications: booster, line and preamplifier.

The amplifiers used on fiber-optic communication systems are mainly based on three technologies: doped fiber amplifiers (basically EDFAs), Raman amplifiers and semiconductor optical amplifiers (SOA). EDFA is the most widely deployed optical amplifier type due to its excellent compatibility with transmission fibers, energy efficiency and low cost [3]. The Raman amplifier is the second on the rank, but its deployment in commercial systems is by far outnumbered by EDFAs [3]. In 1990s, SOAs were expected to emerge as a compact and low-cost alternative to EDFAs. However, because of the short-time constant of their dynamics, they cause unacceptable level of inter-channel and intra-channel distortions making them unsuitable for WDM systems [95]. Otherwise, they can be used for wavelength conversion and as a fast switch for wavelength routing in WDM networks [2]. Currently, they also find applications in access passive optical networks (PON), to extend the total loss budget [95]. Thus, as this work focuses on long-haul systems, SOAs are not covered in this Chapter.

The remainder of this Section focuses on EDFAs and Raman amplifiers, presenting their fundamental concepts in terms of operating principles, noise generation and gain control techniques. Additionally, an optical amplifier characterization process to obtain the amplifier performance is described; an adaptive gain adjustment methodology, used to compare with the proposed Cognitive Methodology, is reviewed; and the difference between amplifier gain control and amplifier gain adjustment is discussed.

2.3.1 EDFA

Since its invention in 1987 [96], the EDFA has revolutionized the telecommunications industry. Today, the EDFA is widely viewed as a mature technology, while new network applications drive new requirements for further enhancement of optical fiber amplifiers [95]. EDFAs have attracted the most attention because they operate in the wavelength region near 1.55 μm [2], which corresponds the low loss region (C-band, in ITU-T[1] grid) in SSMFs.

Operating principle

There are three phenomena behind signal amplification in EDFAs: absorption, spontaneous emission and stimulated emission. Figure 2.3 presents an atomic system with two energy levels ($E1 < E2$) to illustrate the concepts of these three phenomena. Under normal conditions, all materials absorb light rather than emit it [2]. The absorption phenomenon occurs when an incident light photon with energy $h\nu$ (where h is the Planck's constant and ν is the light frequency), equals the energy difference $E2-E1$, is absorbed by the atom. The atom ends up in the excited state (E2) and the incident light is attenuated, as illustrated in Figure 2.3(a). This process is used on photodiodes, to convert light into electrical current, since the transition to excited state generates a pair electron-hole in semiconductors [2].

Atoms do not stay on the excited state for a long time, returning to the energy level E1 and emitting a photon in the process. The photon emitted also has energy $h\nu$, corresponding to $E2 - E1$. If this transition occurs independently of any external radiation, it is a spontaneous emission. In this case, photons are emitted in random

[1] International Telecommunication Union - Telecommunication Standardization Sector, responsible to develop international standards known as ITU-T Recommendations.

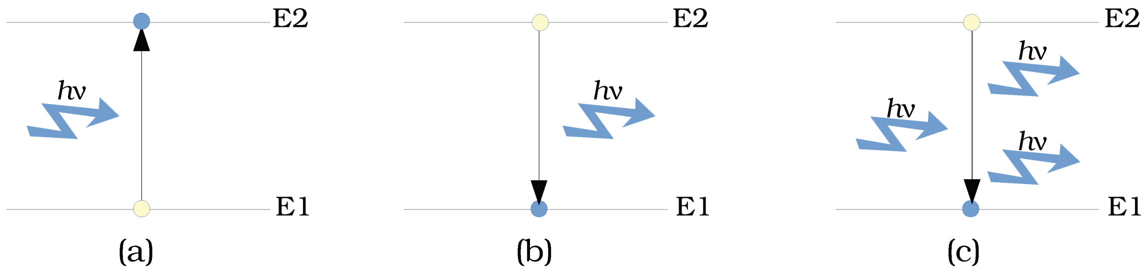

Figure 2.3: Physical phenomena associated to the EDFA amplification process: (a) Absorption, (b) spontaneous emission, and (c) stimulated emission in an atomic system with two energy levels. Adapted from [2].

directions with no phase relationship among them. Spontaneous emission is the operating principle of light emitting diodes (LED) and it is illustrated in Figure 2.3(b). However, if this transition is induced by an electromagnetic field whose frequency ν also satisfies $h\nu = E2 - E1$, it is defined as stimulated emission [97] and it is illustrated in Figure 2.3(c). In stimulated emission, the emitted and original photons are coherent. This means that they have the same characteristics in terms of frequency, phase, direction of propagation, and state of polarization. Besides EDFAs, stimulated emission is also the phenomenon behind the diode lasers, which emit coherent light [2, 87].

However, in EDFAs, three energy levels are involved on the amplification process. Figure 2.4 shows these three energy levels of erbium ions in silica glass ($E1 < E2 < E3$), omitting several others. The amorphous nature of silica broadens all energy levels, represented by discrete lines in Figure 2.3 for a single atom, into bands in Figure 2.4 for the erbium ions in silica glass [88].

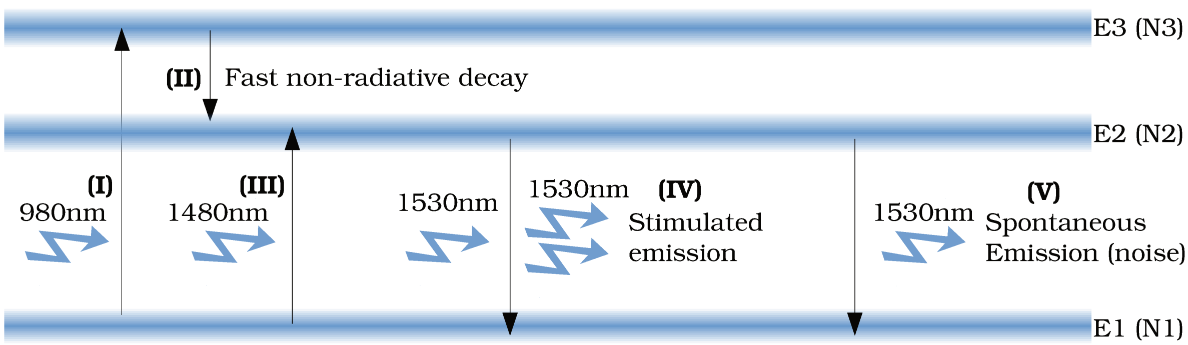

Figure 2.4: First three energy levels of Er^{3+} ions in silica glass. Adapted from [87, 98].

In thermal equilibrium, the populations (number of ions Er^{3+}) of each band are distributed as: $N1 > N2 > N3$, where Nn is the population of the energy level

En. However, the amplification process requires a population inversion, i.e. $N2 > N1$. This condition is achieved by a combination of absorption and spontaneous emission. Injecting light at 980 nm, which corresponds to the energy between $E3$ and $E1$, it will occur absorption and ions transitions from levels $E1$ to $E3$, as indicated in Figure 2.4 by process (I). These ions on level $E3$ quickly transit to level $E2$ in a spontaneous and non-radiative emission process (also illustrated in Figure 2.4 by process (II)). This fast decay is a consequence of the small spontaneous emission lifetime, of around 1 μs, in energy level $E3$. Lifetime is the mean time that an atom remains on an exited level. Once on level $E2$, there are also spontaneous transitions to level $E1$ (see Figure 2.4, process (V)). It is the main noise source in EDFAs, as it will be explained further up. However, it is a slow process, since the lifetime of level $E2$ is near 10 ms. Thus, because of this long permanence of ions on energy level $E2$, the population inversion $N2 > N1$ is guaranteed. The signal at 980 nm used to provide population inversion is denoted as *pump power* [87].

The energy separation of these two bands ($E1$ and $E2$) corresponds to a wavelength range from 1460 to 1620 nm, which coincides with the low-loss region of silica fibers [87, 88]. Thus, once the population inversion is achieved, when a signal at around 1530 nm is injected into the EDFA, it stimulates the emission of coherent photons, as illustrated in Figure 2.4 by process (IV). These stimulated emissions are due to the ions transitions from $E2$ to $E1$, reducing/depleting the population inversion, which is quickly restored by the pump power [87].

Another possible pump wavelength is 1480 nm, providing a direct transition from energy level $E1$ to $E2$ (see Figure 2.4, process (III)). However, a pump at 1480 nm achieves a lower population inversion, which degrades the amplifier performance in terms of noise [87], as it will be explained further up.

A typical optical architecture for EDFA is depicted in Figure 2.5, also illustrating the signal spectrum in some points, for 40 channels in C-band from 1530 to 1561 nm. It consists of a segment of silica fiber doped with ionized erbium atoms (Er^{3+}), named erbium-doped fiber (EDF). This fiber is pumped with lasers at 980 or 1480 nm. Signal and pump powers are combined via a wavelength division multiplexer (WDM). Input isolator (ISO) is used to prevent backward noise reaching previous devices. Output isolator avoids reflections inside the EDF, preventing the optical amplifier acting as a laser. Additionally, power splitters (PS) can be used at the EDFA input and output to provide a small fraction of power to photodetectors (PD) for monitoring reasons.

The energy levels' broad bands in Figure 2.4 are responsible for amplifying several wavelengths simultaneously. However, erbium ions are distributed nonuniformly within these continuous bands [87]. Thus, stimulated emissions are more likely to occur for some wavelengths than others. As a consequence, different wavelengths do not experience the same gain when passing through an EDF. This gain dependence on wavelength is also illustrated in Figure 2.5, by the difference between the spectra at the amplifier input and the second isolator output. Thus, a gain flattening filter (GFF) must be considered. This component applies different attenuations for each channel to overcome the gain inequality, providing a flat spectrum at the amplifier output.

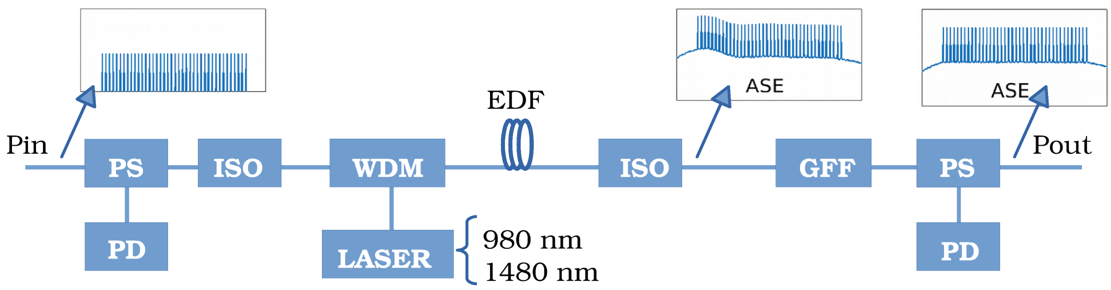

Figure 2.5: Typical EDFA optical circuit.

Back to pump wavelengths, although degrading the noise performance of the amplifier, higher-power pump lasers are available at 1480 nm, compared with 980 nm. Therefore, 1480 nm pumps are suitable for amplifiers designed to deliver high output powers. Another advantage of the 1480 nm pump is that it propagates with low loss in the transmission fiber. Thus, 1480 nm pump lasers are used in remote optically-pumped amplifier (ROPA), in which the pump laser is remotely placed from the EDF itself. ROPA are used in systems where it is not possible to place any active components in the middle of the link [87].

Noise

There are three main noise sources that degrade the signal-to-noise ratio (SNR) in optical transmission systems: thermal noise, shot noise and amplifier noise. The first two produce fluctuations in the current even when the incident optical signal has a constant power. Thermal noise is a consequence of the electrons random movement inside any conductor at a finite temperature. Shot noise is inherent to the photodetection process:

even when the incident power on a photodetector is constant, photons are absorbed at random time intervals, generating electron-hole pairs. Shot and thermal noises must be taken into account for any receiver. However, in long-haul systems, the optical signal is optically amplified periodically for compensating fiber losses. Thus, the accumulated noise added by each amplifier becomes so large that system performance is mostly dominated by amplifier noise, rather than the thermal or shot noises [88].

Noise is inherent to the EDFAs amplification process previously described. Once the population inversion is achieved, ions can spontaneously decay from energy levels $E2$ to $E1$, emitting a photon that is uncorrelated to the signal photons. This spontaneously emitted photon is also amplified, stimulating the emission of new photons (also uncorrelated to the signal). This amplified spontaneous emission (ASE) appears as noise at the output of the amplifier, reducing the signal gain [87, 94]. Figure 2.6 shows the EDFA output spectrum with the signal at 1545 nm and the broadband ASE noise background, obtained in simulation.

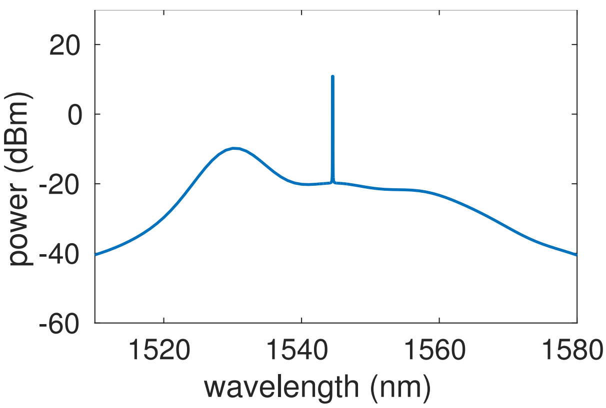

Figure 2.6: EDFA output spectrum illustrating the optical signal at 1545 nm and the ASE noise obtained in simulation with a resolution of 0.1 nm.

An important figure of merit of optical amplifiers is their noise figure (NF), which is defined as the ratio of the SNR at the amplifier input and output:

$$NF = \frac{SNR_{in}}{SNR_{out}}. \tag{2.1}$$

Note that in Equation 2.1, the noise figure is defined in terms of the electrical SNR. Thus, it is assumed that the signal is detected at the amplifier input and output. The detection process requires a photodetector, which is a non-linear square-law device. The photocurrent is therefore composed of a number of beat signals between the signal and noise (ASE) fields in addition to the squares of the signal and noise fields separately. The mixing of the noise with itself and with the signal are commonly referred as the spontaneous-spontaneous and signal-spontaneous beat noises, respectively. These are the two new noise terms in the photocurrent associated to the optical ASE [94].

An expression for the noise figure can be derived considering that the input signal is shot-noise-limited (there is no ASE at the amplifier input). At the output, the ASE contribution is mainly signal-spontaneous beat noise. Spontaneous-spontaneous beat noise can be ignored because the signal power is much larger than the ASE noise power. Moreover, thermal noise is negligible on the noise figure expression when the amplifier gain is large enough [94, 98]. Thus, Equation 2.2 considers just the dominant terms of the expression derived in [94]:

$$NF = 2n_{sp}\frac{G-1}{G} + \frac{1}{G}, \tag{2.2}$$

where G is the amplifier gain in linear units and n_{sp} is the spontaneous emission factor (also referred as the population inversion parameter), and it is given by $N2/(N2 - N1)$ [2]. Considering $G >> 1$, NF is simply $2n_{sp}$. An ideal amplifier, in which n_{sp} is 1 (full population inversion), corresponds to the best NF case of 2 (or 3 dB). For practical amplifiers, NF is typically between 4 and 7 dB [87].

A complete inversion ($n_{sp} = 1$) is only possible considering pumping wavelength at 980 nm. Therefore, a 980 nm pumped EDFA can achieve a better noise figure than a 1490 nm pumped EDFA [94].

Furthermore, EDFA noise figure can also be expressed as a function of the ASE noise power (P_{ASE}) [94]:

$$NF = \frac{P_{ASE}}{h\nu\Delta\nu G} + \frac{1}{G}, \tag{2.3}$$

where P_{ASE} is given by $2n_{sp}h\nu\Delta\nu(G-1)$ in W, ν is the light frequency in Hz, and $\Delta\nu$ is the optical bandwidth in which P_{ASE} is measured, also in Hz. This Equation is very useful to measure noise figure optically, using an optical spectrum analyzer (OSA). In this case, $\Delta\nu$ is related to the OSA resolution ($\Delta\lambda$) by $c/\lambda(\Delta\lambda/\lambda)$, in which c is the light speed and λ is the channel wavelength. Moreover, Equation 2.3 must be applied to measure noise figure only when there is no ASE at the amplifier input (shot-noise-limited) [94].

2.3.2 Raman amplifier

Raman amplifiers are based on the non-linear phenomenon called stimulated Raman scattering (SRS). During SRS, light incident on a medium transfers its energy to a lower frequency light. This process is better explained further up. The main advantages of Raman amplifiers are that they provide gain at any wavelength and they can use the transmission fiber as the gain medium. The drawbacks are the high sensitivity to pump oscillations and the low pump power efficiency. The latter drawback is overcome by high-power pump lasers available for Raman amplifications since mid-nineties [87, 99].

Operating principle

The SRS phenomenon occurs when a photon of an incident light is scattered by one of the molecules of the medium to a lower-frequency photon. This shift to a lower frequency (a longer wavelength or a smaller energy photon) is referred as the Stokes shift, and it is a characteristic of the medium. In SSMF, the Stokes shift peak is nearly 13.2 THz. The energy corresponding to the Stokes shift is transformed to a phonon, which is a vibration mode of the material [98, 99].

Thus, in Raman amplifiers, when a weak signal at frequency ν_S is launched into an optical fiber together with a strong pump power at ν_P, if ν_P and ν_S obey the Stokes shift ($\nu_P - \nu_S = 13.2$ THz), the signal will be amplified [99]. Figure 2.7 shows the gain spectrum obtained in simulation for distributed Raman amplifier (DRA) in a counterpropagating configuration resulted from a pump at 1440 nm. A DRA is a Raman amplifier in which the gain medium is the transmission fiber itself. Observe the gain peak at 1530 nm, which corresponds to a Stokes shift (converted to wavelengths at the C-band) of 90 nm.

Moreover, it is also possible to achieve a gain spectrum flattened by using several pumps at different wavelengths. In this situation, each pump creates the gain spectrum as in Figure 2.7. The superposition of these spectra creates relatively flat gain over a wide spectral region [2].

Figure 2.8 illustrates a typical optical circuit of a counterpropagating DRA, in which signal and pump travel in the opposite direction along the transmission fiber. The counterpropagating DRA is the most popular configuration for Raman amplifiers [2, 87]. Discrete Raman amplifiers, that use special fibers (as dispersion compensating fibers) as

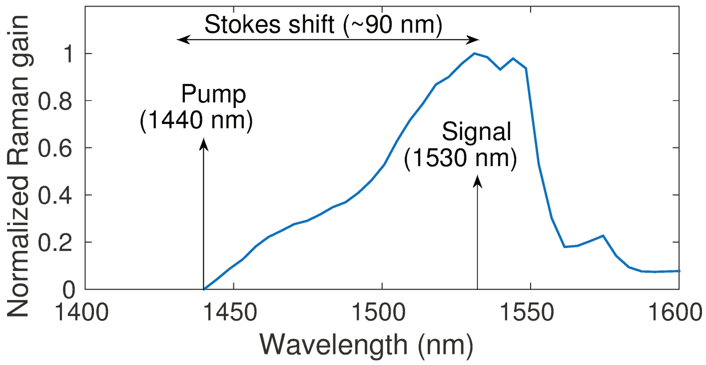

Figure 2.7: Raman gain spectrum for a pump at 1440 nm, providing gain at nearly 1530 nm. Adapted from [98].

the gain medium, and copropagating pumping configurations are also possible.

The DRA circuit shown in Figure 2.8 can have one or more pump lasers at 14xx nm to provide gain for signals at the C-band (1520 to 1560 nm). A pump combiner component is used to gather the power of these pump lasers and a WDM is used to couple the signal and the pump powers. As the amplification occurs along the transmission fiber, the signal at the WDM input is already amplified.

There are two gain definitions in a DRA: the *net gain* and the *on-off gain*. The net gain is the difference between the output signal (Pout) and the system signal input (Pin,sys), both illustrated in Figure 2.8. The net gain considers the Raman gain and the fiber loss. The on-off gain is the difference between the Pout with the lasers turned on and off. Thus, the on-off gain considers just the Raman gain.

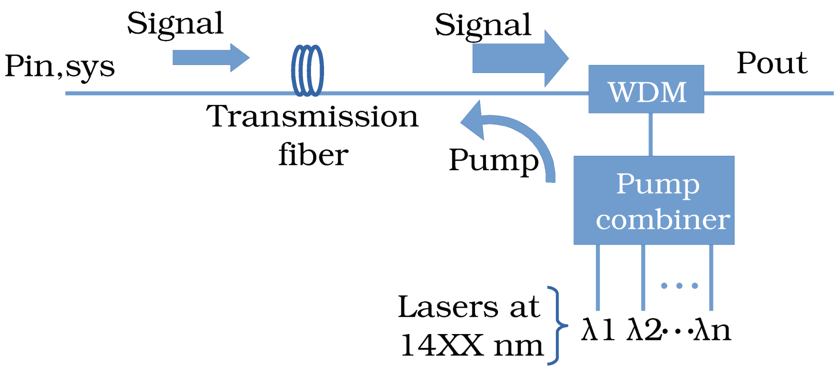

Figure 2.8: Typical optical circuit of a counterpropagating DRA.

(Improved) noise

The noise sources in Raman amplifiers are different from those in EDFAs. The dominant source is the multiple path interference caused by double Rayleigh backscattering (DRB) of the signal along the fiber. DRB copropagates with the signal and is also amplified by the distributed Raman gain, appearing as noise. Other examples of noise sources are the spontaneous Raman scattering and the pump-noise transfer. Spontaneous Raman scattering, similar to ASE in EDFAs, appears as a noise because of the non-coherence associated to all spontaneously generated photons. However, different from ASE in EDFAs, in Raman amplifiers, spontaneous Raman scattering is relatively low. Pump-noise transfer to the signal occurs due to the Raman gain fast response to pump power variations. Therefore, any fluctuation in the pump at frequencies < 1 THz is transferred to the Raman gain and, consequently, to the signal power. This noise can be reduced by using a counterpropagating configuration because fluctuations in pump power are averaged over the propagation time along the fiber [87, 99].

The noise figure of the DRA presented in Figure 2.8 corresponds to the entire system ($NF_R = NF_{sys}$), comprising the transmission fiber, as illustrated in Figure 2.9(a). Thus, it presents a much higher value than EDFA typical noise figures. To emphasize the noise advantage of DRAs, it is commonly used the equivalent noise figure concept ($NFeq$). $NFeq$ represents the noise figure a discrete amplifier would have in the absence of Raman amplification to provide the same on-off gain and SNR as that obtained using the DRA [99].

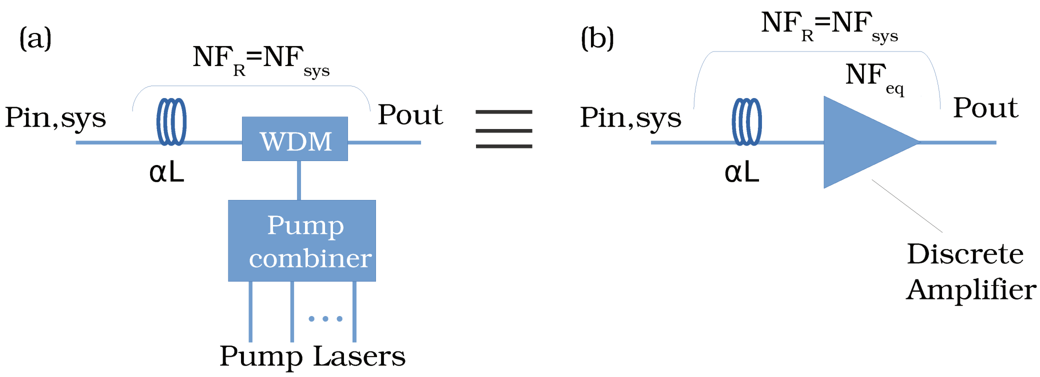

Figure 2.9: Illustration of the equivalent noise figure for DRA.

Replacing the DRA (Pumps, pump combiner and WDM) in Figure 2.9(a) by a discrete amplifier that provides the same output power (Pout) with a noise figure

NF_{eq} (defined above) in Figure 2.9(b), the system noise figure will be given by: $NF_{sys} = NF_{eq}\alpha L$, where α is the fiber attenuation and L is the fiber length. Thus, αL is the total fiber loss. This expression is obtained by considering the total noise figure of a fiber span followed by a discrete amplifier, detailed in [94]. Finally, as $NF_{sys} = NF_R$, it turns out that $NF_{eq} = NF_R/(\alpha L)$, or $NF_{eq}^{dB} = NF_R^{dB} - (\alpha L)^{dB}$. Thus, depending on (αL), N_{eq} can be lower than zero. It is physically not possible, but indicates the higher performance of DRAs over EDFAs [94, 99].

Furthermore, it is possible to use Equation 2.3 to calculate N_{eq} for DRAs just replacing G by the on-off gain.

2.3.3 *Amplifier characterization process*

An experimental characterization process to obtain the optical amplifier performance was proposed in [100]. The process consists on automatically measuring several discrete points, with a pre-defined granularity, along the operating region of the amplifier. This operating region is referred as the amplifier power mask [101], and corresponds to the region in which the amplifier optical performance is guaranteed. Figure 2.10(a) illustrates the power mask, which is defined in the input versus output power plane and is limited by the amplifier maximum output power, minimum input power, and minimum/maximum gains.

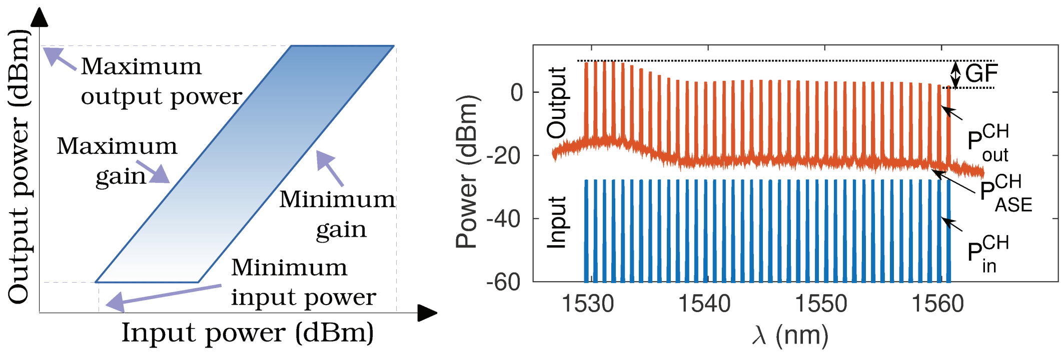

Figure 2.10: Amplifier characterization: (a) optical amplifier power mask and (b) amplifier input and output spectra obtained in simulation considering a resolution of 0.1 nm.

During the characterization process, information of total input/output powers and spectra (see Figure 2.10(b)) are measured and used to obtain the amplifier noise figure and gain flatness for each discrete point inside the power mask.

Noise figure is calculated for each channel using Equation 2.3, following rewritten considering the index CH for channel:

$$NF^{CH} = \frac{P_{ASE}^{CH}}{h\nu^{CH}\Delta\nu^{CH}G^{CH}} + \frac{1}{G^{CH}}, \tag{2.4}$$

in which P_{ASE}^{CH} and G^{CH} are the noise power and the gain for a single channel, respectively. P_{ASE}^{CH} is estimated from the output spectra, at the signal frequency, by extrapolating the adjacent ASE measurements under the signal peak. To improve P_{ASE}^{CH} measure accuracy, it was considered 40 non-modulated channels occupying 50 GHz and distributed uniformly along the C-band (192.1 to 160 THz). This distribution provides empty 50 GHz slots adjacent to each channel. This adjacent slot is reserved to P_{ASE}^{CH} estimations. G^{CH} is calculated using the input (P_{in}^{CH}) and output (P_{out}^{CH}) channel powers obtained from the input and output spectra, respectively, excluding P_{ASE}^{CH} at the output. These powers are illustrated in Figure 2.10(b).

The gain flatness (GF) is defined here as the difference in dB between the highest and lowest channel output powers, for a flat input spectrum, also illustrated in Figure 2.10(b).

Figure 2.11 presents the characterization results inside the power mask for worst noise figure among all channels (Figure 2.11(a)) and gain flatness (Figure 2.11(b)), for an EDFA with a maximum output power of 21 dBm, a minimum input power of -25 dBm, and a gain range from 14 to 24 dB.

Note that the characterization process outcome shown in Figure 2.11 provides valuable information for the amplifier adjustment. Additionally, this characterization process is very important for the Cognitive Methodology proposed in this work since it provides the amplifier models used during the methodology process.

2.3.4 Adaptive gain adjustment (AdGA)

Some local and global approaches for adaptive gain adjustments applied to optical amplifiers were proposed aiming to improve end-to-end system performance [25, 26, 27, 28, 29].

One of them is the adaptive gain adjustment (AdGA). It is a heuristic method described in [25] that adjusts the amplifier operating point automatically, in terms of

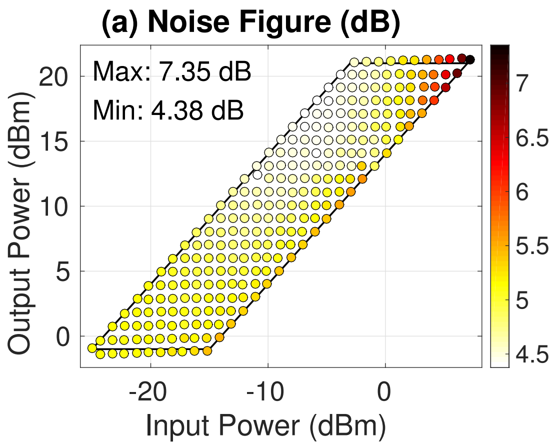

Figure 2.11: Amplifier characterization results for (a) noise figure and (b) gain flatness.

its set point gain, aiming to provide the best trade-off between its noise figure and gain flatness. It is essentially a local approach, not considering any overall performance to adjust the amplifiers. Although, it ends up improving end-to-end performances in terms of OSNR/BER as demonstrated in [25].

Figure 2.12(a) depicts a high-level AdGA flowchart, in which power mask information (PM Info) is a static database and refers to the experimental characterization process outcome described in Section 2.3.3. The AdGA process is composed of three steps: The "Pin Measurement" step monitors the amplifier total input power (Pin) and, when there is a change on its value, the "Gain Search" step queries PM Info for operating points with the same current Pin. These points are plotted in an objective space, illustrated in Figure 2.12(b), with noise figure and gain flatness as the axis (scaled from zero to one). Each point in the objective space refers to a gain value depicted in the right side color bar. Finally, the "Apply Gain" step selects a gain (indicated in Figure 2.12(b) with the minimum Euclidean distance from the origin), and applies it to the amplifier.

The AdGA impact over a cascaded of amplifiers was evaluated in terms of system gain flatness and noise figure, and received OSNR and BER [25], with additional adjustments considering weights applied to noise figure and gain flatness to guarantee BER performance. In [26], AdGA was applied in dynamic and meshed optical networks, together with RWA to improve the connections performance, demonstrating a blocking probability reduction when performance restrictions were considered. Additionally, a demonstration of the AdGA methodology as a primitive cognitive approach, considering the launch power impact on BER measurements, can be found in [103], maintaining

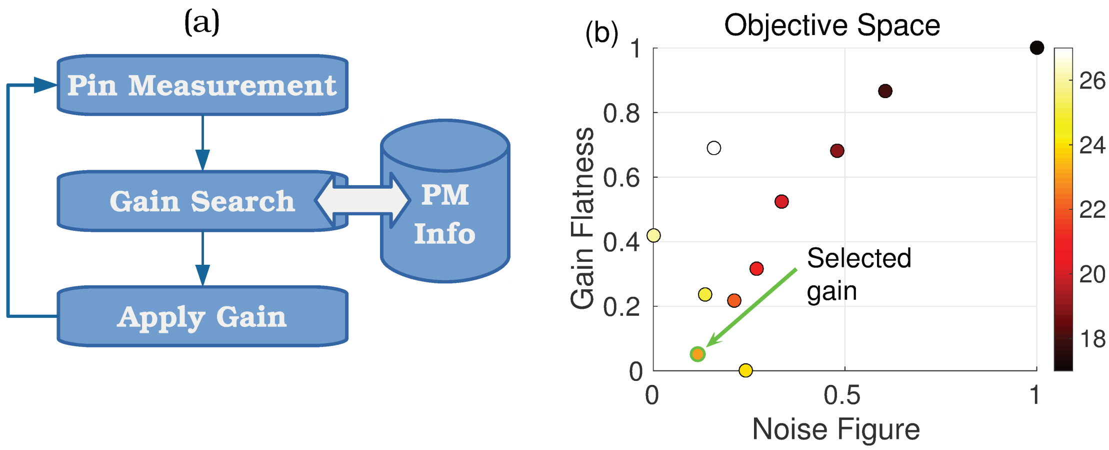

Figure 2.12: AdGA procedure: (a) flowchart and (b) objective space highlighting the selected gain applied to the amplifier [102].

suitable BER values for up to 6 dB of attenuation penalties in an experimental testbed with different modulation formats and bit-rates.

In this work, AdGA is applied in the same scenarios as the proposed Cognitive Methodology for comparison purposes.

2.3.5 *Automatic gain control versus gain adjustment*

Optical amplifiers are used to extend the transmission distances by compensating passive devices' losses. However, optical amplifiers, specially EDFAs, are mostly designed to operate in saturation regime [104]. In this condition, they present a strong gain dependency on the input power. Thus, it is important to control the amplifier gain so that it can remain unchanged with input power variations. Moreover, this gain control must also minimize undesirable output power oscillations caused by input power changes due to reconfigurations by adding or removing channels in dynamic network scenarios [104]. In other words, it is desirable that channels do not feel (in terms of gain/power change) the addition/removal of other channels.

There are different strategies to provide automatic gain control (AGC) for EDFAs. These strategies are based on all-optical, electrical or hybrid (optical/electrical) approaches. All-optical AGC employs optical feedback [105, 106, 107, 108], while electrical AGC applies electric feedfoward [109, 110], feedback [111, 112, 113] or both (feedfoward/feedback) [114, 115, 116] to control the pump laser. Hybrid (optical/electrial) AGC schemes are proposed to overcome the drawbacks of each independent scheme [104, 117, 118]. A detailed description about these AGC techniques can be found in [104]. Additionally, recent studies on EDFA gain control focus on SDM applications [119, 120], which is out of the scope of this work.

AGC schemes for DRAs are also proposed [121, 122, 123]. They employ an open loop control, since it is not possible to measure the total input power of a counter-propagating DRA.

For all cases, the main goal of the AGC techniques, besides to control the gain, is to provide fast response time to suppress output power transients.

In this work, it is important to distinguish these AGC techniques from methodologies that adjust the amplifiers' gain aiming to improve end-to-end performance (by finding the best setpoint gain), such as the Cognitive Methodology proposed in this thesis and the AdGA detailed in Section 2.3.4. These methodologies do not propose a new AGC, they use the amplifier internal AGC, which could be anyone, just to reconfigure the setpoint gain.

2.4 Case-based reasoning (CBR)

As already mentioned in the Introduction, there are different models for machine learning approaches, such as decision trees, neural networks, genetic algorithms and case-based reasoning [52]. In this work, it was considered the case-based reasoning (CBR) because it is relatively simple to implement and, different from genetic algorithms and neural networks, it does not require an explicit problem domain model [124].

CBR is a methodology for both reasoning and learning. It was already defined in the Introduction as a problem solver approach that uses old experience to understand and solve new problems. CBR is on peoples' day-to-day life, in simple tasks like cooking, driving or arguing in a conversation. In these tasks, people are always remembering previous situations and their consequences, and mostly adapting them to fit or to better handle the current situation they are facing. Thus, CBR can mean adapting old solutions to meet new demands; using old cases to explain new situations; using old cases to criticize new solutions; or reasoning from precedents to interpret a new situation (just as lawyers do) [53].

Still according to [53], there are four contributors to the case-based reasoner's solution quality:

- Experience: the second time solving some problem or doing some task is easier than the first time because people get experience, trying not to repeat the same mistakes. Thus, it is intuitive that the quantity of experience of a reasoner has, influence on the quality of its answers to new problems. Those experiences (cases) should include both successful and failed attempts at achieving those goals. Successful attempts will be used to propose solutions to new problems. Failed attempts will be used to warn for potential failures.

- Understanding: in CBR, it is important to understand new problems in terms of old ones. This process is performed by recalling old experiences and interpreting the new situation in terms of the recalled ones.

- Adaptation: adapting old solutions is needed because new problems may be different, or because the last solution did not succeed or just because it is an improvement attempt.

- Evaluation: the answers given by a reasoner must be evaluated to identify if they are good or bad. Thus, evaluation and consequent repair are important contributors to the expertise of a case-based reasoner.

Figure 2.13 presents the classic CBR cycle used for problem solving, composed of four steps: *retrieve*, *reuse*, *revise* and *retain*, referred as the "4 REs" [125]. Using this cycle, a new problem is solved by first obtaining the problem description and retrieving from the database (or memory) one or more similar cases to the new problem. It is the retrieve step, in which similarity assessment plays an important role. Then, the retrieved (similar) cases are used to propose a solution to the new problem in the reuse step. The proposed solution is commonly obtained after applying some adaptations on one or more similar cases. There are different adaptation methods depending on what is changed and how it is changed. Diverse adaptation methods are described in [125]. The proposed solution must be evaluated for success or fail in the revision step. This evaluation can be done by applying the solution and watching the consequences, or by simulation/modeling (before really applying it). Finally, the solution and its evaluation result (success/fail) are stored on the database in the retain step. As indicated in the figure, the database plays an important role on the CBR-cycle, by supporting it as a memory.

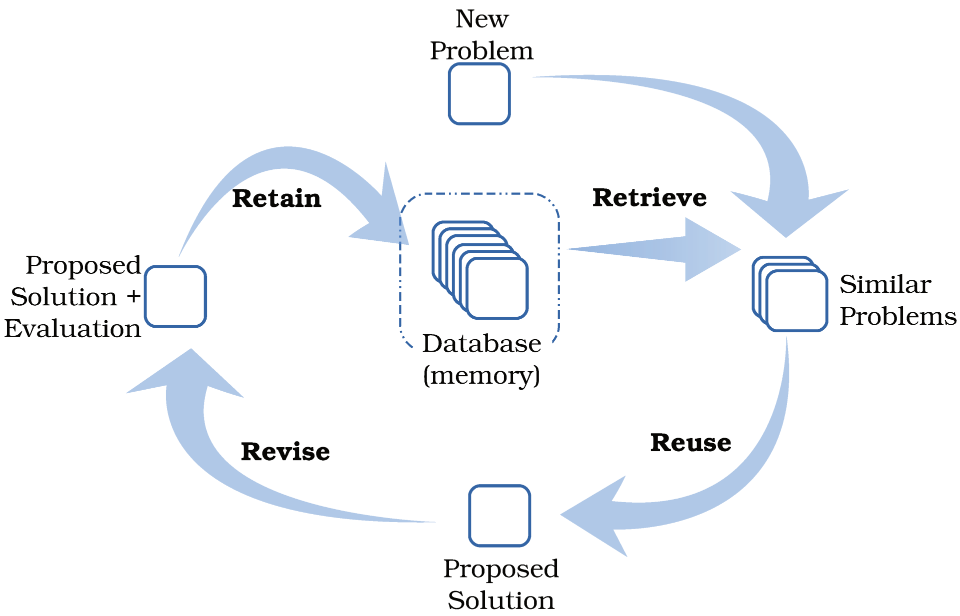

Figure 2.13: CBR cycle with the four steps: retrieve, reuse, revise and retain. Adapted from [52].

Some issues regarding CBR relies on the impact of database growth on retrieval costs. Concerns about how to perform an efficient recall for similar cases and how to remove redundant cases on database to improve the retrieval time have emerged. Improving retrieval performance through more effective approaches to similarity assessment and removal polices (exclude harmful cases from database, for example) for optimizing efficiency have been the focus of a considerable amount of research [125].

Finally, a summary of the main advantages and drawbacks regarding CBR is following detailed:

- CBR is intuitive and relatively simple to implement. However, it may require additional algorithms for searching and adapting the similar cases.
- CBR improves its solution over time, as the database grows. However, database growth has negative consequences, such as the large storage space needed and the large computational time required on the retrieve step.
- CBR reduces knowledge acquisition effort because database is created on-the-fly, while solving the problems. However, the database may not cover the solutions domain in a proper way.

Chapter 3

Cognitive Methodology

The Cognitive Methodology is a global process which can be applied during an RWA procedure in dynamic and meshed WDM optical networks. It aims to improve the connections OSNR performance by using past experience to change the amplifiers' setpoint gain along the lightpath. The cognition is achieved by employing case-based reasoning (CBR), a problem solver approach described in Section 2.4.

Section 3.1 describes the Cognitive Methodology, showing when and how it is applied. Concerns about the size of the database (used to store the old experience on the CBR process) and its consequences on the execution time appear as a drawback for the Cognitive Methodology. Thus, in Section 3.2, a modification aiming to overcome this issue is proposed.

3.1 Amplifier cognitive CBR (AcCBR)

As already mentioned, the Cognitive Methodology is applied in meshed and dynamic networks. In such scenarios, the network state in terms of number of connections and total power at each link changes along the time, also changing the total input power of the amplifiers. As already presented in Section 2.3.3, the amplifier performance in terms of noise figure and gain flatness presents a dependence on its operating point. Thus, these changes on the amplifier total input power can lead to a degradation of the signals passing through it.

As an example, suppose a signal passing through a cascade of three amplifiers. In this scenario, there are three possible ways to improve the signal performance by adjusting the amplifiers' operating points: the First one uses an exhaustive search, evaluating every possible gain combination for these three amplifiers and choosing the best combination. It is worth mentioning that this approach becomes more time consuming as the number of amplifiers increases, due to the high number of possible combinations. In addition, this approach also provides an optimal solution. The Second option considers the amplifier performance to adjust its setpoint gain. Note that the characterization process outcome, described in Section 2.3.3, provides valuable information for the amplifier adjustment aiming to improve its performance. Thus, it is possible to locally adjust each amplifier independently, improving its optical performance in terms of noise figure and gain flatness. In addition, this approach does not guarantee an optimal solution, since the individual optimization of the amplifiers does not imply the optimization of the cascade. However, it does allow a better computational time. Note that this approach is the AdGA, presented in Section 2.3.4. A Third option is a global approach, considering the performance of the entire amplifier cascade when adjusting the gain of the amplifiers, as the proposed alternatives in [27, 28, 29]. The Cognitive Methodology proposed in this work attempts to improve the signal performance by proposing a new gain combination for these three amplifiers, considering previous adjustments and their consequences on the signal performance.

Returning to the meshed and dynamic scenario, the Cognitive Methodology is applied every time the amplifiers total input power change, which occurs mainly when a connection is established or removed. The Cognitive Methodology is named *amplifier cognitive CBR (AcCBR)* because it accomplishes the CBR problem-solving cycle presented in Section 2.4. Thus, AcCBR will use the old connections performance to propose a new gain combination for the amplifiers along the lightpath.

These old connections' performances are stored on a database (DB), which is the key module of the AcCBR, acting as the memory of the CBR process. An example of a DB is presented in Table 3.1. The connection information stored on the DB, referred as cases, are separated into three groups: the features used to distinguish the cases, the proposed AcCBR solution and the performance obtained with the proposed solution.

Table 3.1: An example of an AcCBR DB with some connections (cases).

Features				Solution	Eval
#Link	#Amp	*Pin* (dBm)	αL (dB)	G (dB)	OSNR (dB)
1	[1]	[-25.0]	[8.5]	[25]	28.58
2	[1;2]	[-22.0;-22.0]	[7.8;21.1]	[24;23;14]	23.80
2	[2;1]	[-18.0;-20.2]	[15.5;6.0]	[18;14;22]	23.89
3	[1;1;2]	[-20.2;-22.0;-17.2]	[7.8;8.5;15.5]	[24;25;18;14]	22.59
3	[1;2;2]	[-16.0;-16.5;-19.0]	[10.2;26.8;17.3]	[26;24;19;19;14]	20.53
1	[1]	[-19.0]	[6.0]	[22]	28.38
2	[2;1]	[-18.0;-19.0]	[15.0;10.4]	[17;14;26]	23.95
2	[2;1]	[-16.5;-16.5]	[21.7;7.6]	[24;14;24]	23.97
1	[2]	[-17.2]	[15.5]	[18;14]	26.00
3	[1;1;2]	[-17.2;-22.0;-19.0]	[10.4;8.5;21.1]	[26;25;23;14]	22.56
2	[2;1]	[-19.0;-20.2]	[21.7;8.4]	[24;14;24]	23.94
3	[2;2;1]	[-15.5;-15.5;-16.0]	[15.3;11.5;7.6]	[17;14;14;14;24]	21.63
2	[1;1]	[-20.2;-17.2]	[8.5;7.8]	[25;24]	25.53
3	[2;1;1]	[-22.0;-20.2;-17.2]	[21.1;8.5;10.4]	[23;14;25;26]	22.58
2	[1;2]	[-17.2;-18.0]	[7.8;21.1]	[24;23;14]	23.88
1	[1]	[-14.6]	[7.6]	[24]	28.75
3	[1;1;2]	[-16.0;-19.0;-17.2]	[10.4;8.5;21.1]	[26;25;23;14]	22.61
2	[2;2]	[-20.2;-15.5]	[20.5;14.0]	[23;14;16;14]	22.78
3	[1;2;2]	[-13.5;-15.0;-14.2]	[10.2;15.5;15.3]	[26;17;14;17;14]	21.53
3	[2;1;2]	[-17.2;-15.0;-14.6]	[19.9;8.4;21.7]	[22;14;24;24;14]	21.80
1	[1]	[-15.0]	[7.8]	[25]	28.83
1	[2]	[-15.0]	[15.3]	[17;14]	25.68
2	[2;1]	[-15.5; -15.5]	[21.7; 8.4]	[24;14;24]	24.12

The first group is referred to as the connection *features* and corresponds to the first four columns in Table 3.1, which are the number of links (#Link), the number of amplifiers (#Amp) at each link, the total input power (Pin) at each link in dBm, and the total optical fiber loss at each link, αL in dB (where α is the fiber attenuation in dB/km and L is the total fiber length in km). These information are used by the AcCBR (as it will be further explained) to find similar cases on DB. They are distributed in vectors, each position corresponding to the values for each link. Thus, on the second line in Table 3.1, the connection presents two links, as indicated on the first column; #Amp = [1;2] indicates that there is 1 amplifier at the first link and 2 amplifiers at the second link; Pin = [-22.0;-22.0] (dBm) indicates that the total input power is -22 dBm for both links; and αL = [7.8;21.1] (dB) stands for a total optical fiber loss of 7.8 dB (first link) and 21.1 dB (second link).

The second group of connection information is named *solution* and corresponds to the proposed gain combination, illustrated at the fifth column in Table 3.1. These values are also distributed in a vector, following the order of amplifiers along the lightpath (LP). Thus, considering also the second line on Table 3.1, the gain vector [24;23;14] (dB) corresponds to the gain of the single amplifier on the first link as 24 dB, the gain of the first amplifier on the second link as 23 dB, and the gain of the second amplifier on the second link as 14 dB.

The last group is called *evaluation* (*eval* for short) and corresponds to the performance assessment of the proposed solution in terms of OSNR at channel reception (last column on Table 3.1).

Figure 3.1 presents the main flowchart detailing the sequence of steps to be performed by a centralized controller to handle an optical connection request. AcCBR is applied for each new connection request, after the RWA procedure, which is responsible to compute the LP by considering source and destination nodes and the available resources on the network, as discussed in Section 2.2. It returns the LP information in terms of *path* (P, set of nodes between source and destination) and the *wavelength* (λ) [126]. The RWA is considered as a black box in Figure 3.1. If RWA do not return a LP to establish the connection, either because there is no available resources or because of wavelength continuity constraints, the connection is blocked. Considerations about the RWA process will be detailed further up, when presenting the experimental and simulation assumptions in Chapters 4 and 5.

AcCBR applies the "4 REs" (REtrieve, REuse, REvise and REtain) of the CBR cycle presented in Section 2.4 and highlighted in Figure 3.1, considering the RWA outcome. It first considers that the new connection is already established, increasing the total input power along the links of the LP. Then, AcCBR accomplishes the *retrieve* step, by querying the DB for similar old connections. Depending on the DB size, the retrieve step can be the most time consuming during the whole process. Thus, it is important to use intelligent search algorithms and/or strategies to reduce the DB size and improve the execution time [126]. Similarity assessment considers the connection features in Table 3.1, represented as a vector ([#Link;#Amp;Pin;αL]). Thus, two cases will be considered similar if:

- the total number of links (or nodes) is the same for both cases;

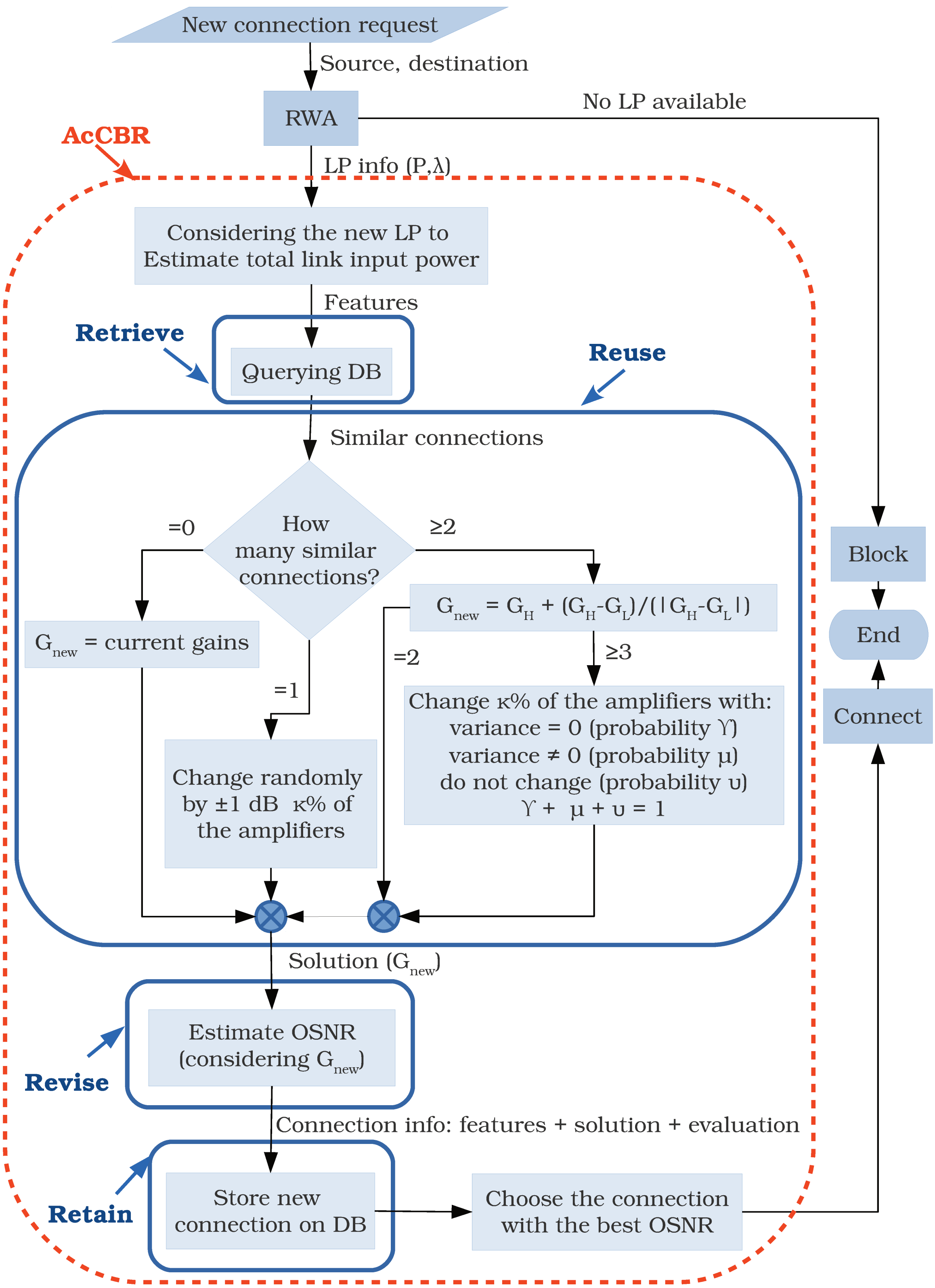

Figure 3.1: AcCBR complete flowchart incorporating the CBR cycle.

- the number of amplifiers for each link is the same for both cases;
- the total input power for each link (Pin) has difference of up to $\pm\beta^{Pin}$ dB and;

- the total optical fiber loss for each link (αL) has difference of up to $\pm\beta^{\alpha L}$ dB.

The *reuse* step on the CBR cycle proposes a new gain combination for the new LP. It comprises some routines, also depicted in Figure 3.1, depending on the number of similar cases on the retrieve outcome:

Routine 1 no similar case (= 0): AcCBR maintains the current gains along the LP;

Routine 2 one similar case (= 1): AcCBR randomly adjusts by ±1 dB the gain of κ% of the amplifiers along the LP of this single case, exploring future improvements;

Routine 3 two or more similar cases (≥ 2): AcCBR adjusts the gains following the Equation:

$$G_{new} = G_H + \frac{G_H - G_L}{\mid G_H - G_L \mid}, \tag{3.1}$$

where G_H and G_L are the gain vectors (as in Table 3.1) of the amplifiers along the LP with the higher and lower OSNRs, respectively. By doing so, G_{new} explores the direction of OSNR improvement provided by these two similar cases in the DB [7];

Routine 4 Three or more similar cases (≥ 3): after applying (3.1), AcCBR also randomly considers one of the following actions:

1. alter the gains of κ% (the same κ previously defined) amplifiers not modified until now in the set of similar LPs by ±1 dB with probability γ. These amplifiers whose gains were not modified until now present a null gain variance;
2. modify the gains of κ% amplifiers that have different gain values (non-null variance) in the set of similar LPs with probability μ and;
3. use the outcome of Equation 3.1 without any modification with probability υ;

with $\gamma + \mu + \upsilon = 1$ [7]. This combination of probabilities addresses the classical well-known exploration and exploitation trade-off in evolutionary algorithms [127].

Considering the new gain combination, AcCBR estimates the OSNR of the new connection at the end of the LP, performing the *revise* step on the CBR cycle. The OSNR estimation uses the following Equation [7]:

$$OSNR^{CH} = \frac{G^{CH,LP} Pin^{CH,LP}}{(G^{CH,LP} NF^{CH,LP} - 1) h\nu^{CH} \Delta\nu^{CH}} \tag{3.2}$$

where $G^{CH,LP}$ and $NF^{CH,LP}$ are the channel gain and noise figure along the LP, $P^{CH,LP}$ is the channel input power at the LP first link, h is the Planck's constant, ν^{CH} is the channel frequency and $\Delta\nu^{CH}$ is the optical bandwidth in which signal and noise were measured [7]. Equation 3.2 is derived in Appendix A.

After estimating the OSNR, AcCBR stores the new connection information (features, solution and evaluation) on the DB, even if it does not have a good OSNR performance, to help future decisions. This action corresponds to the *retain* step on the CBR cycle. The DB is created in this step, if it does not exist yet [7].

As the last actions, AcCBR chooses the gain combination on DB (considering similar cases + G_{new}) with the best OSNR and applies it on the amplifiers along the LP. Then, the connection is finally established.

Note that AcCBR can choose any similar case on DB. Thus, it is not possible to measure the performance of the proposed solution since it might not be applied. This reinforce the importance of the devices' modeling used on the OSNR estimation in Equation 3.2. They should be as realistic as possible.

As an example, suppose that, after applying the RWA to a new connection, it returns a LP with one link, two amplifiers, 21 dB of fiber loss; and a total input power of -10 dBm. Also suppose that these two amplifiers have a gain vector of [21,20] (dB). If there is no similar case on DB, AcCBR considers the current amplifiers' gain as G_{new} (routine 1 on the reuse step), estimates the OSNR, and stores these information on the DB presented on Table 3.2 (first line).

Table 3.2: Illustration of how AcCBR is applied considering the similar cases on DB.

Case	#Link	#Amp	Pin (dBm)	αL (dB)	G (dB)	OSNR (dB)	
1st	1	2	-10	20	[21,20]	27.87	Randomly changed
2nd	1	2	-10	20	[22,20]	28.33	
			$(G_H - G_L)/(\mid G_H - G_L \mid)$		[+1,0]		Applying Eq. 3.1
3rd	1	2	-10	20	[23,20]	28.73	
			$(G_H - G_L)/(\mid G_H - G_L \mid)$		[+1,0]		Applying Eq. 3.1
			variance		[1,0]		+ random change
4th	1	2	-10	20	[24,21]	28.52	

After some time, suppose that a new connection presents this same RWA solution in terms of LP features. Now, there is one similar case on the retrieve outcome (the one previously stored on the first line in Table 3.2). Thus, according to the routine 2 on the reuse step, AcCBR proposes a new gain combination by randomly changing by

± 1 dB the gain of a certain percentage of the amplifiers along the LP. As an example of this random procedure, the gain of the first amplifier is changed from 21 to 22 dB (+1 dB), while the second amplifier remains unchanged, as presented in the second line in Table 3.2. Then, AcCBR estimates the OSNR, stores the new connection information on DB, and apply the gain combination with the best OSNR, which corresponds to the second case (second line).

If the RWA procedure returns this same LP for other new connection for the third time, there would be two cases on DB. In this case, AcCBR applies Equation 3.1, as indicated on the routine 3 in reuse step. Note that randomly changing the first amplifier gain, from 21 to 22 dB (first to second lines in Table 3.2), leads to a better OSNR performance. Thus, as Equation 3.1 explores the direction of OSNR improvements, it results in an increase of the first amplifier gain from 22 to 23 dB. The third line in Table 3.2 presents the gain variation given by the second term in Equation 3.1, that is summed to the gain vector on the second line (which corresponds to the gain with the best OSNR: G_H). Applying Equation 3.1 also results in a better OSNR obtained on the revise step, as presented in the fourth line in Table 3.2. Thus, after storing this new connection on the DB, AcCBR chooses this new gain combination to be applied on the new LP since it presents the best OSNR performance.

Finally, considering a LP with these same characteristics being proposed by the RWA for the fourth time, AcCBR would retrieve three similar cases on DB. In this situation, besides applying Equation 3.1, which changes the first amplifier gain from 23 to 24 dB (as indicated on the fifth line in Table 3.2), AcCBR applies additional random changes, as described on the routine 4 of the reuse step. These random changes consider the gain variance along the similar cases. The sixth line in Table 3.2 shows the gain variance for both amplifiers. In this case, AcCBR adds 1 dB to the second amplifier gain, which presents a null variance, resulting in a gain change from 20 to 21 dB. This solution is then evaluated on the revise step, resulting in an OSNR degradation. Thus, after storing the new connection on DB, AcCBR considers the gain combination of the third case, which presents the best OSNR performance, to be applied to the LP.

For simplification, the cases on the Table 3.2 present links with fixed fiber losses and total input power. However, similar cases can have $Pin \pm \beta^{Pin}$ dBm and $L \pm \beta^{L}$ dB, in which Pin and αL are associated to the new LP.

3.2 Fast AcCBR (fAcCBR)

One factor that influences the quality of the solutions provided by a CBR scheme is its experience [53]. In AcCBR, the experience is associated to the DB size. As it will be seen on the results presented in Chapters 5 and 4, the OSNR improves when the DB size increases for most evaluated scenarios, indicating that the experience plays an important role in the Cognitive Methodology performance. However, this performance improvement has a drawback: the execution time also increases with the DB size because, for larger DB sizes, it takes longer to find similar cases on the retrieve step [126].

To better illustrate this issue, suppose a network with fixed link features, i.e, the same number of amplifiers and fiber losses, as illustrated in Figure 3.2(a). In this scenario, LPs are combinations of the same links, differing from each other only in terms of total link input power. Now consider three similar cases LP_{1-3} (also illustrated in Figure 3.2(a)) already stored on the DB in Figure 3.2(b). For simplification, these LPs present exactly the same total input power (Pin) and fiber loss (αL) per link, even though these values can vary by $\pm\beta^{Pin}$ dB and $\pm\beta^{\alpha L}$ dB, respectively. Then, when a new connection using LP_{new} (similar to LP_{1-3}) appears, AcCBR will find three similar cases on DB.

On the other hand, suppose a more realistic network, where links present different number of amplifiers and total fiber losses, as illustrated in Figure 3.2(c). In this scenario, even with the same total input power per link, the connections LP_{1-3} (also in Figure 3.2(c) and (d)) present different features and cannot be considered as similar cases. Thus, the new connection using LP_{new} (last line in Figure 3.2(d)) will not find similar cases when applying AcCBR.

As it can been seen from the previous example, it is harder to find similar cases on more realistic networks, specially for LPs with high number of links due to the high number of possible combinations. Moreover, the cognitive effect (improvement with time due to learning process) of the AcCBR is just verified when it finds at least two cases on the DB and apply Equation 3.1. Thus, a network with different link characteristics requires a larger DB size to cover for LP diversity and to be able to provide new solutions based on similar cases. This large DB is a drawback for the Cognitive Methodology since it increases the computation time of the retrieve step and the storage resources.

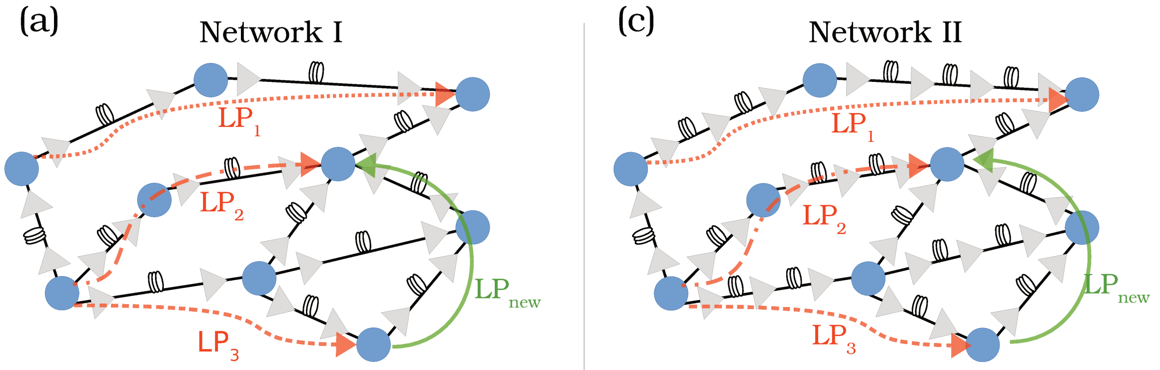

(b)	#Links	#Amps	Pin (dBm)	Fo_{loss} (dB)
LP_1	2	2,2	-10,-10	-20,-20
LP_2	2	2,2	-10,-10	-20,-20
LP_3	2	2,2	-10,-10	-20,-20
LP_{new}	2	2,2	-10,-10	-20,-20

Similar to LP_{new}

(d)	#Links	#Amps	Pin (dBm)	Fo_{loss} (dB)
LP_1	2	3,4	-10,-10	-31,-38
LP_2	2	2,3	-10,-10	-18,-29
LP_3	2	3,2	-10,-10	-32,-21
LP_{new}	2	2,2	-10,-10	-23,-17

Not similar to LP_{new}

Figure 3.2: (a) Networks with the same link features with some LPs, (b) features of the LPs presented on network I, (c) Networks with different link features with some LPs, and (d) features of the LPs presented on network II.

Improving retrieval performance through more effective approaches for similarity assessment has been the focus of a considerable amount of research [125]. Alternatives to improve retrieval time include the use of massively parallel computing [128], better organization of cases in DB [129], and exploring statistical methods [130].

However, in this work, the retrieval time improvement has been performed by wisely reducing the cases on database. The results obtained in [131] for networks with different link characteristics present ONSR improvements when applying AcCBR for most cases, even for LPs with a high number of links. However, analyzing the number of similar cases obtained on the retrieve step for these LPs (with a high number of links), there are few similar cases (mostly zero), indicating that not all steps of the Cognitive Methodology were applied, staying mostly on routines 1 and 2 on the reuse step.

The OSNR improvement for these LPs, even not completely applying AcCBR, may occur when AcCBR optimizes LPs with a few number of links. In these situations, AcCBR might end up also optimizing LPs with higher number of links, since there are shared links between these LPs. Figure 3.3 illustrates this situation, in which the optimization of LPs with single links (LP_1 to LP_3) could also optimize LP_4, which is composed of the three links in LP_1 to LP_3.

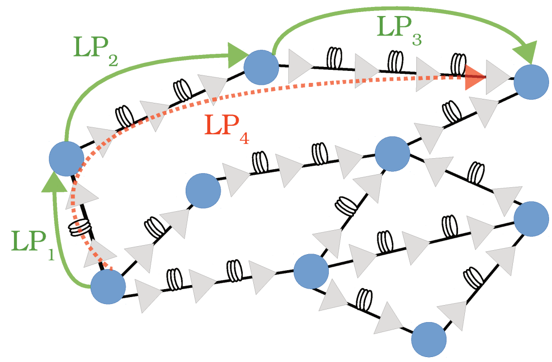

Figure 3.3: Networks with different link features showing some LPs examples.

Thus, it is worth to analyze the application of the Cognitive Methodology just for LPs with a few number of links (as LP_1 to LP_3), since the higher links LPs will be a combination of these optimized few links LPs. Moreover, the DB size can be significantly reduced, since few links LPs have a small number of possible combinations.

This modification on the Cognitive Methodology is denoted by *fast AcCBR-maximum link n (fAcCBR-MLn)* and refers to applying AcCBR just for LPs with up to n links. By doing so, fAcCBR attempts to improve also LPs with higher number of links, and reduces the execution time during the retrieve step due to a smaller DB. However, it is important that the fAcCBR does not degrade the optical performance in terms of OSNR compared with the original AcCBR [126].

A high level flowchart for fAcCBR, abstracting the AcCBR process (already presented in Figure 3.1), is depicted in Figure 3.4. It consists of the same steps already detailed for the original AcCBR, just adding the condition about the number of links on the LP information on the RWA outcome. If this value is higher than n, AcCBR is not applied and the connection is established with the current amplifier gains. If lower or equal to n, AcCBR is normally applied before establishing the connection.

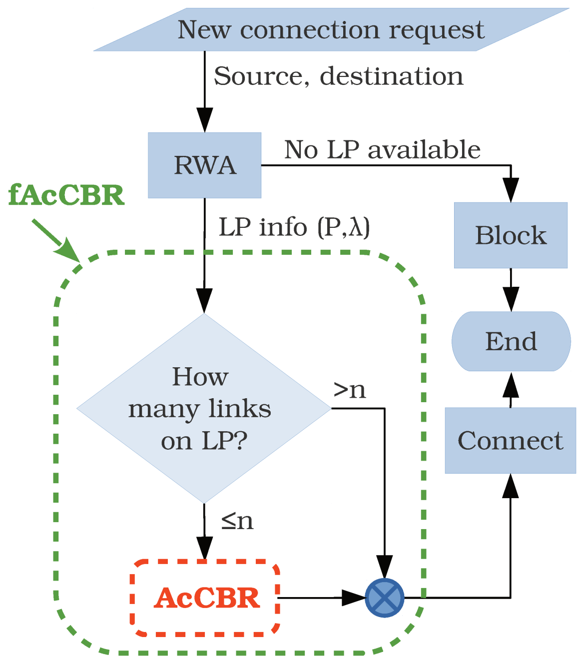

Figure 3.4: fAcCBR high level flowchart.

Chapter 4

Testbed results[1]

The Cognitive Methodology is experimentally validated in a meshed five-node network testbed. Additionally, simulated and experimental results are compared with assess the devices' modeling assumed during the OSNR estimation on the reuse step. This Chapter is divided into the following Sections: Section 4.1 describes the validation environment regarding the experimental network (Section 4.1.1), the modeling of the network devices (Section 4.1.2), and the RWA and traffic generation assumptions (Section 4.1.3); Section 4.2 shows the preliminary simulations performed to serve as a reference to the experiments; Section 4.3 presents the network experimental validation, considering the proposed Cognitive Methodology; and Section 4.4 reviews the results and presents partial conclusions.

[1]This Chapter is based on the following papers published by the author: U. Moura et al.,"SDN-enabled EDFA gain adjustment cognitive methodology for dynamic optical networks," 2015 European Conference on Optical Communication (ECOC), Valencia, 2015, pp. 1-3; and U. Moura et al., "Cognitive Methodology for Optical Amplifier Gain Adjustment in Dynamic DWDM Networks," Journal of Lightwave Technology, vol. 34, pp. 1971-1979, April 2016.

4.1 General assumptions

4.1.1 Autonomous Network (AN)

The experimental validation considers the Autonomous Network (AN) testbed depicted in Figure 4.1(a). The AN is a five-node metropolitan optical network located at CPqD Foundation[2]. It is pioneer in software modeling of hardware equipment to propose adaptive and cognitive algorithms and in performing experimental demonstrations [132].

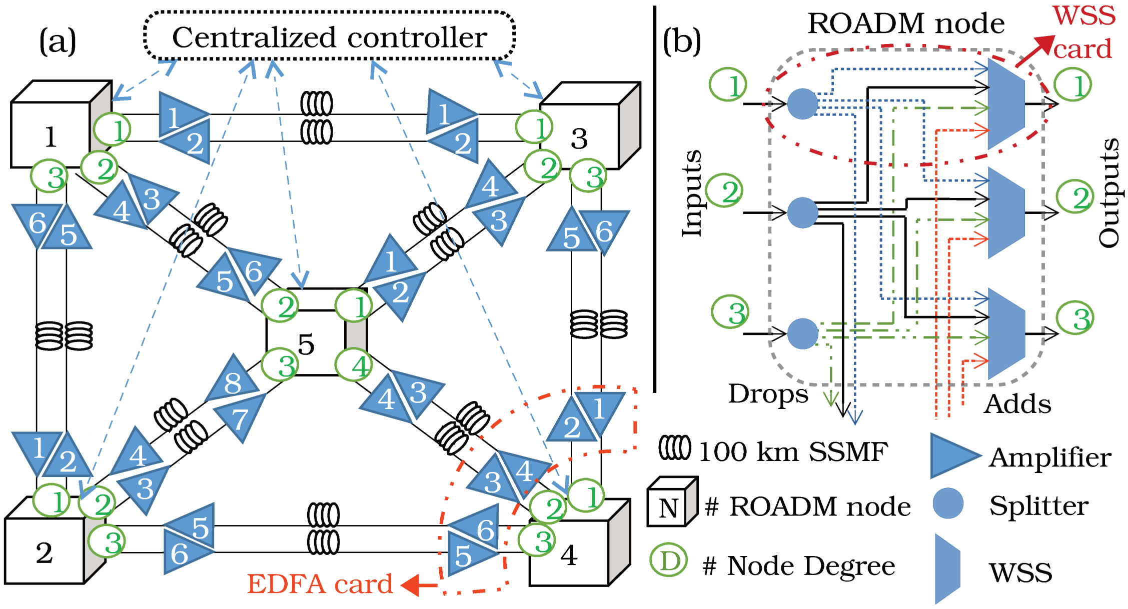

Figure 4.1: Autonomous Network (AN) (a) topology and (b) broadcast-and-select (B&S) ROADM of degree three used at AN. Adapted from [132, 133].

AN consists of four ROADM nodes of degree three and a central ROADM node of degree four. The node degree is defined as the cardinality of its neighboring nodes [134]. These five ROADM nodes are interconnected through bidirectional links composed of SSMF 100-km spans, forming the directed graph illustrated in Figure 4.1(a) with a high density (D = 0.8) [132]. The density of a directed graph $G(V, E)$, where V is the set of vertices (nodes) and E is the set of edges (twice the number of bidirectional links), is defined as the current number of edges divided by the total possible number of edges: $D = \mid E \mid / (\mid V \mid (\mid V \mid -1))$, $D \in (0, 1]$ [134]. Density indicates the graph connectivity, measuring how close a graph is to its corresponding complete graph [7].

Each ROADM node is based on a broadcast-and-select (B&S) structure, illus-

[2]http://www.cpqd.com/

trated in Figure 4.1(b) for a three-degree B&S ROADM node. It is implemented using splitters at each input. These splitters are full-connected with three WSSs at each output, used to filter undesired lightpaths. Add and drop ports are directly accessed between splitters and WSSs. Thus, the ROADMs are not directionless-enabled [132]. A directionless ROADM is able to access any direction at any add/drop port.

AN physical infrastructure[3] is depicted in Figure 4.2 and it is distributed along four racks. From left to right, the first containing the nodes one and two and optical fiber coils; the second containing just the node five; the third containing nodes three and four and more optical fiber coils [132]. The fourth rack is responsible for optical spectrum analysis of the results from each one of the sixteen drop ports. These ports are connected to the OSA by a 16x1 optical switch responsible to choose the drop port to be observed at the OSA.

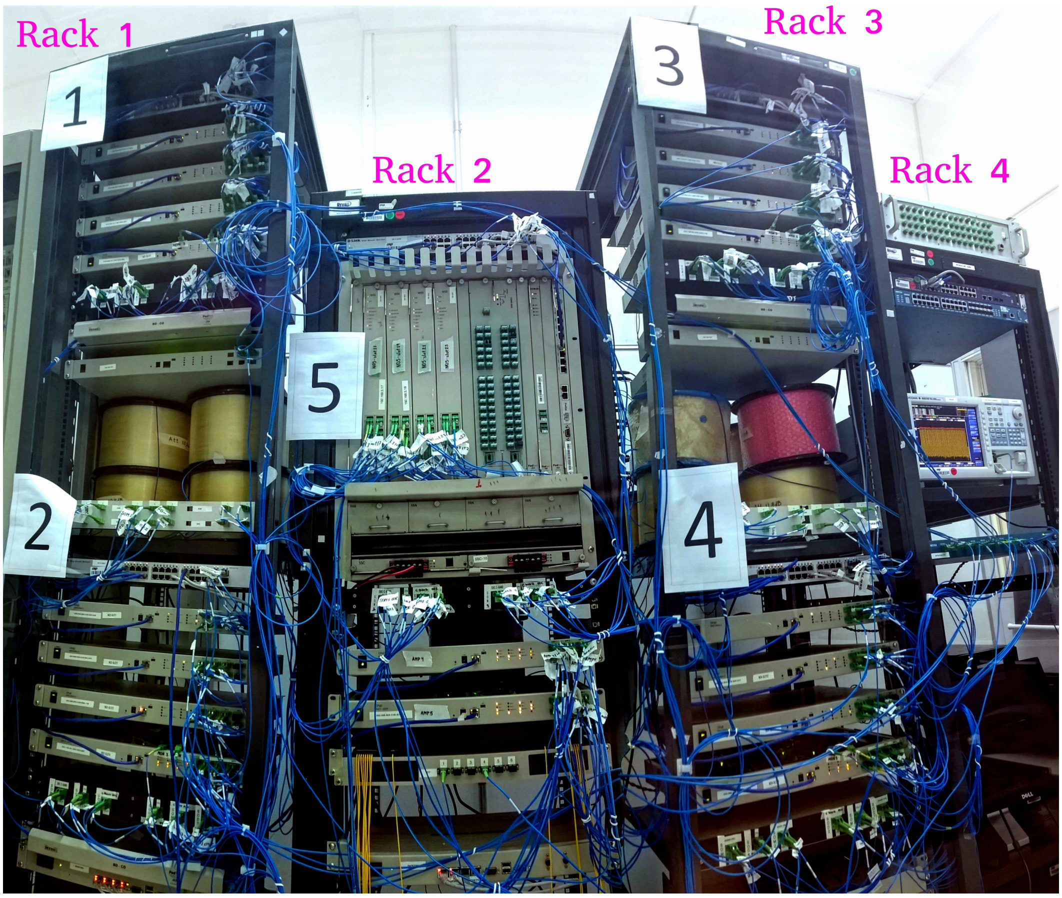

Figure 4.2: Laboratorial setup for the AN.

[3]The AN setup was assembled by the Transmission team, inside the Optical Technologies Division at CPqD Foundation, composed by Heitor Carvalho, Matheus Svolenski, Alexandre Andrade, and Matheus Magalhães under the leadership of Miquel Garrich and Juliano Oliveira. Experiments accomplished in this setup led to several publications, such as [132, 135, 136, 137, 138, 139, 140, 141, 142, 143, 144, 145, 146, 147].

The nodes are composed of the following devices: nodes one to four have three WSS cards (highlighted in Figure 4.1(b)) where each one contains the devices of an ROADM degree, such as splitter, WSS, photodiodes for monitoring, etc (Figure 4.1(b) is a simplification). These WSSs are based on Liquid Crystal on Silicon (LCoS) technology and are able to apply attenuations at each 12.5 GHz slot independently. Nodes one to four also have an EDFA card (highlighted in Figure 4.1(a) for node 4) containing six single stage EDFAs (with a maximum output power of 21 dBm) corresponding to one per degree and per direction. Node five has four WSS cards, based on legacy microelectromechanical system (MEMS) technology with 50-GHz fixed-grid switching capability (also able to provide independent attenuations), and two EDFA cards each one containing 4 amplifiers (i.e., 8 EDFAs corresponding to one per degree and per direction) [132].

The communication from/to the centralized controller to/from the network devices is performed through the node five, which is directly connected to the centralized controller via an Ethernet cable. From node five, inter-node control communications use an Ethernet switch placed at each node, by means of an optical supervisory channel (OSC) at 1510 nm (out of EDFA band). This OSC is multiplexed by a supervisory optical multiplexer (SOM) card placed at the egress of the node just after each EDFA output port. Similarly, the OSC is demultiplexed by a supervisory optical demultiplexer (SOD) card placed at the arrival of the node just before each EDFA input port [132].

In AN, the transmission employs 40 continuous-wave lasers (ITU-T WDM grid from C21 to C60), 100 GHz spaced, modulated by four multiplexed lines of 32 Gb/s (PRBS $2^{31} - 1$) that generate 128 Gb/s DP-QPSK coherent channels. Channels occupy 50 GHz alternate slots in the spectrum enabling proper OSNR measurements considering the adjacent channel reserved for noise. These OSNR measurements are performed to compare simulation and experimental results. Since AcCBR estimates the OSNR (as described in Section 3.1), this allows operators to use full loaded 80 channels in real applications. A 1x16 splitter is used after the transmitter setup in order to feed the sixteen add ports of the network. The input power per channel at the first amplifier of each link is set to -25 dBm using the WSSs attenuation capability. Thus, it is possible to establish a connection between any two nodes in the network [7].

4.1.2 Devices' modeling

As described in Section 3.1, the revise step on the Cognitive Methodology performs an analytical estimation (and not a measurement) of the lightpath quality, because the proposed solution (G_{new}) cannot be applied until the end of the AcCBR process. At this point, AcCBR selects the best gain combination in DB that may not correspond to G_{new}. This OSNR estimation must assume models for the network devices, such as optical fibers, optical amplifiers and ROADM nodes [7]. Therefore, the devices' modeling is important not only for the simulations performed in this work, but also for the Cognitive Methodology itself.

In this work, the network devices are modeled considering the following restrictions:

- The optical fiber assumes fixed attenuation independent to channel, considering an SSMF with an attenuation of 0.2 dB/km;
- The ROADM nodes consider an attenuation per channel, dynamically adjusted by the output WSSs to equalize the channels power level at the input of the first amplifier on the next link. The WSS insertion loss considered in this work is 16 dB for pass (splitter + WSS) and 9 dB (just splitter) for drop (see Figure 4.1(b));
- The optical amplifier is based on the characterization (Section 2.3.3) outcome. It considers the noise figure dependence on operating point, but not on the channel frequency. Thus, all channels present the same noise figure for a given operating point, which corresponds to the worst noise figure along the channels, as presented in Figure 2.11(a). It also considers the gain dependence on channel, in order to simulate the accumulated tilt effect along a cascade of amplifiers. This information is obtained on the characterization process, being used to plot the gain flatness graph presented in Figure 2.11(b).

Regarding the optical amplifier, the noise figure assumption may cause discrepancies between simulation and experimental OSNRs due to noise figure variations higher than 1 dB across the C band. However, it can be negligible in this first approach since the current focus is to evaluate if the AcCBR methodology will properly work considering a simplified environment. Although, even not considering the noise figure dependence on channel, OSNR estimations using Equation 3.2 are consistent with the experimental OSNR measurements presented in Section 4.3 [7].

Three amplifier models were considered in this Chapter. Their power masks, with noise figure and gain flatness performances, were obtained by the experimental process described in Section 2.3.3, and are presented in Figure 4.3. Their characteristics are following detailed:

- Model 1: it is an EDFA prototype with a 14-m EDF stage, co-propagating pump power up to 600 mW at 980 nm, and no GFF. Its minimum total input power is - 25 dBm, maximum total output power is + 21 dBm, and the gain varies from 14 to 24 dB. Its noise figure and gain flatness dependencies on operating point are presented in Figure 4.3(a) and (b), respectively, considering a granularity of 0.5 dB. Model 1 is the model used on the AN;

- Model 2: it is a commercial EDFA with one stage of EDF and up to 300 mW of pump power at 980 nm in a co-propagating configuration. Its minimum total input power is - 30 dBm, maximum total output power is + 14 dBm, and the gain varies from 14 to 24 dB. Its noise figure and gain flatness dependencies on operating point are presented in Figure 4.3(c) and (d), respectively, considering a granularity of 1 dB. Its internal optical circuit is unknown in terms of EDF length and GFF presence. Although, low gain flatness values around the 19 dB gain-diagonal indicate the GFF presence (see Figure 4.3(d));

- Model 3: it is also a commercial EDFA with one stage of EDF but with up to 600 mW of pump power at 980 nm in a co-propagating configuration. Its minimum total input power is - 25 dBm, maximum total output power is + 21 dBm, and the gain varies from 14 to 24 dB. Its noise figure and gain flatness dependencies on operating point are presented in Figure 4.3(e) and (f), respectively, considering a granularity of 1 dB. Its internal optical circuit is also unknown in terms of EDF length and GFF presence. Again, it is possible to infer the GFF presence by the low gain flatness values around the 19 dB gain-diagonal, observed in Figure 4.3(f);

Furthermore, considerations of non-linear effects are outside the scope of this work. However, the most powerful channel at the input of all optical fibers does not surpass 0 dBm to avoid nonlinearities [148].

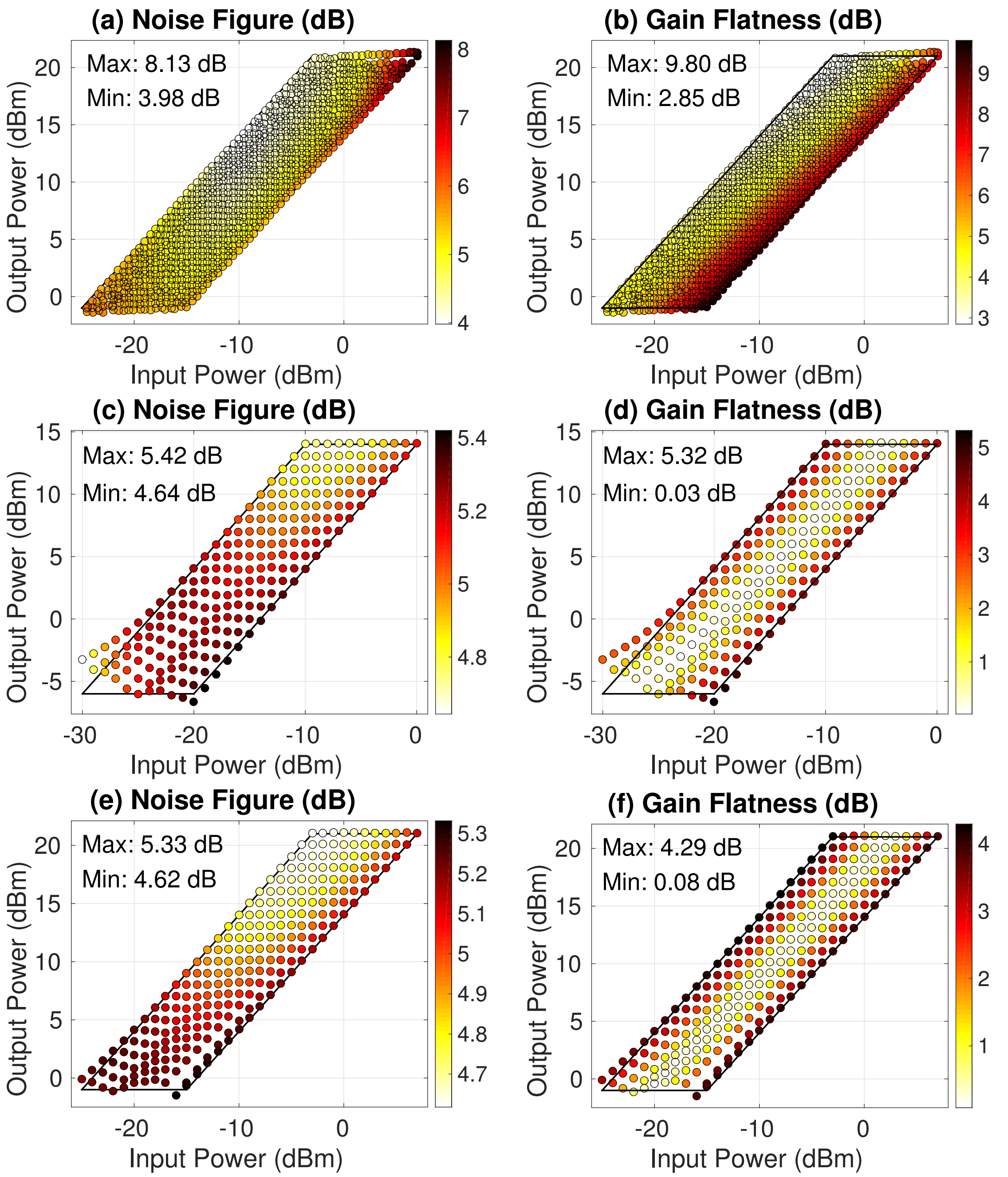

Figure 4.3: Optical amplifier performance dependence with the amplifier operating point for amplifier model 1: (a) noise figure and (b) gain flatness; mode 2 (c) noise figure and (d) gain flatness; and model 3: (e) noise figure and (f) gain flatness; obtained experimentally using the characterization process described in Section 2.3.3.

4.1.3 RWA and traffic generation

As already mentioned in Chapter 3, the Cognitive Methodology is designed to be applied together with the RWA, so that every time a new connection is established, causing changes on the amplifiers total input power, it is possible to adjust their operating point based on end-to-end performances [7].

Thus, in this Chapter, the Cognitive Methodology is applied when solving an RWA problem considering a classical optical circuit-switched network, with ad hoc dynamic demand and traffic generated according to a Poisson process, with connections arrival time and duration modeled by a negative exponential distribution (see Appendix B). They consider 1,000 unidirectional connections (Simplex) and 500 erlang of traffic load, in a transparent optical network, with wavelength continuity constraint, i.e., the lightpath must have the same wavelength available in all links. As in AN, 40 channels at C band, 100 GHz spaced, are considered to establish the connections. Additionally, there is no grooming. Thus, every new connection uses a new channel, even if some existing channel has available band to support this new connection. Dijkstra is applied on the route subproblem to find the path with the lowest cost. It considers the total loss and the number of wavelength used as the link cost. The last consideration aims to better distribute the connections inside the network. Moreover, first-fit is considered to wavelength assignment subproblem [133].

4.2 Preliminary simulations

To serve as reference for the experiments, simulations developed in Matlab® were performed considering the AN topology and the general assumptions presented in Section 4.1. In these simulations, two sets of amplifier models for the first and second amplifiers on each link have been considered. The first set, referred as B21/P14, considers the booster amplifier model 3 placed just before the optical fiber and a pre-amplifier model 2, placed after the optical fiber. The second set is referred as B21/B21, and considers that all amplifiers in the network (before and after the optical fibers) are booster amplifiers model 1. These models are detailed in Section 4.1.2. The last set of amplifiers stands for the AN and will be used to compare with the experimental results.

In these simulations, the performance of the Cognitive Methodology is compared with two amplifier gain conditions: fixed gain (FG) and AdGA. In FG, the amplifiers' gains are set to compensate fiber and ROADM losses and remain unchanged during all the simulation/experiment. AdGA acts as presented in Section 2.3.4. For AcCBR methodology, the DB starts empty and increases along the time, reaching 75 KBytes at the end of the simulations. For AcCBR and AdGA, the network is set as in FG condition at the beginning of the simulations. Thus, for the initial connections, when there is no similar case in DB and AcCBR considers the current gains, it is applying the gains as in FG. Thus, FG condition can be seen as a initial state for AcCBR [7]. Furthermore, for the reuse step, AcCBR considers the probabilistic parameters' values as $\kappa = 50\%$, $\beta^{Pin} = 0.5$ dB, and $\beta^{\alpha L} = 1$ dB; and the exploration and exploitation parameters' values as $\gamma = 0.5$, $\mu = 0.1$, and $\upsilon = 0.4$.

Figure 4.4 shows the simulation OSNR (mean and standard deviation) results for all the connections presented at the AN as a function of the connection start time. Figure 4.4(a) stands for B21/P14 set, while Figure 4.4(b) stands for B21/B21. Upper graphs in Figure 4.4 are for lightpath (LP) with one link and bottom graphs for LP with two links. Upper graphs in Figure 4.4 also show the number of total connections (# connec) present in AN, which is the same for both sets of amplifier models since they consider the same traffic [7].

For B21/P14, Figure 4.4(a) shows that OSNRs in FG condition remain almost constant along all simulation for LPs with 1 link, with values around 24 dB, and presenting a little degradation at the beginning of the simulations for LPs with 2 links, but improving to values higher than 20 dB. AdGA presents the worst OSNR values, with some OSNR degradation at the beginning of the simulation, followed by an OSNR improvement, achieving values lower than 23 dB and 20 dB for 1 and 2 links/LP, respectively. AcCBR, on the other hand, presents the best OSNR results, with an increase of OSNR values at the beginning of the simulation, due to the learning process, and achieving around 24.5 dB for LPs with 1 link. For LPs with 2 links, AcCBR presents the same behavior as FG at the beginning of the simulations, i.e., presenting a small degradation at around 5 s. However, as the time increase and so the DB, AcCBR obtains more experience and starts to present an OSNR improvement with the time, achieving values near 21 dB.

For B21/B21 models, FG presents the same OSNR behavior as in B21/P14 for LPs with 1 link, with an almost constant OSNR value of 24 dB, as shown in Figure 4.4(b). For LPs with 2 links, it presents a considerable OSNR degradation when the time increase, followed by an increase of the standard deviation. Recall that, in FG condition, the gains are set to compensate exactly fiber span and ROADM-node losses. If the amplifiers have a high gain tilt, as the amplifier model 1 (see Figure 4.3(b)), some channels will have a smaller gain, being attenuated when passing from one link to the other. Thus, for LPs

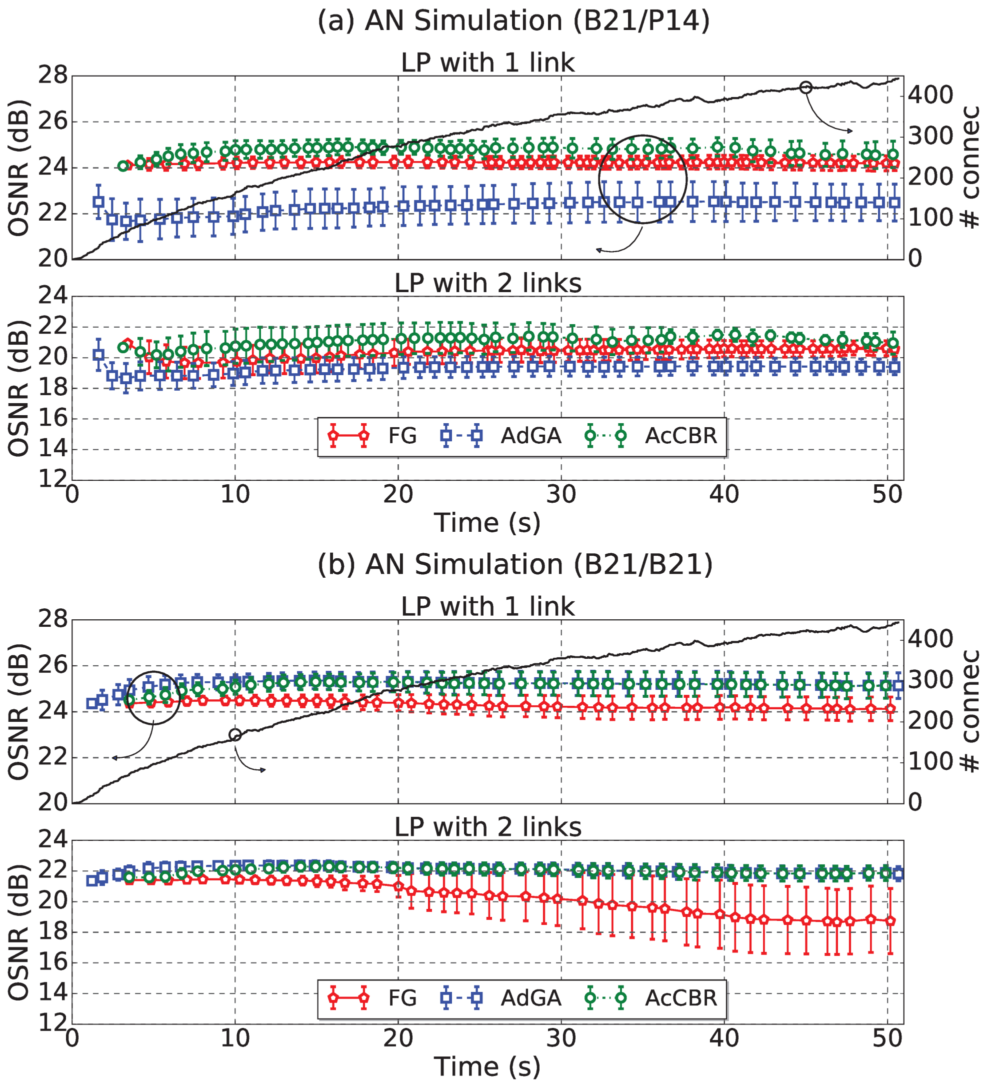

Figure 4.4: AN simulation results for (a) B21/P14 and (b) B21/B21. For AcCBR: $\kappa = 50\%$, $\beta^{Pin} = 0.5$ dB, $\beta^{\alpha L} = 1$ dB, $\gamma = 0.5$, $\mu = 0.1$, and $\upsilon = 0.4$. Adapted from [7, 133].

with 2 links, in FG condition, it is expected a higher degradation. Note that the higher standard deviation is due to the high differences in gain along the channels, leading to different levels of degradation.

Still in Figure 4.4(b), AdGA presents the opposite behavior observed in B21/P14. It increases the OSNRs at the beginning of the simulation from around 24 to around 25 dB for LPs with 1 link, and from near 21 to values around 22 dB, for 2 links/LP. These different OSNR behaviors between B21/P14 and B21/B21 show that AdGA performance depends on the amplifiers models used in the network.

Finally, AcCBR, as in B21/P14, presents OSNR improvements from near 24 to 25 dB for LPs with 1 link, and from 21 to around 22 for LPs with 2 links, as can be seen in Figure 4.4(b). These final values are higher than the values achieved in B21/P14, maybe because of the smallest minimum noise figure for amplifier model 1, used on the B21/B21 set, compared with models 2 and 3, used on the B21/P14 set.

4.3 Experiments

The experiments, performed at the AN to validate the simulation results for the amplifier models B21/B21, consist of taking a snapshot near 50 s in Figure 4.4(b) considering all the connections present in the network and the amplifier gains for the three amplifier gain conditions (FG, AdGA and AcCBR). Then, the OSNRs were experimentally measured for all sixteen-drop ports and compared with the simulation results presented in Figure 4.4(b) [7]. These experiments were held with the support of the Transmission team[4], at the CPqD Foundation.

Figure 4.5 shows the comparison between simulation and experimental OSNR results for FG, AdGA and AcCBR (subfigures (a), (b) and (c), respectively) for all channels dropped at node 1 and port drop degree 1. The channels from LPs with one link (high OSNRs) and two links (low OSNRs) are easy to identify. Moreover, the best performance for AdGA and AcCBR compared with FG is also verified.

The experimental spectra associated to the OSNRs are shown at the bottom of each graph in Figure 4.5. Note that the splitter stage in the passive B&S ROADM structure (Figure 4.1(b)) provides multiple copies of the input signals for selective filtering at the WSS stage, thus bypassing channels appear at the drop port (spectra plots) but not in the OSNR plots (dropped channels) [7].

Table 4.1 summarizes the experimental results showing OSNR mean and standard deviation ($\pm\delta$) at all drop ports for each gain condition. Mean OSNR values in FG condition also presents the worst result, with a degradation of around 4 dB (for LPs with 2 links) in mean OSNR when comparing with AcCBR [7]. AdGA and AcCBR present the same OSNR performance, as observed on Figure 4.4(b), for OSNR values near 50 s.

These OSNR comparisons between simulation and experiment validate the simulation tool in terms of devices' modeling and OSNR estimation for all network nodes. Moreover, it is worth mentioning that, although AcCBR is applied during the connections establishment, considering just the OSNRs of the new connections, there are im-

[4]Heitor Carvalho, Matheus Svolenski, and Alexandre Andrade.

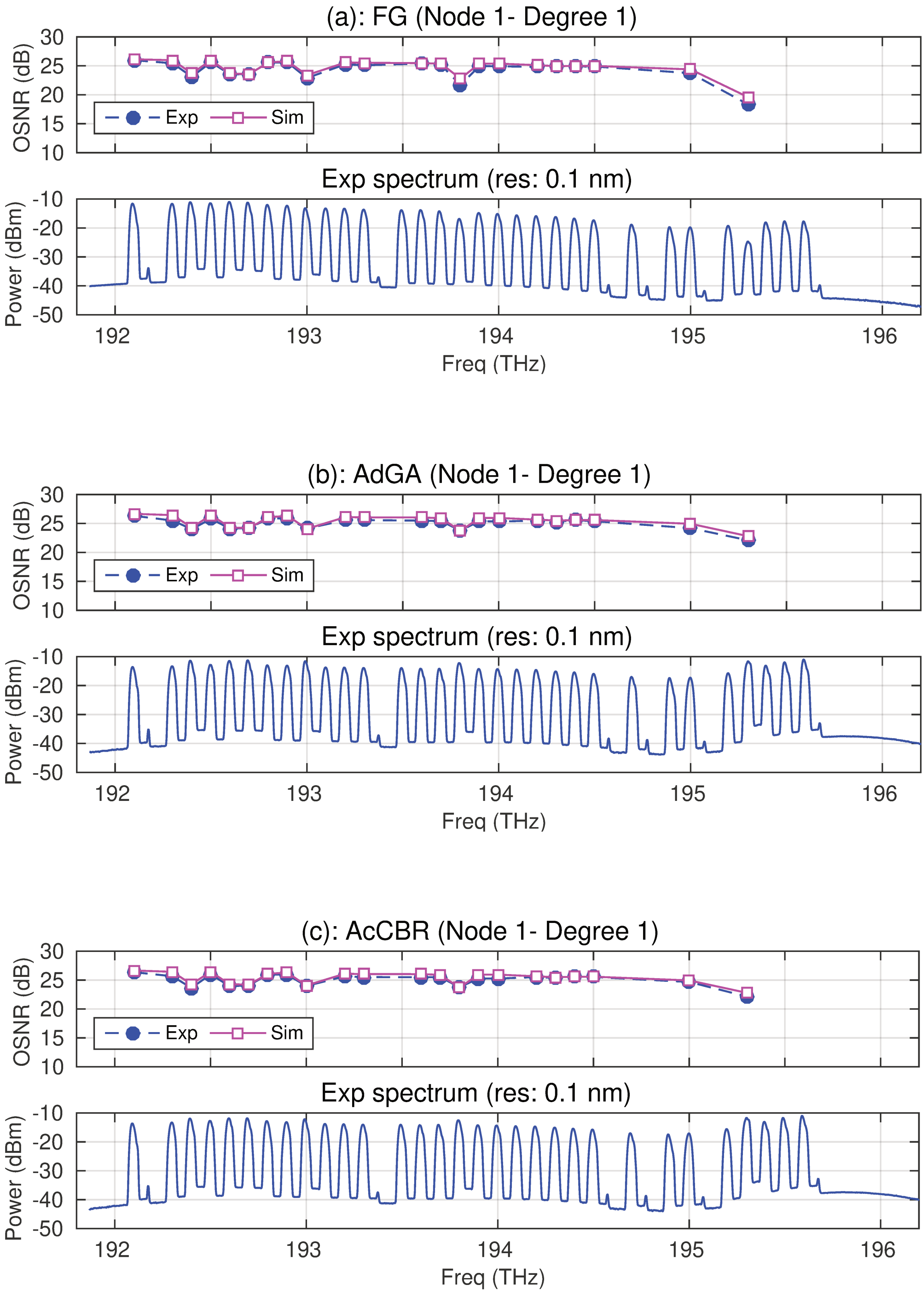

Figure 4.5: AN experimental OSNR measurements at node 1 and drop port degree 1 for (a) FG, (b) AdGA and (c) AcCBR [7].

provements on the mean OSNR for all connections presented in the network as shown in Table 4.1. This indicates that the performance improvement achieved by the Cognitive

Mean $\pm\delta$ OSNR (dB)

LP size	1 link	2 links
FG	24.09 $\pm$1.49	18.57 $\pm$3.44
AdGA	24.78 $\pm$1.30	22.37 $\pm$1.88
AcCBR	24.76 $\pm$1.02	22.59 $\pm$1.29

Table 4.1: Experimental results at AN showing mean and standard deviation OSNR for FG, AdGA and AcCBR [7].

Methodology can be extended for all the connections already established [7].

4.4 Concluding remarks

The Cognitive Methodology was experimentally validated in a meshed five-node network testbed. Additionally, simulated and experimental results were compared with assess the devices' models assumed during the OSNR estimation on the reuse step.

Chapter 5

Computer simulations[1]

After experimentally validate the Cognitive Methodology in Autonomous Network and evaluate the devices' models, this Chapter evaluates by simulation the Cognitive Methodology in real networks scenarios. First, in Section 5.1, networks with different topologies are considered, assuming fixed span lengths and different traffic loads. Then, in Section 5.2, different network topologies are also explored, considering their real link distances. Additionally, Section 5.2 also evaluates the Cognitive Methodology in terms of execution time and the effect of applying the Cognitive Methodology just for lightpaths with a few number of links (fast AcCBR (fAcCBR)) on the execution time and on the optical performance.

5.1 Fixed 100-km links

This Section investigates the optical performance of the Cognitive Methodology applied to practical networks with different topologies and traffic loads.

[1]This Chapter is based on the following papers submitted by the author: U. C. Moura et al.,"Optical amplifier cognitive gain adjustment methodology for dynamic and realistic networks.", Springer, Cognitive Technologies, 2017; and U. C. Moura et al., "Execution Time Improvement for Optical Amplifier Cognitive Methodology in Dynamic WDM Networks.", SBMO/IEEE MTT-S International Microwave and Optoelectronics Conference (IMOC), 2017.

5.1.1 General assumptions

To validate the versatility of the Cognitive Methodology against different network topologies, three real networks, shown in Figure 5.1, were selected from [149]. Biz Networks (Figure 5.1(a)) is an Indonesian network and it is the smallest network in terms of number of nodes (29). However, it has the highest density (D = 0.081), presenting 33 links. It contains five interconnected rings, leading to lightpaths with high number of links. CESNET (Figure 5.1(b)) is from Czech Republic and presents 45 nodes and 56 links. It has the particularity to have a few nodes with a high connectivity degree and a considerable number of nodes (more than 50%) with just one connection. Because of this characteristic, it has the lowest graph density (D = 0.057) and lightpaths with a small number of links. Finally, Palmetto (Figure 5.1(c)) is from South and North Caroline, USA. It is numerically similar to CESNET in terms of number of nodes (45), links (64) and density (0.065). However, it has a very different topology, presenting a more uniform link distribution along nodes [7].

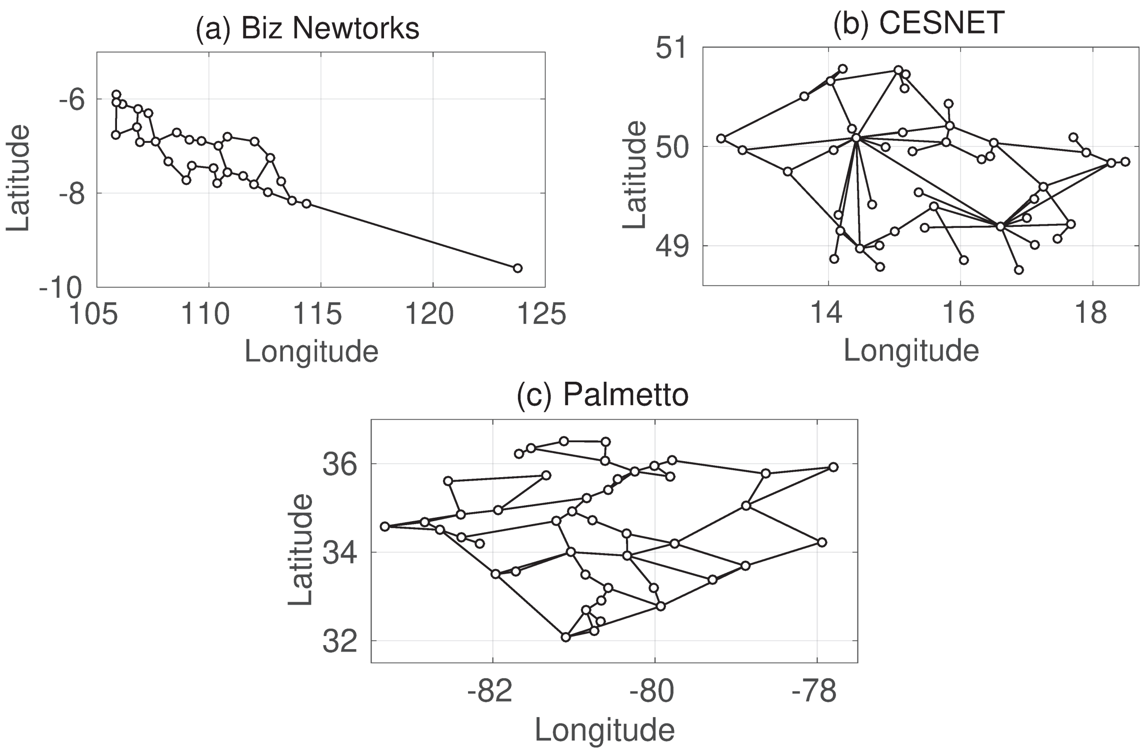

Figure 5.1: Networks considering fixed 100-km link distances: (a) Biz Networks: 29 nodes, 33 links (66 edges), D = 0.081. (b) CESNET: 45 nodes, 56 links (112 edges), D = 0.057. (c) Palmetto: 45 nodes, 64 links (128 edges), D = 0.065 [149].

This evaluation is restricted to networks with link distances near 100 km, so that this distance can be assumed fixed for all the links along the networks. Thus, it is assumed bidirectional links with a fixed 100-km SSMF and two optical amplifiers for each direction [7]. The same two sets of amplifier models considered in Section 4.2 are investigated: B21/P14 (models 3/2) and B21/B21 (models 1/1).

The computer simulations, developed in Matlab®, consider the traffic generation and RWA assumptions described in Section 4.1.3. The only difference is that two traffic loads (low/high) are considered. These traffic loads are associated to the blocking probability and depend on the network topology. A "low" load leads to a 0% of blocking probability and "high" load leads to a blocking probability near 30% for Biz Networks and 15% for CESNET and Palmetto. Devices' modeling assumptions are the same used on the experimental validation described in Section 4.1.2. These simulations are repeated 10 times for each network, for each amplifier gain control conditions (FG, AdGA and AcCBR), for each amplifier models per link (B21/P14 and B21/B21), and for each load condition (low/high). Moreover, four different initial DB sizes are considered for AcCBR, starting from zero and sequentially increasing [7]. Additionally, for the reuse step, AcCBR considers the probabilistic parameters' values as $\kappa = 50\%$, $\beta^{Pin} = 0.5$ dB, and $\beta^{\alpha L} = 1$ dB; and the exploration and exploitation parameters' values as $\gamma = 0.5$, $\mu = 0.1$, and $\upsilon = 0.4$.

5.1.2 Results

Figures 5.2, 5.3, and 5.4 summarize the results for Biz Networks, CESNET and Palmetto, respectively, showing the OSNR values for the two evaluated set of amplifier models, where subfigures (a) stand for B21/P14 and subfigures (b) stand for B21/B21. During the simulations, the OSNRs of all the connections presented at the network are estimated each time a new connection was established (when AcCBR and AdGA are applied). It enables to evaluate the impact of the gain adjustments also on the connections already established on the network [7]. At the end of the simulations, these OSNR values are used to obtain the mean and standard deviation for the 10 repetitions. Left and right graphs inside subfigures stand for "low" and "high" loads, which are 100 and 800 erlang for Biz Networks (Figure 5.2), 200 and 1600 erlang for CESNET (Figure 5.3), and 100 and 900 for Palmetto (Figure 5.4). AcCBR OSNRs (mean and standard deviation) are plotted as a function of the DB size, while FG and AdGA OSNRs (just mean) are continuous to serve as a reference for AcCBR results [7].

Furthermore, as the OSNR value depends on the number of amplifiers along the lightpath (LP), the mean OSNRs are calculated for different sets of connections, depending on their number of links (or amplifiers). Thus, for each load in Figures 5.2, 5.3, and 5.4, there are three graphs standing for LPs with 1/7/14 links for Biz Networks (Figure 5.2); 1/3/6 links for CESNET (Figure 5.3); and 1/5/9 links for Palmentto (Figure 5.4). These values are associated to up/middle/bottom graphs, respectively.

Moreover, Biz Networks shows LPs with up to 17 links, due to its characteristics of ring connections; while CESNET has up to 10 links per LP, due to its hub characteristics, and Palmetto has up to 15 links per LP. From the results shown in Figures 5.2, 5.3, and 5.4, a high level analysis shows the same behavior previously seen in AN results (Figure 4.4): AdGA presenting the worst performance for B21/P14 and FG presenting the worst performance for B21/B21 [7].

It is important to recall that AN single simulation for one traffic pattern with 1,000 connections reported in Section 4.2 is sufficient for AcCBR reach a good performance at the end of the simulation (Figure 4.4). This occurs because, for a small network, such as AN, the set of possible cases is also small, and a DB size with a magnitude of KBytes has sufficient cases to help AcCBR obtain good solutions. However, it is not true for larger networks, such as Biz, CESNET and Palmetto [7].

Back to Figures 5.2, 5.3, and 5.4, the OSNR performance of AcCBR with an empty DB is near FG for all graphs, which is expected, since FG is the initial condition for AcCBR (when there is no similar case in DB). For larger networks, the set of possible cases is also larger (because the diversity of LPs in terms of link number) in a way that AcCBR needs a magnitude of Mbytes to have a DB with sufficient cases to improve its results [7].

Note that, similar to the results for AN (Figure 4.4), there are different OSNR performances when applying AdGA: for B21/P14, it presents the worst performance and for B21/B21 it presents the best one. On the other hand, AcCBR improves the OSNR as the DB increases, showing its learning capability for both set of amplifier models. Furthermore, for high DB sizes, AcCBR achieves the best OSNR results for all cases, considering the standard deviation, showing its robustness regardless the amplifier models used in the network [7].

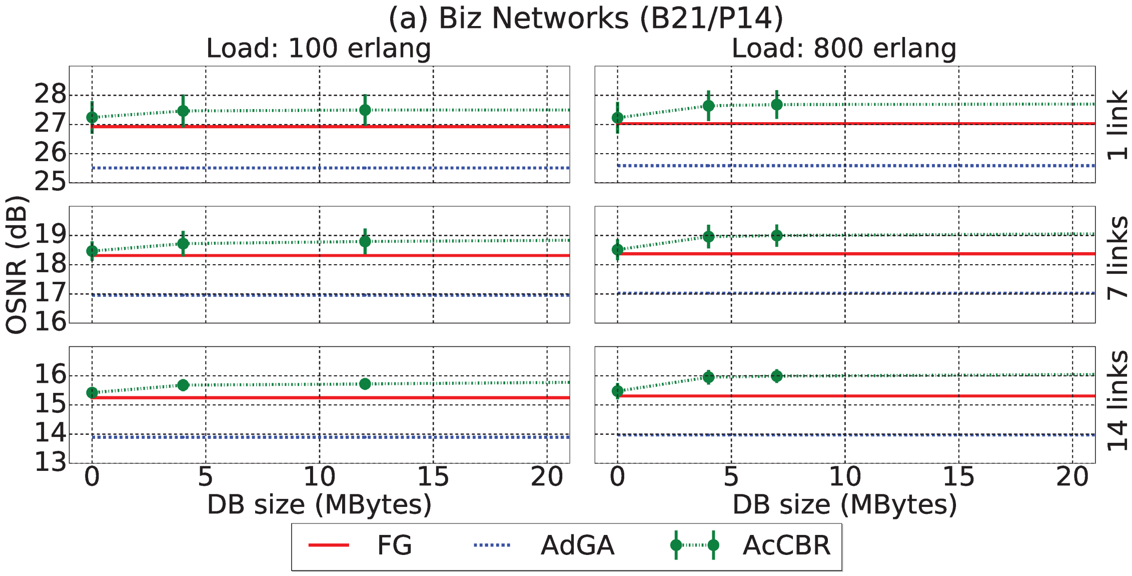

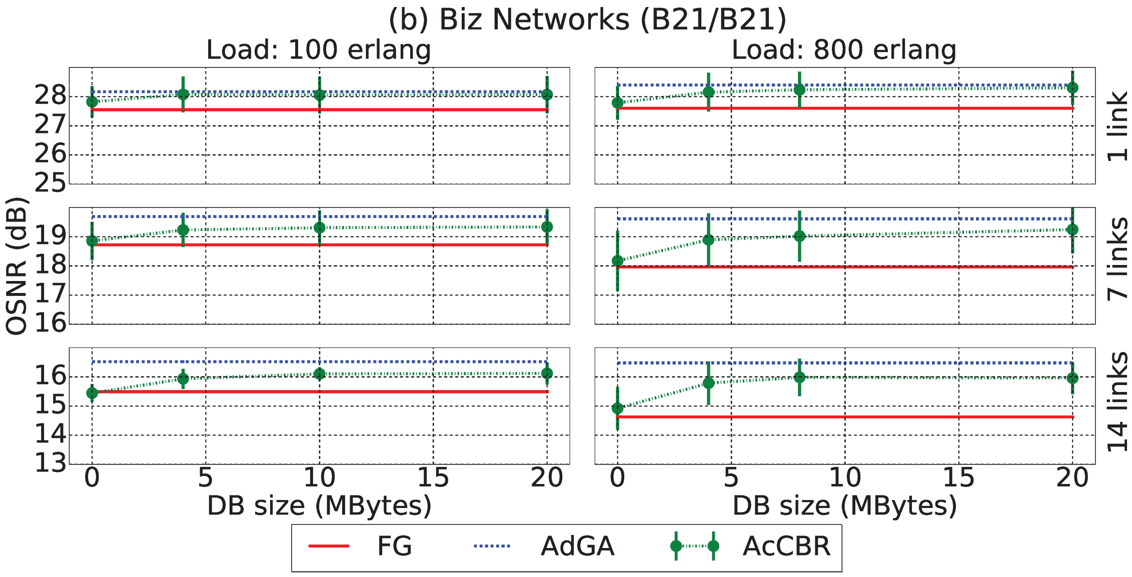

Figure 5.2: OSNR values at the end of the LP for Biz Networks (considering fixed link distances): mean and standard deviation per DB size (AcCBR) and just mean (FG and AdGA) for amplifier models (a) B21/P14 and (b) B21/B21, with 100 and 800 erlang of traffic loads. For AcCBR: $\kappa = 50\%$, $\beta^{Pin} = 0.5$ dB, $\beta^{\alpha L} = 1$ dB, $\gamma = 0.5$, $\mu = 0.1$, and $\upsilon = 0.4$ [7].

Moreover, the traffic load has an effect on the mean OSNR for FG with B21/B21 amplifier models: there is an OSNR degradation as the load increase. This degradation, of up to 1.2 dB, is more perceptible for LP with high number of links. It may be caused by the high gain tilt in amplifier model 1 considered in B21/B21 (see Figure 4.3(b)), that causes a high gain difference along the channels, specially when there are more channels (high load). Recall that in FG condition, the amplifiers are set to

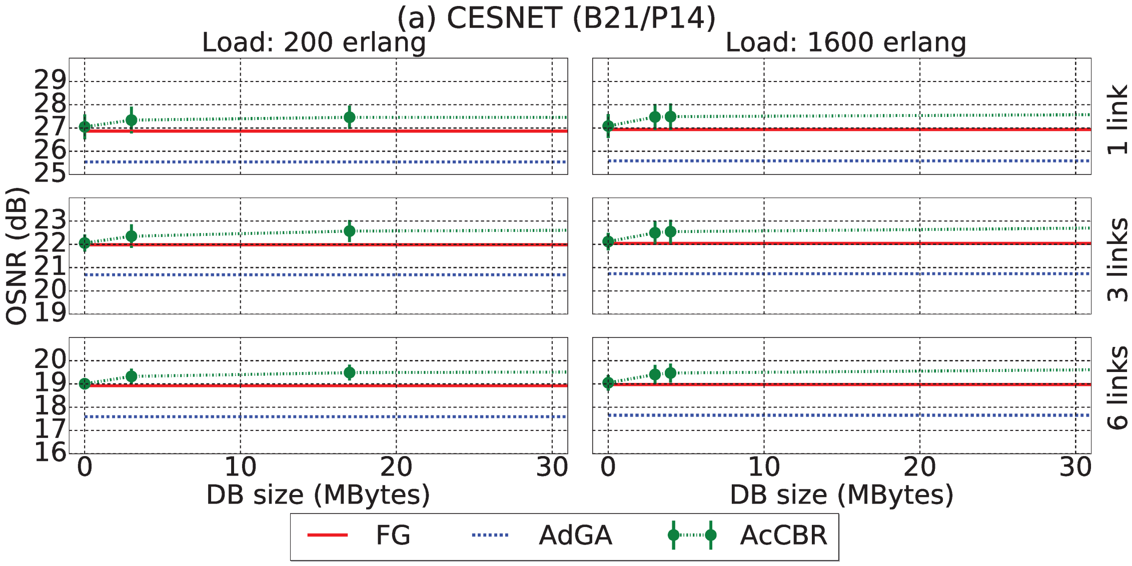

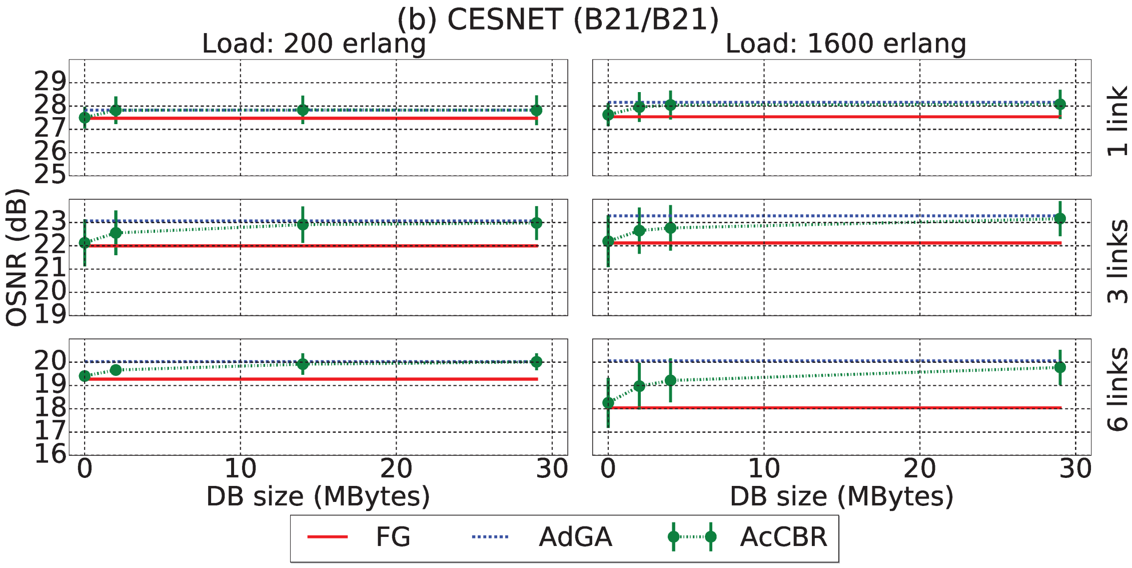

Figure 5.3: OSNR values at the end of the LP for CESNET (considering fixed link distances): mean and standard deviation per DB size (AcCBR) and just mean (FG and AdGA) for amplifier models (a) B21/P14 and (b) B21/B21, with 200 and 1600 erlang of traffic loads. For AcCBR: $\kappa = 50\%$, $\beta^{Pin} = 0.5$ dB, $\beta^{\alpha L} = 1$ dB, $\gamma = 0.5$, $\mu = 0.1$, and $\upsilon = 0.4$ [7].

compensate the link losses. Thus, any gain difference can lead some channels without sufficient gain to compensate the link losses. This degradation is accumulated along the links, being more critical for connections with a high number of links.

On the other hand, AdGA presents small variations of OSNR (up to 0.2 dB) with traffic load (for both set of amplifier models) because when the input power changes, AdGA searches a new operating point with a better gain flatness and noise figure [7].

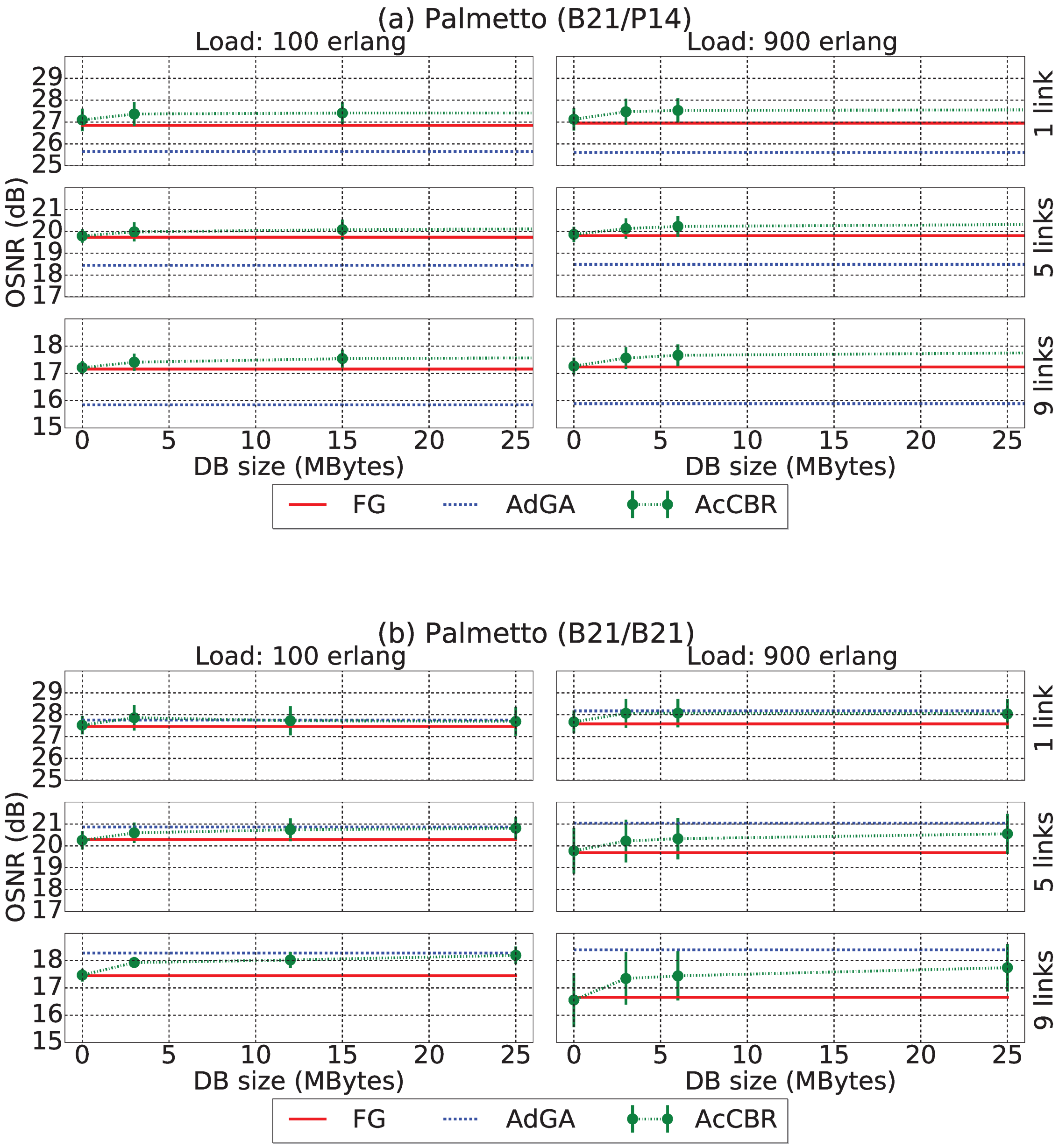

Figure 5.4: OSNR values at the end of the LP for Palmetto (considering fixed link distances): mean and standard deviation per DB size (AcCBR) and just mean (FG and AdGA) for amplifier models (a) B21/P14 and (b) B21/B21, with 100 and 900 erlang of traffic loads. For AcCBR: $\kappa = 50\%$, $\beta^{Pin} = 0.5$ dB, $\beta^{\alpha L} = 1$ dB, $\gamma = 0.5$, $\mu = 0.1$, and $\upsilon = 0.4$ [7].

For AcCBR, considering B21/P14 models, it achieves almost the same OSNR for both traffic loads. It is also true for B21/B21, at LPs with 1 link. However, for LPs with higher number of links, the traffic loads also influence the AcCBR performance, which presents a little difficult to achieve the same performance as in low load condition (specially for Palmetto). Recall that AcCBR starts from FG condition when DB is empty, which is more degraded in high load scenarios. Even though, at high DB sizes, AcCBR achieves almost the same OSNR values for low and high loads, showing its suitability in terms of initial conditions and traffic loads [7].

Finally, in Figures 5.2, 5.3, and 5.4, it is observed a slightly OSNR improvement with the increase in traffic load for B21/P14 (all LPs) and B21/B21 (just for LPs with 1 link). One possible reason for these OSNR improvements is because a higher traffic load increases the number of channels on the link. In this situation, the signal "steal" power from the noise: there are more signal than noise photons to stimulate new photon emissions (see Section 2.3.1). On the other hand, the OSNR degradation with the increase in traffic load for B21/B21 and LPs with higher number of links was already explained on previous paragraphs.

5.1.3 Partial conclusions

The Cognitive Methodology was evaluated in three practical topologies, with different topologies, considering the same distance (and the same number of amplifiers) for all links. The performance of the Cognitive Methodology was compared with two amplifier gain conditions: FG and AdGA, considering different scenarios in terms of traffic load and amplifier models.

The obtained results showed that, regardless the network topology (number of nodes, links and density), amplifier models, traffic load and LP size (in terms of number of links), AcCBR presented a learning capability, with OSNR improvements of up to 2 dB as DB size increased. Furthermore, AcCBR achieved the best performance in terms of OSNR results, after the learning process, for most cases.

5.2 Different link distances

In this Section, the Cognitive Methodology is evaluated for different network sizes, considering their real link distances, with different number of amplifiers per link. Moreover, the execution time is also evaluated and compared with different amplifier gain conditions. Finally, the proposed modification for the Cognitive Methodology (fAcCBR), presented in Section 3.2, is evaluated in terms of time reduction and its impact on the OSNR performance.

5.2.1 General assumptions

Three real networks from [149] with different topology and link distances are explored. Biz Networks (Figure 5.1(a)), from Indonesia (already used in Section 5.1); Tata (Figure 5.5(a)), from India; and China Telecom (Figure 5.5(b)), from China. For these networks, the real distances between nodes were calculated using latitude and longitude information also shown in Figures 5.1 and 5.5. As in previous simulations, bidirectional links (directed graphs) [131] are considered.

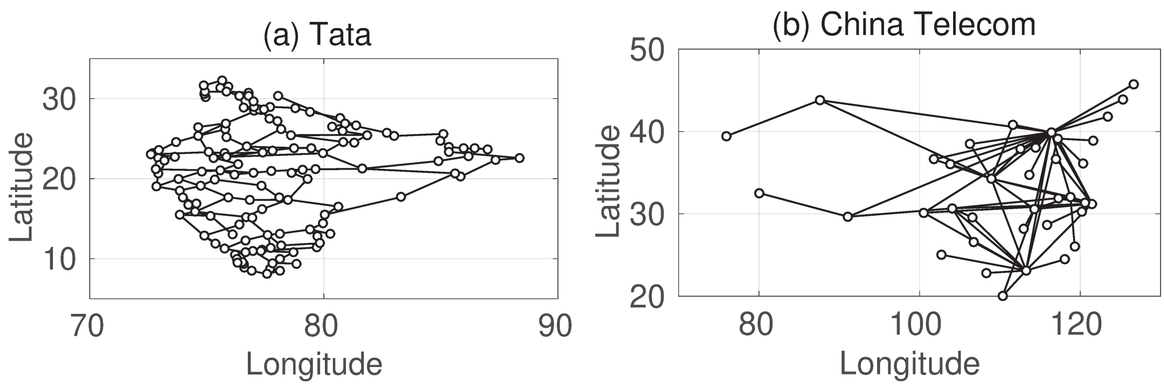

Figure 5.5: Networks considering the real link distances: (a) Tata, midsize network, from India, and (b) China Telecom, large-size network, from China (adapted from [131]).

Considering the real link distances implies in assuming different number of amplifiers per link. Figure 5.6 helps to understand the definition of the number of amplifiers per link considered in this work. The amplifiers should compensate the total link loss experienced by the signal when coming out from one node (point A in Figure 5.6(a)) to the output of the next node (point B in Figure 5.6(a)). This total loss depends on the optical fiber loss and the insertion loss of the ROADM-node pass (splitter and WSS in Figure 4.1(b)). For each link, just the node at the end of the link (filled nodes in Figure 5.6) is considered to calculate the total link loss. Previous nodes (non-filled nodes in Figure 5.6) are compensated by the amplifiers on previous links. The fiber loss is related to the total link distance (L, also the total fiber length) and the fiber attenuation (α), in dB/km, and is given by αL. In this work, fiber spans are SSMF with an attenuation of 0.2 dB/km. The node insertion loss is fixed, and considered as 16 dB, as already mentioned in Section 4.1.2.

Thus, the number of amplifiers per link is defined according the following rule: for links with αL between 1 to 11.5 dB (or 17 to 27.5 dB considering total link loss), one amplifier placed before the optical fiber (acting as a booster) is considered, as illustrated in Figure 5.6(a). To compensate the total link loss, this single amplifier must have a gain variation from 17 to 27.5 dB. For links with αL between 11.5 to 32 dB (or 27.5 to 48 dB considering the total link loss), 2 amplifiers are considered, at the edges of the fiber span (a booster and a preamplifier), as illustrated in Figure 5.6(b), with gains varying from 13.75 to 24 dB each. Note that these two amplifiers provide a total gain range from 27.5 to 48 dB, corresponding to the total link loss range. For αL above 32 dB (or above 48 dB for total link loss), besides the booster and preamplifier on the edges, line amplifiers are placed along the link for each fiber loss interval of 27 dB. These line amplifier additions split the fiber into equal spans, as illustrated in Figure 5.6(c-e). They must be able to provide a gain of up to 27 dB.

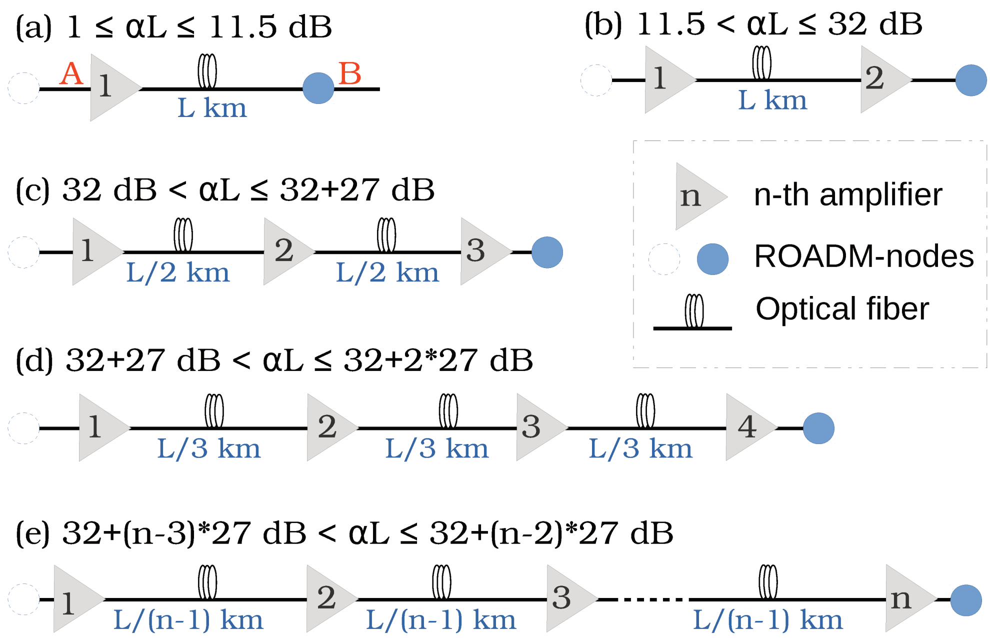

Figure 5.6: Number of amplifier, n, per link as a function of the total link loss, αL (α is the fiber attenuation and L the total link distance).

Furthermore, span loss higher than 20 dB is avoided for total link losses higher than 200 dB (or 1000 km). In other words, if after applying the previous rule, there are still span lengths with loss higher than 20 dB for a link with more than 200 dB of total loss, line amplifiers will be still added to this link until it presents spans loss lower than 20 dB. It is done to minimize performance degradation due to low signal powers at the amplifiers input [131]. The total link distance/fiber loss (left y axis) and the number of amplifiers per link (right y axis) are shown in Figure 5.7 for Biz Networks (Figure 5.7(a)), Tata (Figure 5.7(b)) and China Telecom (Figure 5.7(c)) [131].

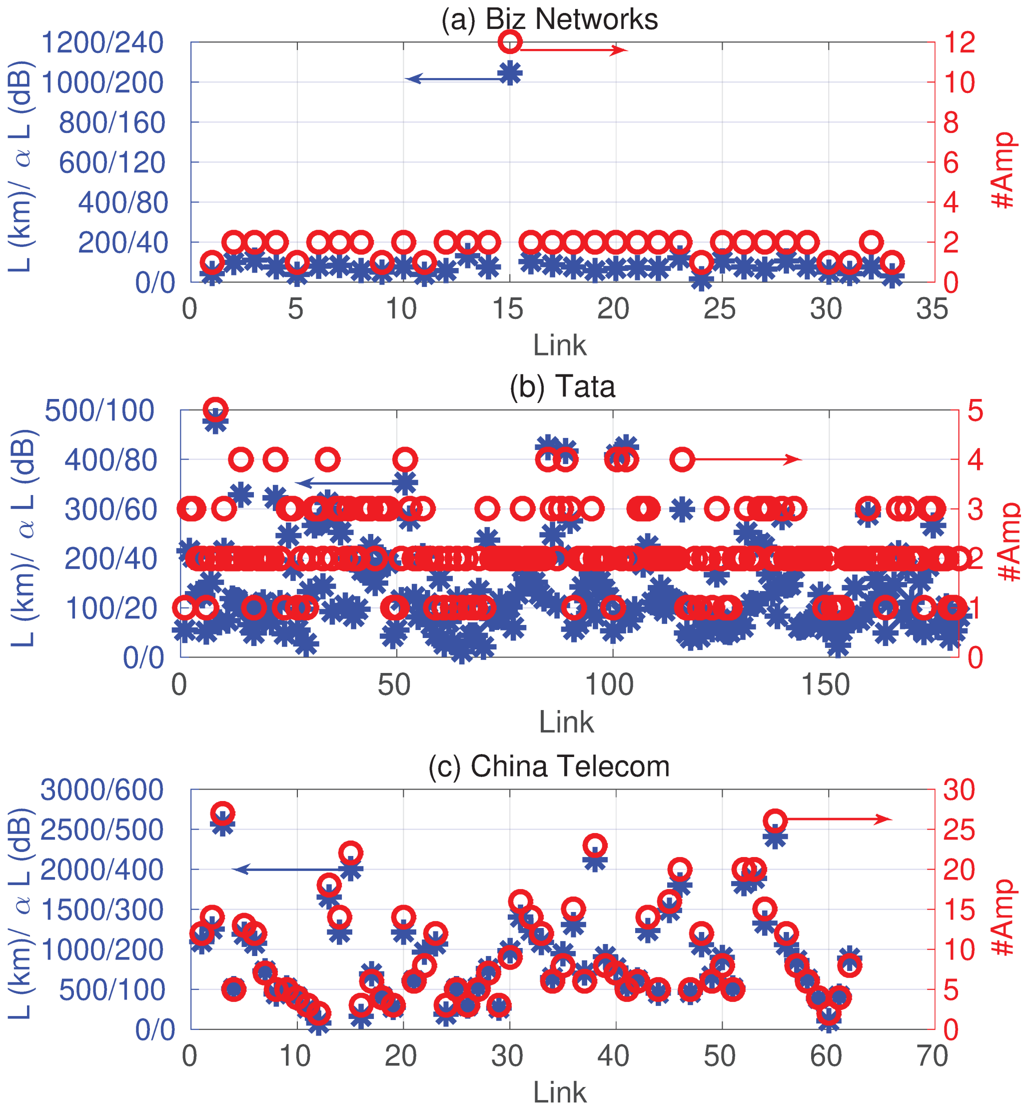

Figure 5.7: Total link distance (L), total link loss (αL) and number of amplifiers (#Amp) per link for (a) Biz Networks, (b) Tata and (c) China Telecom (adapted from [131]).

Table 5.1 summarizes the networks' parameters in terms of number of links (edges) and nodes, density, distance, link loss and number of amplifiers per link (Amp/ Link), considering minimum, maximum, mean and standard deviation values. Biz Networks is the smallest network, with distances from 18.63 to 133.95 km, and just one link with 1,044.47 km. This long link increases mean and standard deviation to 102.29 $\pm$ 171.16 km (not considering this link, mean and standard deviation are reduced to 72.85 $\pm$ 26.23 km). It presents a ring topology, with 29 nodes and 33 links, which leads to a density of 0.081. It was used in Section 5.1, considering fixed 100-km span lengths. Tata is a mid-size network with a more uniform distance distribution, with a mean of 133.85 $\pm$ 87.63 km (from 12.03 to 477.94 km). It presents the highest number of links and nodes, 180 and 143, respectively, forming interconnected rings. Although, due to the high number of nodes, it presents the lowest density (0.018). Finally, China Telecom is a large-size network, with link distances from 80.45 to 2,564.26 km. It presents a low number of nodes (38) considering its area, with 62 links, resulting in a density of 0.088, forming a hub topology. Due to this characteristic, China Telecom presents LPs with the smallest number of links.

Table 5.1: Biz Networks, Tata and China Telecom networks' parameters: number of links (#Links), number of nodes (#Nodes), total link distance (L), total link loss (αL) and number of amplifiers per link (#Amp/Link) [131].

	Biz Networks	Tata	China Telecom
#Links (#edges)	33 (66)	180 (360)	62 (124)
#Nodes	29	143	38
Density	0.081	0.018	0.088
Min. L (km)	18.63	12.03	80.45
Max. L (km)	1,044.47	477.94	2,564.26
Mean L (km)	102.29±171.16	133.85±87.64	911.97±567.47
Min. αL (dB)	3.73	2.41	16.09
Max. αL (dB)	208.89	95.59	512.85
Mean αL (dB)	20.46±34.23	26.77±17.53	182.39±113.49
Min. #Amp/Link	1	1	2
Max. #Amp/Link	12	5	27
Mean #Amp/Link	2.06±1.82	2.16±0.78	9.61±6.25

The devices' modeling is the same described on the experimental validation, in Section 4.1.2, except for the amplifier, in which the gain dependence on channel is no longer considered. This simplification is necessary because the gain difference along the channels impacts too much the signal performance for long links, such as the ones considered in this Section. Before considering the channel gain information for network with long distance links, it is important to update the Cognitive Methodology to also consider this information as a feature on the DB.

The amplifier models considered in this Section were restricted to models 2 and 3 (described in Section 4.1.2). These two models were used as the first (model 3) and the last (model 2) amplifiers on the links with two or more amplifiers. A new model (model 4) is used as inline amplifiers (or as the single link amplifier, in Figure5.6(a)). The model 4 is an EDFA amplifier with two stages of EDFs (7 m each) and a GFF between them. Both stages in a co-propagating 980 nm pump configuration with up to 300 and 600 mW for first and second stage, respectively. Its minimum total input power is -28 dBm, maximum total output power is +24 dBm, and the gain varies from 17 to 27 dB. Its noise figure and gain flatness dependence on operating point is presented in Figure 5.8(a) and (b), respectively, also obtained using the characterization process described in Section 2.3.3.

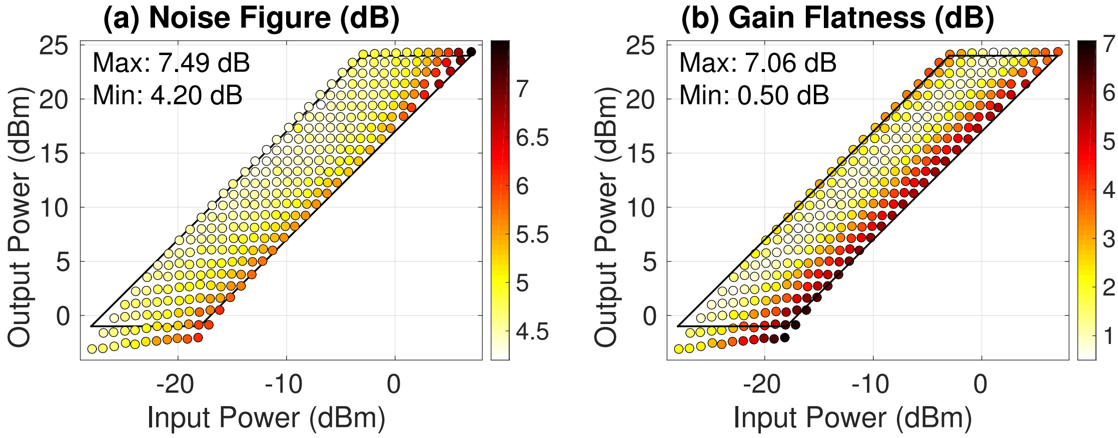

Figure 5.8: Noise figure and gain flatness dependence with the amplifier operating point for amplifier model 4 obtained experimentally using the characterization process described in Section 2.3.3.

Recall that the rule used to define the number of amplifiers per link (described at the beginning of this Subsection) requires that in the link with a single amplifier, this amplifier provides a gain from 17 to 27.5 dB. However, amplifier model 4 has a gain variation from 17 to 27 dB. Thus, these links will be under-compensated by up to 0.5 dB when considering the amplifier model 4. Moreover, links assigned with two amplifiers present total loss from 27.5 to 48 dB. Considering models 3 and 2 for booster and pre amplifier, respectively, the total gain provided by these two amplifiers ranges from 28 to 48 dB. In this situation, these links will be over-compensated by up to 0.5 dB considering these two amplifiers models (2 and 3). However, for the networks considered in this Section, just a few links present a total loss between 27 and 28 dB.

The computer simulations, also performed using Matlab®, runs in an Intel Core i7 4500u @ 1.80 GHz and 8 GB of RAM. They consider the traffic generation and RWA assumptions described in Section 4.1.3. The simulations are also repeated 10 times for each network, for each amplifier gain control conditions (FG, AdGA and AcCBR), and considering a fixed traffic load of 500 erlang. It is also considered four different initials DB sizes for AcCBR, starting from zero and sequentially increasing [7]. Moreover, for the reuse step, AcCBR considers the probabilistic parameters' values as $\kappa = 50\%$,

$\beta^{Pin} = 1$ dB, and $\beta^{\alpha L} = 2$ dB; and the exploration and exploitation parameters' values as $\gamma = 0.5$, $\mu = 0.1$, and $\upsilon = 0.4$.

5.2.2 Results

Mean and standard deviation OSNR results for Biz Networks are shown in Figure 5.9. For this network, connections commonly have up to 40 amplifiers. Thus, in Figure 5.9, the OSNR results are separated into a set of nine representative connection paths in terms of total number of links and amplifiers per connection. Furthermore, x-axis indicates the gain adjustment scheme applied: FG, AdGA, DB0-4 for AcCBR, and ML1-4 for the AcCBR modification to improve the execution time: fast AcCBR-maximum link (fAcCBR-MLn), defined in Section 3.2. DB0 indicates that the 10 repetitions were performed starting with an empty DB. DB1 to DB4 stand for different DB sizes: 1.3, 2.4, 3.5 and 4.6 MB, respectively. fAcCBR-MLn applies AcCBR just for LPs with up to n links. The DB sizes for fAcCBR were: 0.07, 0.46, 1.0 and 1.6 MB for n from 1 to 4, respectively. The DBs in fAcCBR-MLn were obtained from DB4, by extracting all cases with up to n links. Thus, fAcCBR does not start with an empty DB, as AcCBR. Moreover, during the following analysis, it is compared fAcCBR-MLn with the highest DB size: AcCBR-DB4 [126].

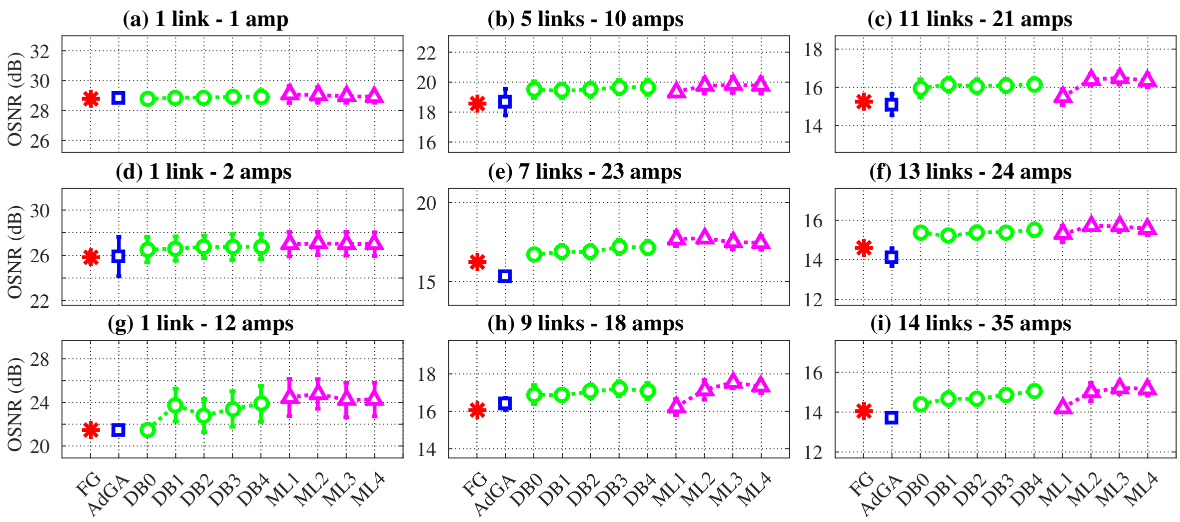

Figure 5.9: OSNR mean and standard deviation results for all the connections present in Biz Networks (considering the real link distances) at the time a new connection is established. DB0-DB4 refers to AcCBR. MLn refers to fAcCBR (the AcCBR modification to improve the execution time presented in Section 3.2). For AcCBR: $\kappa = 50\%$, $\beta^{Pin} = 1$ dB, $\beta^{\alpha L} = 2$ dB, $\gamma = 0.5$, $\mu = 0.1$, and $\upsilon = 0.4$ [126].

Figure 5.10 shows the mean execution time including the standard deviation (with bars) for each gain condition. These values are obtained from summing the time duration of the RWA and AcCBR executions at the AcCBR flowchart in Figure 3.1 for each of the 10,000 connections (10 repetitions x 1,000 connections). For AcCBR and fAcCBR, x-axis corresponds to the DB size, in MB, making it possible to evaluate the relationship between execution time and DB size. In addition, Table 5.2 summarizes mean OSNR and execution time values for the same connection paths presented in Figures 5.9 and 5.10 [126]. Table 5.2 also compares the OSNR variations from AcCBR-DB0 to DB4, and from DB4 to fAcCBR-MLx. These OSNR variations are highlighted with different colors to be better visualized. For OSNR improvements higher than 0.1 dB, the color is set to green. OSNR degradation higher than 0.1 dB is set to red. Variations less than ±0.1 dB are not considered a change, and their associated color are orange.

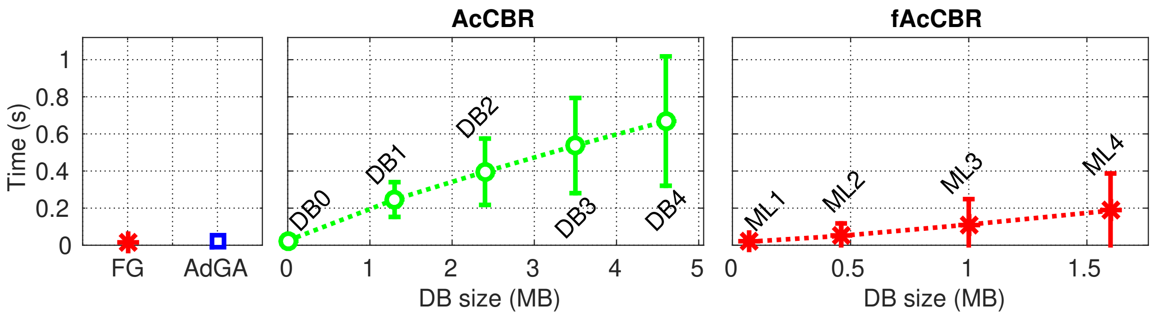

Figure 5.10: Execution time (mean and standard deviation) results for Biz Networks (considering the real link distances). DB0-DB4 refers to AcCBR. MLn refers to fAcCBR (the AcCBR modification to improve the execution time presented in Section 3.2). A visible execution time reduction is achieved when applying fAcCBR comparing with AcCBR-DB4. For AcCBR: $\kappa = 50\%$, $\beta^{Pin} = 1$ dB, $\beta^{\alpha L} = 2$ dB, $\gamma = 0.5$, $\mu = 0.1$, and $\upsilon = 0.4$ [126].

In Figure 5.9, note that FG condition and AdGA methodology present the worst OSNR performances for most cases. On the other hand, AcCBR (DB0-DB4) presents a cognitive behavior, with mean OSNR improving as DB increases. These OSNR improvements range from +0.14 dB (for LPs with 13/24 links/amps) to +2.37 dB (for LPs with 1/12 link/amps), as it can be seen on the fifth column in Table 5.2. Regarding the execution time in Figure 5.10, FG and AdGA present the lowest values: 17.38 and 20.40 ms, respectively (see Table 5.2). These values can be considered as a lower bound for the results here reported as it is mainly devoted to a non-optimized RWA calculation. AcCBR requires an execution time that increases linearly with the DB size, ranging from

Table 5.2: Mean OSNR in dB and mean execution time for Biz Networks (considering the real link distances), presenting an execution time reduction of up to 97.13% after applying fAcCBR (the AcCBR modification to improve the execution time presented in Section 3.2) when comparing with the most time consuming approach (AcCBR-DB4). For AcCBR: $\kappa = 50\%$, $\beta^{Pin} = 1$ dB, $\beta^{\alpha L} = 2$ dB, $\gamma = 0.5$, $\mu = 0.1$, and $\upsilon = 0.4$.

Link/amp	FG	AdGA	AcCBR		fAcCBR (MLx − DB4)			
			DB0	DB4 (DB4-DB0)	ML1	ML2	ML3	ML4
(a) 1/1	28.76	28.85	28.78	28.94 (+0.16)	29.07 (+0.13)	29.04 (+0.10)	28.95 (+0.01)	28.94 (-0.00)
(b) 5/10	18.57	18.66	19.50	19.66 (+0.16)	19.35 (-0.30)	19.75 (+0.10)	19.82 (+0.16)	19.77 (+0.12)
(c) 11/21	15.23	15.10	15.96	16.17 (+0.21)	15.49 (-0.68)	16.41 (+0.24)	16.50 (+0.33)	16.36 (+0.19)
(d) 1/2	25.82	25.89	26.49	26.79 (+0.29)	26.99 (+0.20)	27.05 (+0.26)	27.02 (+0.24)	26.98 (+0.19)
(e) 7/23	16.21	15.34	16.71	17.17 (+0.46)	17.71 (+0.54)	17.74 (+0.58)	17.50 (+0.33)	17.47 (+0.30)
(f) 13/24	14.60	14.12	15.37	15.50 (+0.14)	15.30 (-0.20)	15.71 (+0.21)	15.68 (+0.18)	15.57 (+0.06)
(g) 1/12	21.50	21.48	21.50	23.88 (+2.37)	24.46 (+0.58)	24.78 (+0.90)	24.23 (+0.35)	24.27 (+0.39)
(h) 9/18	16.05	16.40	16.90	17.09 (+0.19)	16.23 (-0.86)	17.15 (+0.06)	17.54 (+0.45)	17.32 (+0.24)
(i) 14/35	14.08	13.71	14.40	15.05 (+0.65)	14.21 (-0.84)	15.01 (-0.04)	15.21 (+0.17)	15.17 (+0.12)
Time (ms)	17.38	20.40	24.66	669.13	19.20	50.57	111.19	186.58
Time reduction compared with fAcCBR-DB4					97.13%	92.44%	83.38%	72.12%

24.66 ms for DB0 to 669.13 ms for DB4 (see Table 5.2) [126].

Table 5.3 presents the number of similar connections (mean and standard deviation) obtained during the retrieve step as a function of the DB size for the same evaluated connection paths in Biz Networks. When the number of similar cases is zero, it means that the Cognitive Methodology was not (completely) applied, since it does not have previous similar cases to help propose a new solution. In this situation, the amplifiers' gains along the LP remain constant (G_{new} = current gains, as presented at the flowchart in Figure 3.1). As DB size increases, the number of similar connections also increases (see columns 2 to 6, in Table 5.3. However, it is important to observe that just some LPs ((a), (b), (d) and (g), highlighted in Table 5.3) present a significant amount of similar connections that helps the Cognitive Methodology to improve OSNR. The other LPs remain with mean similar connections near zero. It is not consistent with

Table 5.3: Similar connections (mean and standard deviation) returned by the retrieve step for Biz Networks (considering the real link distances) demonstrating that just some connection paths present a considerable amount of similar connections. For AcCBR: $\kappa = 50\%$, $\beta^{Pin} = 1$ dB, $\beta^{\alpha L} = 2$ dB, $\gamma = 0.5$, $\mu = 0.1$, and $\upsilon = 0.4$.

Link/amp	DB0	DB1	DB2	DB3	DB4
(a) 1/1	1.34 ± 1.63	37.83 ± 26.53	52.41 ± 36.81	65.99 ± 49.33	$\mathbf{76.70 \pm 54.61}$
(b) 5/10	0.11 ± 0.31	3.08 ± 4.08	5.32 ± 6.69	7.97 ± 8.77	$\mathbf{9.50 \pm 10.73}$
(c) 11/21	0.00 ± 0.00	0.24 ± 0.63	0.25 ± 0.65	0.54 ± 1.15	0.54 ± 0.92
(d) 1/2	2.52 ± 3.08	53.87 ± 37.97	78.55 ± 50.85	96.30 ± 60.96	$\mathbf{105.02 \pm 70.04}$
(e) 7/23	0.06 ± 0.24	0.71 ± 0.92	1.48 ± 1.62	0.95 ± 1.43	2.00 ± 2.24
(f) 13/24	0.04 ± 0.21	0.00 ± 0.00	0.07 ± 0.26	0.03 ± 0.17	0.13 ± 0.34
(g) 1/12	0.33 ± 0.55	8.23 ± 2.70	7.75 ± 2.81	7.95 ± 2.65	$\mathbf{8.97 \pm 2.76}$
(h) 9/18	0.00 ± 0.00	0.53 ± 0.92	1.29 ± 1.68	1.61 ± 2.00	1.32 ± 1.89
(i) 14/35	0.00 ± 0.00	0.00 ± 0.00	0.00 ± 0.00	0.00 ± 0.00	0.00 ± 0.00

the results presented in Figure 5.9, where AcCBR improve the OSNR performance as the DB increase for all cases. These result mismatches can be explained by taking into account that, according to Figure 5.7(a), Biz Networks has just three kinds of links: with 1, 2 and 12 amplifiers. Thus, since all LPs are composed by a combination of these links, when AcCBR attempts to optimize single link LPs (Figure 5.9(a), (d) and (g)), it ends up optimizing larger LPs that share these single link LPs [131].

The comparison of the results shown in Table 5.3 against Figure 5.9 (or Table 5.2) is very important because they show that the AcCBR does not need to be applied for all the connections. Furthermore, it is sufficient to apply AcCBR for LPs with a few number of links. It is the main idea of the fAcCBR described in Section 3.2.

According to Table 5.2 or Figure 5.9, when fAcCBR is applied just for LPs with one link (ML1), there is an OSNR performance degradation, with respect to AcCBR-DB4, mostly for high path lengths (see sixth column in Table 5.2). On the other hand, the execution time drops from 669.13 to 19.20 ms. This value is very close to FG, AdGA and AcCBR-DB0, and corresponds to a reduction of 97.13% compared with AcCBR-DB4 [126].

Considering fAcCBR-ML2, i.e., applying AcCBR just for LPs with up to 2 links, there is no OSNR degradation when comparing with AcCBR-DB4, presenting even improvements of up to +0.9 dB (1/12 link/amps), as it can be seen in Table 5.2. Note that the OSNR improvements when compared with AcCBR-DB0 is up to 3.3 dB (also for 1/12 link/amps). The single degradation of -0.04 dB for LPs with 15 links and 35 amplifiers is not considered because it is less than 0.1 dB. The execution time presents a small increase (compared with fAcCBR-ML1), reaching 50.57 ms [126].

Applying fAcCBR-ML3, all LPs present an OSNR improvement or the same performance when comparing with AcCBR-DB4. There is also an execution time increase in Figure 5.10 when compared with fAcCBR-ML2, going to 111.19 ms (see Table 5.2). However, it is still very low when compared with AcCBR-DB4 [126].

Finally, when applying fAcCBR-ML4, just 1/1 and 13/24 link(s)/amp(s) remain with almost the same OSNR as AcCBR-DB4, with a variation less than 0.1 dB. The other LPs present an OSNR improvement. Moreover, the execution time is still very low when comparing with AcCBR-DB4: 186.58 ms, as presented in Table 5.2 [126].

It is expected that, when applying fAcCBR, the best result should be OSNRs with the same performance as AcCBR-DB4. However, there are OSNR improvements when using fAcCBR compared with AcCBR-DB4. These improvements may be explained by considering that, when fAcCBR is applied, the number of connections affected is very small when compared with applying AcCBR for all new connections, because, in fAcCBR, the amplifies' gains are not changing all the time a new connection is established [126].

Therefore, from the Biz Networks results, it can be conclude that, applying AcCBR for LPs with up to 2 links (fAcCBR-ML2) is sufficient to maintain (or even improve) the OSNR performance and improve (reduce) significantly the execution time. This reduction is nearly 92% when compared with AcCBR-DB4. The fAcCBR-ML3 presents almost the same OSNR performance as AcCBR-ML2. However, with a low execution time reduction of nearly 83% compared with AcCBR-DB4 [126].

Before presenting Tata and China Telecom results, it is important to show the number of links distribution along the connections. Figure 5.11 shows this information, where x-axis represents the number of links (#links) and y-axis represents the percentage of the connections associated to each #links. Note that Biz Networks (first bar), as already mentioned, presents connections with up to 17 links. However, most connections present up to 5 links. For Biz Networks, a good result was achieved when applying fAcCBR-ML2, which means applying the Cognitive Methodology to approximately 25% of the connections according to Figure 5.11.

Tata, on the other hand, presents connections with up to 35 links. The remainder link distribution for Tata is presented at the inner graph of the Figure 5.11. Note that the number of links is more distributed along the connections and 50% of the connections are at the range from 5 to 11 links. A few connections present links higher than 18 connections. Regarding China Telecom, it presents connections with up to 5 links. The most concentration occurs for connection with 2 and 3 links.

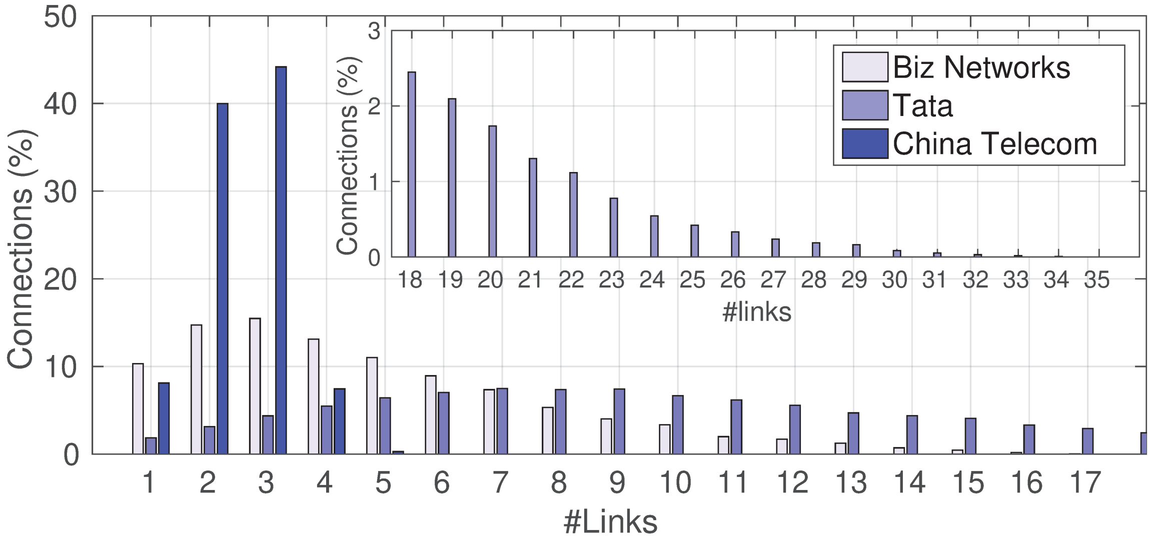

Figure 5.11: Number of links (#Links) distribution along the connections (%) for Biz Networks, Tata, and China Telecom, obtained during the simulations considering the real link distances.

Thus, these three networks present very different link distribution, according to each network topology. These differences must be taken into account when defining the number of links to be considered in fAcCBR, as well as in the analysis of the following results.

Figure 5.12 presents the OSNR results for Tata, also separated into a set of nine representative connection paths. DB1 to DB4 stand for 7.5, 15, 22.5, 30.8 MB, respectively. As Tata Networks presents a more uniform link distribution, fAcCBR is tested for LPs with up to 1 and 2 Links, which correspond to around 2% and 3% of the connections, respectively; and for LPs with up to 7 and 8 links, which correspond to around 35% and 45% of the connections, respectively. The DB size for ML1,2,6 and 7 are 0.12, 0.50, 3.7, and 9.6 MB, respectively. These reduced DBs are also obtained from DB4, by extracting all cases with up to n links. Regarding the number of amplifiers, considering Tata real distances, connections commonly have up to 68 amplifiers.

From the results shown in Figure 5.12, FG has a better performance than AdGA, that presents the worst OSNR performance for most cases. AcCBR, on the other hand, presents different behaviors according to the connection path. However, for most cases, it does not show a cognitive behavior (OSNR improvements with the DB

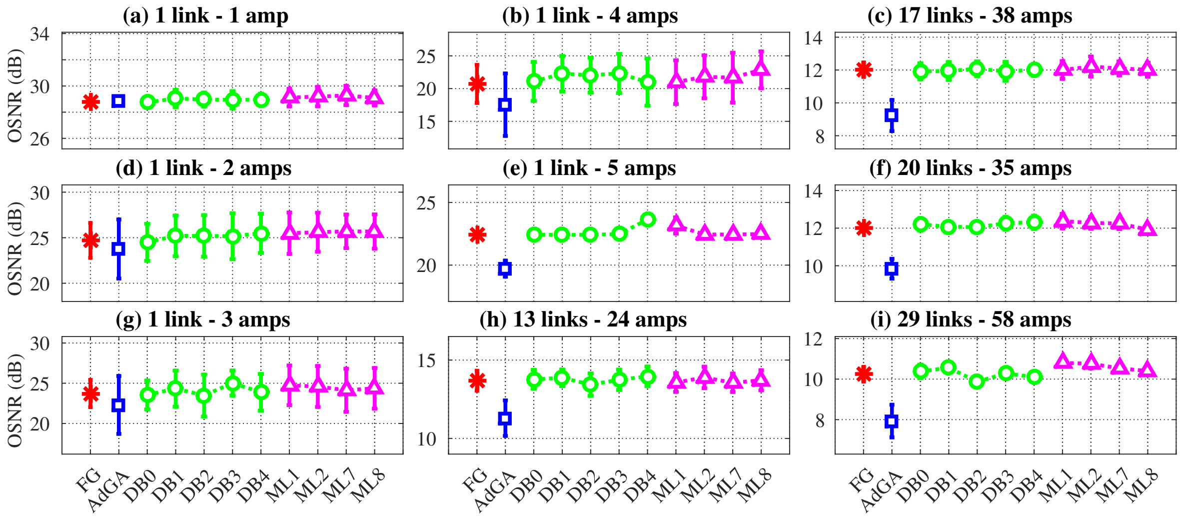

Figure 5.12: OSNR mean and standard deviation results for all the connections present in Tata (considering the real link distances) at the time a new connection is established. DB0-DB4 refers to AcCBR. MLn refers to fAcCBR (defined in Section 3.2). For AcCBR: $\kappa = 50\%$, $\beta^{Pin} = 1$ dB, $\beta^{\alpha L} = 2$ dB, $\gamma = 0.5$, $\mu = 0.1$, and $\upsilon = 0.4$.

size), presenting an OSNR performance oscillating near the FG condition. These OSNR oscillations may indicate the Cognitive Methodology non-convergence and its need for more experience. This might be a consequence of Tata link diversity, that requires a higher DB to converge.

Table 5.4 summarizes the results for Tata, showing the mean OSNR values. For AcCBR, there are OSNR improvements for most cases when going from DB0 to DB4. However, it is clear from Figure 5.12 that these OSNR improvements are not guaranteed due to the already mentioned OSNR oscillations for most cases.

Regarding the execution time presented in Figure 5.13, FG, AdGA and AcCBR-DB0 present the lowest values (as expected). In Table 5.4, these values are near 100 ms (almost 150 ms for AdGA). Comparing with Biz results presented in Table 5.2, they are very high, indicating that a more complex network, such as Tata, needs more time to establish the connections. Note that this high execution time just for Tata may be caused by the non-optimized RWA calculation. On the other hand, when the DB increases from DB0 to DB4, the execution time increases linearly from around 100 ms to 2.6 s.

Thus, when applying AcCBR in Tata, besides the high execution time, another important issue is the non-convergence behavior for most cases considering the DB sizes of up to around 31 MB (AcCBR-DB0 to DB4). The need for a higher DB to improve the

Table 5.4: Mean OSNR in dB and mean execution time for Tata (considering the real link distances), presenting an execution time reduction of up to 96.21% after applying fAcCBR (the AcCBR modification to improve the execution time presented in Section 3.2) when comparing with the most time consuming approach (AcCBR-DB4). For AcCBR: $\kappa = 50\%$, $\beta^{Pin} = 1$ dB, $\beta^{\alpha L} = 2$ dB, $\gamma = 0.5$, $\mu = 0.1$, and $\upsilon = 0.4$.

Link/amp	FG	AdGA	AcCBR		fAcCBR (MLx − DB4)			
			DB0	DB4 (DB4-DB0)	ML1	ML2	ML7	ML8
(a) 1/1	28.78	28.88	28.75	28.96 (+0.21)	29.11 (+0.16)	29.19 (+0.23)	29.28 (+0.32)	29.09 (+0.13)
(b) 1/4	20.72	17.55	21.09	21.00 (-0.09)	20.98 (-0.02)	21.80 (+0.80)	21.67 (+0.67)	22.86 (+1.86)
(c) 17/38	12.02	9.23	11.92	12.01 (+0.08)	12.00 (-0.01)	12.22 (+0.21)	12.10 (+0.09)	12.02 (+0.01)
(d) 1/2	24.71	23.76	24.50	25.49 (+0.99)	25.49 (+0.01)	25.61 (+0.12)	25.70 (+0.21)	25.68 (+0.19)
(e) 1/5	22.44	19.72	22.44	23.64 (+1.20)	23.17 (-0.47)	22.44 (-1.20)	22.45 (-1.19)	22.48 (-1.16)
(f) 20/35	12.00	9.84	12.20	12.31 (+0.11)	12.37 (+0.06)	12.28 (-0.03)	12.24 (-0.07)	11.93 (-0.38)
(g) 1/3	23.72	22.31	23.55	23.88 (+0.33)	24.74 (+0.87)	24.59 (+0.72)	24.13 (+0.25)	24.37 (+0.49)
(h) 13/24	13.68	11.30	13.77	13.96 (+0.19)	13.57 (-0.39)	13.89 (-0.07)	13.55 (-0.41)	13.71 (-0.25)
(i) 29/58	10.24	7.93	10.38	10.10 (-0.28)	10.80 (+0.70)	10.76 (+0.66)	10.53 (+0.43)	10.40 (+0.30)
Time (ms)	87.55	140.13	99.98	2607.15	98.87	101.12	471.96	665.08
Time reduction compared with fAcCBR-DB4					96.21%	96.12%	81.90%	74.49%

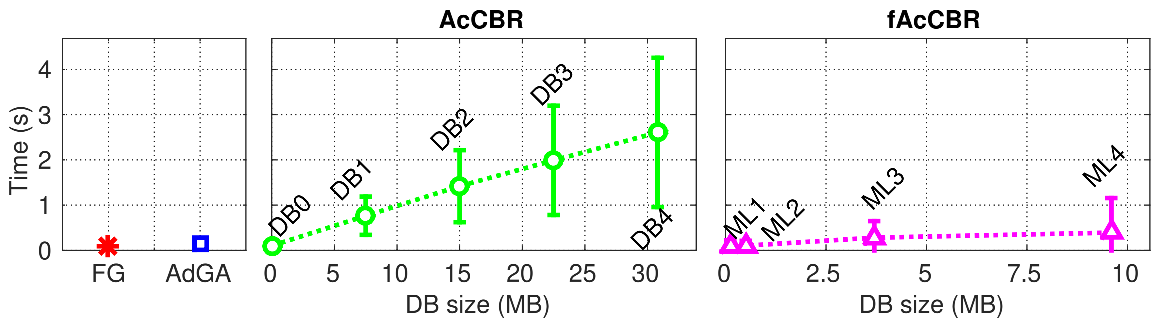

Figure 5.13: Execution time (mean and standard deviation) results for Tata (considering the real link distances). DB0-DB4 refers to AcCBR. MLn refers to fAcCBR (defined in Section 3.2). A visible execution time reduction is achieved when applying fAcCBR comparing with AcCBR-DB4. For AcCBR: $\kappa = 50\%$, $\beta^{Pin} = 1$ dB, $\beta^{\alpha L} = 2$ dB, $\gamma = 0.5$, $\mu = 0.1$, and $\upsilon = 0.4$.

OSNR also requires a higher execution time, which is unacceptable for real applications. However, it is important to point out that, regardless these OSNR oscillations and non-

Table 5.5: Similar connections (mean and standard deviation) returned by the retrieve step for Tata (considering the real link distances) demonstrating that just some connection paths present a considerable amount of similar connections. For AcCBR: $\kappa = 50\%$, $\beta^{Pin} = 1$ dB, $\beta^{\alpha L} = 2$ dB, $\gamma = 0.5$, $\mu = 0.1$, and $\upsilon = 0.4$.

Link/amp	DB0	DB1	DB2	DB3	DB4
(a) 1/1	0.15 ± 0.43	15.70 ± 9.90	26.17 ± 15.24	26.84 ± 15.71	$\mathbf{35.39 \pm 22.14}$
(b) 1/4	0.00 ± 0.00	2.48 ± 2.21	5.65 ± 5.12	8.22 ± 6.28	$\mathbf{7.20 \pm 2.95}$
(c) 17/38	0.00 ± 0.00	0.01 ± 0.09	0.00 ± 0.00	0.00 ± 0.00	0.41 ± 1.19
(d) 1/2	0.12 ± 0.36	14.70 ± 11.00	30.64 ± 20.47	40.30 ± 29.37	$\mathbf{58.47 \pm 40.26}$
(e) 1/5	0.00 ± 0.00	1.00 ± 1.41	1.67 ± 1.03	2.50 ± 0.71	$\mathbf{4.00 \pm 0.00}$
(f) 20/35	0.00 ± 0.00	0.00 ± 0.00	0.00 ± 0.00	0.00 ± 0.00	0.00 ± 0.00
(g) 1/3	0.03 ± 0.17	5.91 ± 4.68	11.12 ± 8.15	17.57 ± 9.27	$\mathbf{19.19 \pm 11.60}$
(h) 13/24	0.00 ± 0.00	0.02 ± 0.13	0.00 ± 0.00	0.00 ± 0.00	0.23 ± 1.07
(i) 29/58	0.00 ± 0.00	0.00 ± 0.00	0.00 ± 0.00	0.00 ± 0.00	0.00 ± 0.00

convergence, there is no significant OSNR degradation when comparing DB4 with FG or AdGA, also considering the standard deviation in Figure 5.12. Thus, it is expected that, when solved the execution time issue, it will be possible to continue applying the Cognitive Methodology in Tata, until finally it converges.

Table 5.5 presents the similar connections obtained during the retrieve process, indicating that some LPs do not have similar cases. However, even for LPs with 1 link (highlighted in Table 5.5), that present a significant amount of similar cases, OSNR improvements with DB size are observed just for LPs with 2 and 5 amplifiers (see Figure 5.12). Therefore, it is not possible to guarantee that applying AcCBR just for LPs with one link will improve the OSNR. Even though, fAcCBR is also evaluated Tata.

Considering fAcCBR-ML1, the OSNR performance remains almost the same as in AcCBR-DB4, with two main degradation of 0.47 dB and 0.39 dB and a maximum improvement 0.87 dB, as presented in the sixth column in Table 5.4. The execution time, in this case, is 98.87 ms. Considering fAcCBR-ML2, there are mostly improvements, with a single degradation of -1.2 dB and a maximum improvement of 0.8 dB, comparing with AcCBR-DB4. The execution time reduction is almost the same achieve with fAcCBR-ML1, near 101 ms, according to the seventh column in Table 5.4.

By increasing the number of links in fAcCBR to 7 and 8 (ML7 and ML8, respectively), there are not significantly OSNR improvements when comparing with ML1 and ML2, as it can be seen in Figure 5.12. Comparing with AcCBR-DB4, it is possible to see two OSNR degradations of 1.19 dB and 0.41 dB for fAcCBR-ML7 (see eighth column in Table 5.4); and three OSNR degradations for fAcCBR-ML8, of 1.16, 0.38, and

0.25 dB (see ninth column in Table 5.4). fAcCBR-ML8 also achieves the best OSNR improvement achieved so far by the fAcCBR, of 1.86 dB for connections 1 link and 4 amplifiers. However, the improvements for the other LPs are very small. Regarding the execution time for these two fAcCBRs, the reduction is 81.90% and 74.49%, for ML7 and ML8, respectively, when compared with AcCBR-DB4.

Therefore, because of the low OSNR improvements and no significant reduction of the execution time, AcCBR-ML7 and ML8 are not viable candidates to be used in Tata. On the other hand, although fAcCBR-ML1 and ML2 present a little degradation for some LPs, they are capable to maintain the OSNR performance for most cases, with a considerable time reduction of near 96% for both. Furthermore, considering these OSNR performance maintenance after applying the fAcCBR for Tata, it is expected that, once the convergence is achieved by the original AcCBR (no OSNR oscillations), it is likely that applying fAcCBR for LPs with up to 2 links will provide the same OSNR performance with a considerable time reduction.

Finally, Figure 5.14 and Table 5.6 present the OSNR results for China Telecom, also for nine representative connection paths. DB1 to DB4 stand for DB sizes of 1.5, 3.0, 4.5, 6 MB, respectively. Figure 5.11 shows that applying AcCBR for up to 3 LPs means to apply it for most connections, and the result in terms of execution time would remain the same. Thus, for this network, AcCBR is applied just for LPs with 1 and 2 links (fAcCBR-ML1 and ML2), with a DB size of 0.16 and 2.2 MB, respectively. These DBs for fAcCBR are also obtained from DB4, by extracting all cases with up to n links. Considering the real distances in China Telecom, connections commonly have up to 77 amplifiers. This maximum number of amplifiers is nearly the same as in Tata (68). However, there are a small number of maximum links per LP, just 5, against 35 in Tata. This means that LPs in China Telecom presents links with long amplifier cascades.

From Figure 5.14, FG presents a better performance than AdGA, just as in previous networks. AcCBR, on the other hand, presents an OSNR improvement with the DB size for all connection paths, even with a small oscillation for LPs with 4 link and 46 amplifiers. These OSNR improvements are also shown in Table 5.6, fifth column, where all values for DB4 - DB0 are positive numbers, ranging from 0.38 to 1.76 dB.

Regarding the execution time, presented in Figure 5.15, FG and AdGA present the lowest values (25.50 and 32.25 ms, respectively), as expected. Observe that these

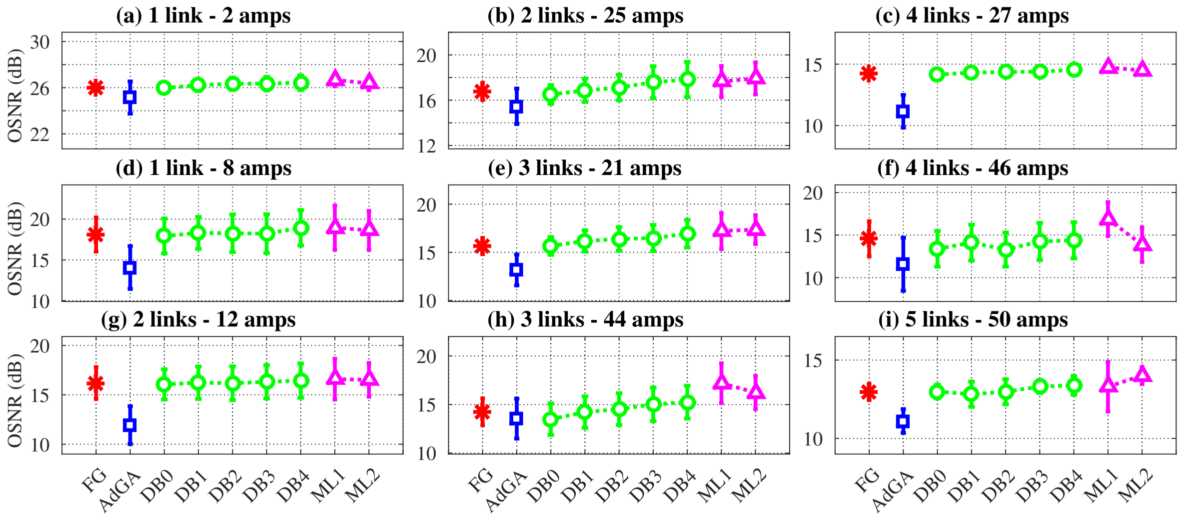

Figure 5.14: OSNR mean and standard deviation results for all the connections present in China Telecom (considering the real link distances) at the time a new connection is established. DB0-DB4 refers to AcCBR. MLn refers to fAcCBR (the AcCBR modification to improve the execution time presented in Section 3.2). For AcCBR: $\kappa = 50\%$, $\beta^{Pin} = 1$ dB, $\beta^{\alpha L} = 2$ dB, $\gamma = 0.5$, $\mu = 0.1$, and $\upsilon = 0.4$.

values are a little higher than what were achieved in Biz Networks, and very small when compared with Tata. The more complex connections in Tata, with high number of links per connections (see Figure 5.11), must contribute to the execution time increase on the non-optimized RWA calculation. Returning to China Telecom, for AcCBR, there is an significant execution time increase from 35.75 ms to 1.03 s from DB0 to DB4. The relationship between DB size and execution time in China Telecom is almost linear.

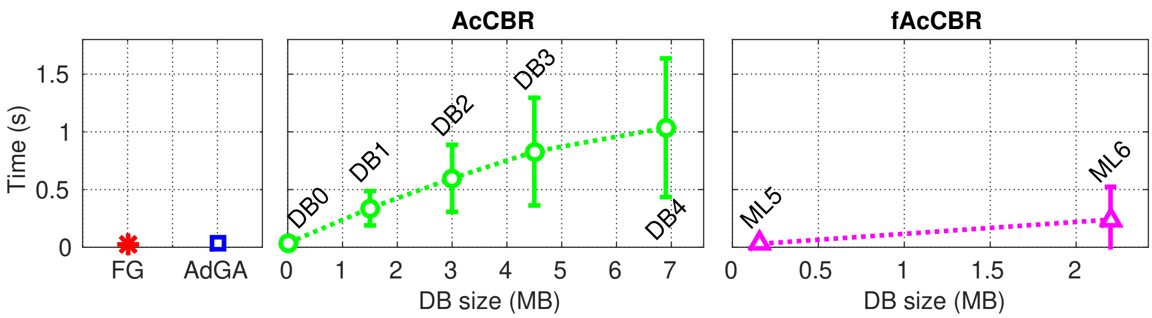

Figure 5.15: Execution time (mean and standard deviation) results for China Telecom (considering the real link distances). DB0-DB4 refers to AcCBR. MLn refers to fAcCBR (the AcCBR modification to improve the execution time presented in Section 3.2). A visible execution time reduction is achieved when applying fAcCBR comparing with AcCBR-DB4. For AcCBR: $\kappa = 50\%$, $\beta^{Pin} = 1$ dB, $\beta^{\alpha L} = 2$ dB, $\gamma = 0.5$, $\mu = 0.1$, and $\upsilon = 0.4$.

Table 5.7 presents the similar connections achieved by the retrieve step when applying AcCBR. Observe that most cases present non-null values for mean similar con-

Table 5.6: Mean OSNR in dB and mean execution time for China Telecom (considering the real link distances), presenting an execution time reduction of up to 97.08% after applying fAcCBR (the AcCBR modification to improve the execution time presented in Section 3.2) when comparing with the most time consuming approach (AcCBR-DB4). For AcCBR: $\kappa = 50\%$, $\beta^{Pin} = 1$ dB, $\beta^{\alpha L} = 2$ dB, $\gamma = 0.5$, $\mu = 0.1$, and $\upsilon = 0.4$.

Link/amp	FG	AdGA	AcCBR		fAcCBR (MLx − DB4)	
			DB0	DB4 (DB4-DB0)	ML1	M2
(a) 1/2	26.01	25.14	25.98	26.43 (+0.46)	26.67 (+0.24)	26.38 (-0.05)
(b) 2/25	16.78	15.46	16.50	17.83 (+1.33)	17.65 (-0.18)	17.93 (+0.10)
(c) 4/27	14.22	11.16	14.16	14.53 (+0.37)	14.73 (+0.20)	14.49 (-0.03)
(d) 1/8	18.11	14.07	17.93	18.94 (+1.01)	18.96 (+0.02)	18.62 (-0.32)
(e) 3/21	15.65	13.17	15.66	16.94 (+1.27)	17.22 (+0.28)	17.36 (+0.42)
(f) 4/46	14.56	11.58	13.39	14.39 (+1.01)	16.87 (+2.48)	13.88 (-0.51)
(g) 2/12	16.20	11.94	16.05	16.44 (+0.39)	16.59 (+0.15)	16.51 (+0.07)
(h) 3/44	14.26	13.55	13.49	15.25 (+1.76)	17.19 (+1.95)	16.24 (+0.99)
(i) 5/50	12.97	11.11	12.99	13.38 (+0.39)	13.30 (-0.09)	14.01 (+0.62)
Time (ms)	25.50	32.25	35.76	1037.94	30.31	239.83
Time reduction compared with fAcCBR-DB4					97.08%	76.89%

nections. However, these values are followed by standard deviations very close to the mean values, meaning that the Cognitive Methodology is not completely applied for some LPs. Thus, the OSNR improvements observed in Figure 5.14 and Table 5.6 are achieved when applying the Cognitive Methodology just for a few LPs, indicating that applying fAcCBR maybe reduce the execution time and maintain the AcCBR performance.

When applying fAcCBR for LPs with just one link (ML1), there are OSNR improvements for most connection paths, except for LPs with 2 links and 2 amplifiers, which present a small degradation of -0.18 dB compared with DB4, as seen in Table 5.6. For the other LPs, the OSNR performances stay almost the same or present improvements of up to 2.48 dB. This high improvement is achieved by the same set of LPs that presents the OSNR oscillation for original AcCBR (4 links and 46 amplifiers). The time reduction for fAcCBR-ML1 is 97.08% when compared with AcCBR-DB4, since the Cognitive

Table 5.7: Similar connections (mean and standard deviation) returned by the retrieve step for China Telecom (considering the real link distances) demonstrating that just some connection paths present a considerable amount of similar connections. For AcCBR: $\kappa = 50\%$, $\beta^{Pin} = 1$ dB, $\beta^{\alpha L} = 2$ dB, $\gamma = 0.5$, $\mu = 0.1$, and $\upsilon = 0.4$.

Link/amp	DB0	DB1	DB2	DB3	DB4
(a) 1/2	0.23 ± 0.50	7.21 ± 4.62	8.38 ± 4.89	11.59 ± 6.94	$\mathbf{14.03 \pm 10.19}$
(b) 2/25	0.04 ± 0.21	1.88 ± 2.24	2.67 ± 2.79	4.08 ± 4.42	$\mathbf{4.91 \pm 4.98}$
(c) 4/27	0.00 ± 0.00	0.34 ± 0.98	0.58 ± 1.06	1.22 ± 1.57	1.23 ± 1.40
(d) 1/8	0.12 ± 0.37	4.78 ± 4.00	10.64 ± 8.92	14.75 ± 10.21	$\mathbf{14.34 \pm 13.12}$
(e) 3/21	0.07 ± 0.25	0.77 ± 1.40	1.70 ± 2.22	2.74 ± 3.12	$\mathbf{3.25 \pm 3.84}$
(f) 4/46	0.00 ± 0.00	0.07 ± 0.26	0.33 ± 0.82	0.45 ± 0.90	1.25 ± 1.37
(g) 2/12	0.07 ± 0.26	1.73 ± 2.23	2.96 ± 3.35	4.70 ± 4.93	$\mathbf{6.15 \pm 6.54}$
(h) 3/44	0.04 ± 0.21	0.43 ± 0.78	0.85 ± 1.33	1.27 ± 1.83	1.89 ± 2.25
(i) 5/50	0.00 ± 0.00	0.10 ± 0.31	0.20 ± 0.41	0.53 ± 0.80	0.35 ± 0.61

Methodology is applied just for less than 10% of the connections, according to Figure 5.11.

For fAcCBR-ML2, there are two main OSNR degradation, -0.32 and -0.51 dB, when compared with AcCBR-DB4, as seen on Table 5.6, last column. In this case, the highest improvement is less than 1 dB. Regarding the execution time, there is a reduction of 76.89% when compared with AcCBR-DB4. It is not a considerable reduction, because for fAcCBR-ML2, the Cognitive Methodology is applied for almost 50% of the connections, as indicated in Figure 5.11.

Thus, for China Telecom, considering applying AcCBR just for LPs with 1 link is sufficient to reduce significantly the execution time (near 98%), while remaining or, for most cases, improving the OSNR performance when compared with AcCBR-DB4. These OSNR improvements may occur by the same reasons detailed in Biz Networks, i. e., the number of connections affected is smaller when applying fAcCBR because the amplifies' gains are not changing all the time a new connection is established.

5.2.3 Partial conclusions

Optical and execution time performances were assessed for AcCBR and fAcCBR, comparing with other two gain conditions: FG and AdGA. These evaluations consider more realistic scenarios, assuming three meshed and dynamic optical networks with different characteristics in terms of size, topology, number of links and nodes. It was also assumed different link distances and number of amplifiers between nodes.

The obtained results showed an OSNR improvement when AcCBR was applied for most cases, demonstrating that the Cognitive Methodology can be applied for networks with different characteristics, presenting performance improvements regardless some oscillations and convergence issues mostly observed in one of the networks. However, these issues do not degrade the optical performance when compared with other gain conditions.

Furthermore, as the AcCBR got more experience, it also became more time consuming. Aiming to overcome this issue, fAcCBR was applied, presenting a considerable execution time reduction of up to 97%, and preserving (or sometimes improving) the optical performance achieved with the original Methodology (AcCBR).

5.3 Concluding remarks

This Chapter evaluated the optical performance of the Cognitive Methodology for different networks topologies, first in a fixed 100-km link scenario, with fixed two amplifiers per link, different traffic loads and amplifier models. Then, considering the real distances between nodes. On the last scenario, the execution time was also explored.

All the results have shown that the Cognitive Methodology (AcCBR) had a learning capability for most evaluated scenarios. It shown OSNR improvements of up to 2 dB as DB size increase for 100-km fixed links networks, and up to 2.4 dB for different link distances. On the last scenario, the Cognitive Methodology also had some convergence issues for the network with the most lighpath diversity (Tata). However, as already mentioned, these convergence issues did not degrade the OSNR performance when compared with other gain condition approaches.

Moreover, it was also observed that these OSNR improvements come with a high cost: the execution time increase. Thus, the Cognitive Methodology was modified aiming to mitigate this drawback. This modification (named fAcCBR) was applied to the last evaluated scenario, which considers different link distances. The results showed a significant execution time reduction when compared with the original Methodology, of up to around 97%. And, the most important, this modification did not degrade the optical performance improvement achieved with the original Methodology.

Therefore, the main contribution of this Thesis, which is a Cognitive Methodology that improves the optical performance of the connections over the time, is achieved. It is possible to apply this Methodology in different networks topologies, considering different scenarios of amplifier models, traffic loads, link distances and number of amplifiers per link, ensuring optical performance improvements and low execution time.

Chapter 6

Conclusions

This Thesis comprised the proposal and validation of the Cognitive Methodology to improve the optical performance of the connections in dynamic and WDM networks. The Cognitive Methodology is designed to be applied during the RWA procedure, when a connection is established. It adjusts the operating point of the amplifiers along the lightpath based on the optical performance of previous connections using a problem solve approach called CBR.

The main results achieved when applying the Cognitive Methodology (presented in Chapters 4 and 5) are following summarized:

- Simulations considering the Autonomous Network (AN) presented cognitive behavior (OSNR improvements over time);
- Experimental validation at AN presented OSNR improvements of up to 4 dB when compared with other gain conditions;
- In simulations considering real and different network topologies, with fixed link distances and considering different amplifier models and traffic loads, the Cognitive Methodology achieved the best OSNR performance, after the learning process, for most cases;

- Also in simulations, considering the real distances between nodes, there were OSNR improvements over time for most cases. There were also some non-convergence issues, that did not degrade the OSNR performance when compared with other gain conditions (considering an error margin);

- Still considering the real distances between nodes, it was shown that the Cognitive Methodology became more time consuming when the database (DB) increase.

- Aiming to address the execution time drawback, it was proposed a modification on the Cognitive Methodology. This modification presented a considerable execution time reduction (of up to 97%), preserving (or improving) the optical performance achieved with the original Methodology.

Therefore, the main contribution of this work is an amplifier gain adjustment methodology that improves the optical performance of the connections over time in a cognitive approach. Furthermore, the Methodology is upgraded to reduce the execution time, without degrade the optical performance.

It is important to point out that these OSNR improvements are very important from the operators point of view, since the network upgrade normally occurs on the edge of the network (by evolving the modulation formats and increasing the data rates). The core elements, such as the optical fibers and amplifiers remain the same. Thus, achieving up to 3.3 dB of OSNR improvement by controlling the amplifiers is very positive since it can be done with the optical resources already on field.

Moreover, the main advantages of the proposed Methodology are:

- The Cognitive Methodology is able to learn by itself, without human intervention;

- The Methodology can be applied without previous solution domain knowledge;

- It can be applied to any amplifier technology (EDFA, Raman, hybrid, SOA), since it has an automatic gain control (AGC) and has been previously characterized;

- It does not need any real time measurement, since it estimates the OSNR performance;

- It can be applied to any network topology, any amplifier model, any traffic load, as demonstrated on the results presented in Chapters 4 and 5;

- Even with some convergence issues for networks with high number of links and more diverse lighpaths, the Cognitive Methodology does not degrades the OSNR when compared with other gain conditions (FG and AdGA), achieving, at least, the same optical performance (considering an error margin).

On the other hand, the Cognitive Methodology shares the same limitations and drawbacks as CBR, listed bellow:

- The DB growth, which is related to the performance improvement, requires large memory resources and increases the computational time;
- The DB may not cover the solutions domain in a proper way;
- Because it estimates the OSNR, the devices' modeling must be reliable;
- The amplifier gain adjustments for each connection establishment may cause power transients that must be evaluated in-depth;
- Increase the number of features on DB also increase the computational time;

6.1 Future works

Some ideas for further investigation arise from the current work. These ideas are listed below:

- Consider the non-linear effects on the OSNR estimation by the analytical model proposed by [150];
- Consider WSS filtering impact;
- Evolve the Cognitive Methodology to be applied in flexgrid scenarios;
- Study of power transients caused by the gain adjustment at each new connection;
- Improve retrieve step to reduce to execution time [125];
- Consider the channel (frequency) information as a feature of the DB;
- Consider noise figure per channel to estimate the OSNR on simulations;

- Investigate other values for the probabilistic parameters considered on the reuse step (κ, β^{Pin} and $\beta^{\alpha L}$);
- Investigate other values for the exploration and exploitation parameters considered on the reuse step (γ, μ and υ);
- Investigate other adaptation methods on the reuse step;
- Evaluate also the worst OSNR, instead of the mean OSNR;
- Compare the Cognitive Methodology results with the exhaustive search in a small network (for reference);
- Evaluate the Cognitive Methodology in terms of some global metric, such as the block probability with OSNR constraints;
- Apply the cognitive methodology also on dealocation events.

6.2 Publications

First results were accepted for oral presentation at an international conference in 2015. This paper was selected as one of the 10% top-scored papers in the conference and was invited to be expanded into a journal paper. These two publications are following described:

- U. Moura et al.,"SDN-enabled EDFA gain adjustment cognitive methodology for dynamic optical networks," 2015 European Conference on Optical Communication (ECOC), Valencia, 2015, pp. 1-3.
- U. Moura et al., "Cognitive Methodology for Optical Amplifier Gain Adjustment in Dynamic DWDM Networks," Journal of Lightwave Technology, vol. 34, pp. 1971-1979, April 2016.

Additional simulation results were published in book chapter and other international conference (also for oral presentation):

- U. C. Moura, M. Garrich, A. C. Cesar, J. D. Reis, J. Oliveira, and E. Conforti,"Optical amplifier cognitive gain adjustment methodology for dynamic and realistic networks.", Springer, Cognitive Technologies, 2017.

- U. C. Moura, M. Garrich, A. C. Cesar, E. d. S. Rosa, J. Oliveira, and E. Conforti, "Execution Time Improvement for Optical Amplifier Cognitive Methodology in Dynamic WDM Networks." SBMO/IEEE MTT-S International Microwave and Optoelectronics Conference (IMOC), 2017.

Moreover, a national patent application and a software registration are also important outcomes of this work:

- Title: "*Método Cognitivo para o Ajuste do Ponto de Operação de Amplificadores Ópticos em Redes Ópticas Dinâmicas*". Process number: BR 10 2015 030459-5 and INPI. Filing date: 4th of December, 2015.

- Title: "*Código de Controle de Ganho Cognitivo para Amplificadores Ópticos - v1.0*". Process number: BR 51 2015 001373-4 at INPI. Publication date: 5th of april, 2016.

Bibliography

[1] Cisco, *The Zettabyte Era: Trends and Analysis*, 6 2016. white paper. 22

[2] P. A. Govind, *Fiber-Optic Communication Systems*. John Wiley & Sons, New York, 2002. 22, 34, 35, 36, 37, 41, 42

[3] E. Agrell, M. Karlsson, A. Chraplyvy, D. J. Richardson, P. M. Krummrich, P. Winzer, K. Roberts, J. K. Fischer, S. J. Savory, B. J. Eggleton, *et al.*, "Roadmap of optical communications," *Journal of Optics*, vol. 18, no. 6, p. 063002, 2016. 23, 31, 32, 34, 35

[4] Y. Zhu, K. Zou, and F. Zhang, "C-band 112Gb/s nyquist single sideband direct detection transmission over 960km SSMF," *IEEE Photonics Technology Letters*, 2017. 23

[5] L. Velasco, A. P. Vela, F. Morales, and M. Ruiz, "Designing, operating, and reoptimizing elastic optical networks," *Journal of Lightwave Technology*, vol. 35, pp. 513–526, Feb 2017. 23

[6] G. M. Fernandes, N. J. Muga, and A. N. Pinto, "Space-demultiplexing based on higher-order poincaré spheres," *Optics Express*, vol. 25, no. 4, pp. 3899–3915, 2017. 23

[7] U. Moura, M. Garrich, H. Carvalho, M. Svolenski, A. Andrade, A. C. Cesar, J. Oliveira, and E. Conforti, "Cognitive methodology for optical amplifier gain adjustment in dynamic DWDM networks," *Journal of Lightwave Technology*, vol. 34,

pp. 1971–1979, April 2016. 23, 24, 57, 58, 65, 67, 68, 69, 70, 72, 73, 74, 75, 76, 78, 79, 80, 81, 82, 83, 84, 89,

[8] J. P. Fernandez-Palacios, V. López, B. Cruz, and O. G. de Dios, “Elastic optical networking: An operators perspective,” in *European Conf. on Optical Communication (ECOC), Cannes, France*, 2014. 24

[9] H. Zang, J. P. Jue, B. Mukherjee, *et al.*, “A review of routing and wavelength assignment approaches for wavelength-routed optical WDM networks,” *Optical networks magazine*, vol. 1, no. 1, pp. 47–60, 2000. 24, 33

[10] A. G. Rahbar, “Review of dynamic impairment-aware routing and wavelength assignment techniques in all-optical wavelength-routed networks.,” *IEEE Communications Surveys and Tutorials*, vol. 14, no. 4, pp. 1065–1089, 2012. 24

[11] C. J. A. Bastos-Filho, R. C. L. Silva, D. A. R. Chaves, A. V. S. Xavier, and J. F. Martins-Filho, “Comparing OSNR based policies for an adaptive-alternative IA-RWA algorithm applied to all-optical networks,” *Journal of Microwaves, Optoelectronics and Electromagnetic Applications*, vol. 12, pp. 694 – 706, 12 2013. 24

[12] X. Wang, M. Brandt-Pearce, and S. Subramaniam, “Distributed grooming, routing, and wavelength assignment for dynamic optical networks using ant colony optimization,” *J. Opt. Commun. Netw.*, vol. 6, pp. 578–589, Jun 2014. 24

[13] Y. Li, H. Dai, G. Shen, and S. K. Bose, “Adaptive FEC-based lightpath routing and wavelength assignment in WDM optical networks,” *Optical Switching and Networking*, vol. 14, Part 3, pp. 241 – 249, 2014. 24

[14] J. D. Reis, M. Garrich, D. M. Pataca, J. C. M. Diniz, V. N. Rozental, L. H. H. Carvalho, E. C. Magalhães, U. Moura, N. G. Gonzalez, J. R. F. Oliveira, and J. C. R. F. Oliveira, “Flexible optical transmission systems for future networking,” in *Telecommunications Network Strategy and Planning Symposium (Networks), 2014 16th International*, pp. 1–6, Sept 2014. 24

[15] F. Cugini, G. Meloni, F. Paolucci, N. Sambo, M. Secondini, L. Gerardi, L. Poti, and P. Castoldi, “Demonstration of flexible optical network based on path computation element,” *Journal of Lightwave Technology*, vol. 30, pp. 727–733, March 2012. 24

[16] H. Y. Choi, L. Liu, T. Tsuritani, and I. Morita, "Demonstration of BER-Adaptive WSON employing flexible transmitter/receiver with an extended openflow-based control plane," *Photonics Technology Letters, IEEE*, vol. 25, no. 2, pp. 119–121, 2013. 24

[17] Q. Zhuge, M. Morsy-Osman, X. Xu, M. Chagnon, M. Qiu, and D. V. Plant, "Spectral efficiency-adaptive optical transmission using time domain hybrid QAM for agile optical networks," *Journal of Lightwave Technology*, vol. 31, pp. 2621–2628, Aug 2013. 25

[18] Q. Zhuge, X. Xu, M. Morsy-Osman, M. Chagnon, M. Qiu, and D. Plant, "Time domain hybrid QAM based rate-adaptive optical transmissions using high speed DACs," p. OTh4E.6, Optical Society of America, 2013. 25

[19] C. Franciscangelis, L. H. H. Carvalho, J. D. Reis, V. E. Parahyba, F. D. S. oes, D. M. Pataca, E. S. Rosa, V. N. Rozental, J. R. F. Oliveira, N. G. Gonzalez, and J. C. R. F. Oliveira, "Network survivability field trial over brazilian legacy optical fiber links through advanced transponder reconfiguration," in *2014 The European Conference on Optical Communication (ECOC)*, pp. 1–3, Sept 2014. 25

[20] L. H. H. Carvalho, C. Franciscangelis, U. R. Duarte, V. N. Rozental, J. D. Reis, F. B. Fideles, G. J. Suzigan, F. D. Simões, V. E. Parahyba, N. G. Gonzalez, A. C. Bordonalli, and J. C. R. F. Oliveira, "Multidimensional optimization of optical spectral shaping for fiber nonlinearities mitigation in high baud-rate systems," in *2014 The European Conference on Optical Communication (ECOC)*, pp. 1–3, Sept 2014. 25

[21] C. de A. S. Diniz, M. Garrich, G. J. Suzigan, J. S. Assine, J. D. Reis, J. R. F. de Oliveira, and D. A. A. Mello, "Embedded system for optical spectral optimization based on a genetic algorithm," in *Microwave and Optoelectronics Conference (IMOC), 2015 SBMO/IEEE MTT-S International*, pp. 1–4, Nov 2015. 25

[22] E. Magalhães, M. Garrich, H. Carvalho, M. Magalhães, N. González, J. Oliveira, A. Bordonalli, and J. Oliveira, "Global WSS-based equalization strategies for SDN metropolitan mesh optical networks," in *European Conference on Optical Communications (ECOC)*, 2014. 25

[23] X. Wang, Y. Fei, M. Razo, A. Fumagalli, and M. Garrich, "Network-wide signal power control strategies in WDM networks," in *Optical Network Design and Modeling (ONDM), 2015 International Conference on*, pp. 218–221, IEEE, 2015. 25

[24] V. V. Nascimento, J. C. de Oliveira, V. B. Ribeiro, and A. C. Bordonalli, "Dynamic gain equalization for erbium doped fiber amplifiers based on optoceramic sinusoidal filter cascade," *Microwave and Optical Technology Letters*, vol. 53, no. 3, pp. 623–626, 2011. 25

[25] U. C. de Moura, J. R. Oliveira, J. C. R. Oliveira, and A. C. Cesar, "EDFA adaptive gain control effect analysis over an amplifier cascade in a DWDM optical system," in *Microwave & Optoelectronics Conference (IMOC), 2013 SBMO/IEEE MTT-S International*, pp. 1–5, IEEE, 2013. 25, 46, 47

[26] U. C. de Moura, J. R. Oliveira, and A. C. Oliveira, "Roteamento de tráfego em redes WDM dinâmicas utilizando amplificadores ópticos com controle adaptativo de ganho," in 16° *SBMO - Simpósio Brasileiro de Micro-ondas e Optoeletrônica e* 11° *CBMag - Congresso Brasileiro de Eletromagnetismo*, pp. 7–12, MOMAG, 2014. *In portuguese.* 25, 46, 47

[27] D. A. Barboza, C. J. Bastos-Filho, J. F. Martins-Filho, U. C. de Moura, J. R. de Oliveira, *et al.*, "Self-adaptive erbium-doped fiber amplifiers using machine learning," in *Microwave & Optoelectronics Conference (IMOC), 2013 SBMO/IEEE MTT-S International*, pp. 1–5, IEEE, 2013. 25, 46, 53

[28] E. d. A. Barboza, M. J. da Silva, L. D. Coelho, J. F. Martins-Filho, C. J. A. Bastos-Filho, U. C. de Moura, and J. R. F. de Oliveira, "Impact of nonlinear effects on the performance of 120 Gb/s 64 QAM optical system using adaptive control of cascade of amplifiers," in *2015 SBMO/IEEE MTT-S International Microwave and Optoelectronics Conference (IMOC)*, pp. 1–5, Nov 2015. 25, 46, 53

[29] E. d. A. Barboza, C. J. A. Bastos-Filho, J. F. M. Filho, M. J. da Silva, L. D. Coelho, U. C. de Moura, and J. R. F. de Oliveira, "Local and global approaches for the adaptive control of a cascade of amplifiers," *Photonic Network Communications*, vol. 33, no. 2, pp. 194–207, 2017. 25, 46, 53

[30] Q. H. Mahmoud, *Front Matter*, pp. i–xxxii. John Wiley & Sons, Ltd, 2007. 25, 26

[31] G. S. Zervas and D. Simeonidou, "Cognitive optical networks: Need, requirements and architecture," in *Transparent Optical Networks (ICTON), 2010 12th International Conference on*, pp. 1–4, IEEE, 2010. 25

[32] R. W. Thomas, D. H. Friend, L. DaSilva, A. B. Mackenzie, *et al.*, "Cognitive networks: Adaptation and learning to achieve end-to-end performance objectives," *Communications Magazine, IEEE*, vol. 44, no. 12, pp. 51–57, 2006. 25

[33] "Community research and development information service," 2010. 26

[34] I. T. Monroy, D. Zibar, N. G. Gonzalez, and R. Borkowski, "Cognitive heterogeneous reconfigurable optical networks (CHRON): Enabling technologies and techniques," in *Proc. ICTON*, vol. 11, 2011. 26

[35] I. Rodríguez, R. J. Durán, D. Siracusa, I. de Miguel, A. Francescon, J. C. Aguado, E. Salvadori, and R. M. Lorenzo, "Minimization of the impact of the TED inaccuracy problem in PCE-based networks by means of cognition," in *Optical Communication (ECOC 2013), 39th European Conference and Exhibition on*, pp. 1–3, IET, 2013. 26

[36] R. J. Durán, N. Fernández, D. Siracusa, A. Francescon, I. de Miguel, I. Rodríguez, J. C. Aguado, E. Salvadori, and R. M. Lorenzo, "Experimental assessment of a cognitive mechanism to reduce the impact of outdated TEDs in optical networks," *Photonic Network Communications*, vol. 31, no. 2, pp. 259–271, 2016. 26

[37] N. Fernández, R. J. Durán, I. de Miguel, J. C. Aguado, N. Merayo, R. M. Lorenzo, D. Siracusa, A. Francescon, and E. Salvadori, "Demonstration of proactive restoration in cognitive heterogeneous reconfigurable optical networks," in *10th International Conference on Heterogeneous Networking for Quality, Reliability, Security and Robustness*, pp. 131–132, Aug 2014. 26

[38] R. Borkowski, A. Caballero, D. Klonidis, C. Kachris, A. Francescon, I. de Miguel, R. J. D. Barroso, D. Zibar, I. Tomkos, and I. Tafur, "Advanced modulation formats in cognitive optical networks: EU project CHRON demonstration," in *Optical Fiber Communication Conference*, pp. W3H–1, Optical Society of America, 2014. 26

[39] D. Siracusa, F. Pederzolli, R. L. Cigno, and E. Salvadori, "Energy saving through traffic profiling and prediction in self-optimizing optical networks," p. W4H.1, Optical Society of America, 2014. 26

[40] R. Duran, N. Fernandez, I. de Miguel, M. Angelou, D. Sánchez, J. Aguado, T. Jiménez, P. Fernandez, N. Merayo, N. Atallah, *et al.*, "Advantages of using cognition when solving impairment-aware virtual topology design problems," in *Transparent Optical Networks (ICTON), 2011 13th International Conference on*, pp. 1–4, IEEE, 2011. 26

[41] N. Fernández, R. J. Durán, I. De Miguel, J. C. Aguado, T. Jiménez, M. Angelou, D. Sánchez, P. Fernández, N. Merayo, N. Atallah, *et al.*, "Cognitive algorithm to solve the impairment-aware virtual topology design problem in reconfigurable optical networks," in *Cognitive Methods in Situation Awareness and Decision Support (CogSIMA), 2012 IEEE International Multi-Disciplinary Conference on*, pp. 170–173, IEEE, 2012. 26

[42] D. Siracusa, A. Francescon, N. Fernández, I. de Miguel, R. J. Durán, J. C. Aguado, and E. Salvadori, "Experimental evaluation of virtual topology design and reconfiguration in optical networks by means of cognition," in *OFC 2014*, pp. 1–3, March 2014. 26

[43] R. Borkowski, R. J. Durán, C. Kachris, D. Siracusa, A. Caballero, N. Fernández, D. Klonidis, A. Francescon, T. Jiménez, J. C. Aguado, *et al.*, "Cognitive optical network testbed: EU project CHRON [invited]," *Journal of Optical Communications and Networking*, vol. 7, no. 2, pp. A344–A355, 2015. 26

[44] N. Fernández, R. J. D. Barroso, D. Siracusa, A. Francescon, I. de Miguel, E. Salvadori, J. C. Aguado, and R. M. Lorenzo, "Virtual topology reconfiguration in optical networks by means of cognition: Evaluation and experimental validation [invited]," *J. Opt. Commun. Netw.*, vol. 7, pp. A162–A173, Jan 2015. 26

[45] D. Siracusa, E. Salvadori, A. Francescon, A. Zanardi, M. Angelou, D. Klonidis, I. Tomkos, D. Sánchez, R. Durán, and I. de Miguel, "A control plane framework for future cognitive heterogeneous optical networks," in *Transparent Optical Networks (ICTON), 2012 14th International Conference on*, pp. 1–4, IEEE, 2012. 26

[46] G. Zervas, K. Banias, B. R. Rofoee, N. Amaya, and D. Simeonidou, "Multi-core, multi-band and multi-dimensional cognitive optical networks: An architecture on demand approach," in *Transparent Optical Networks (ICTON), 2012 14th International Conference on*, pp. 1–4, IEEE, 2012. 26

[47] X. Zhang, W. Hou, L. Guo, S. Wang, Y. Sun, and X. Yang, "Failure recovery solutions using cognitive mechanisms for software defined optical networks," in *2016 15th International Conference on Optical Communications and Networks (ICOCN)*, pp. 1–3, Sept 2016. 26

[48] X. Zhang, L. Guo, W. Hou, Q. Zhang, and S. Wang, "Failure recovery solutions using cognitive mechanisms based on software-defined optical network platform," *Optical Engineering*, vol. 56, no. 1, p. 016107, 2017. 26

[49] G. Papadimitriou, P. Nicopolitidis, E. Varvarigos, *et al.*, "Towards power consumption in optical networks: a cognitive prediction-based technique," *International Journal of Communication Systems*, 2015. 26

[50] T. R. Tronco, M. M. Feres, A. C. César, and M. de Lacerda Rocha, "Self-configuration and self-healing for cognitive optical networks," *Journal of Microwaves, Optoelectronics and Electromagnetic Applications (JMOe)*, vol. 12, pp. 193–205, 2013. 26

[51] T. R. Tronco, M. Garrich, A. C. César, and M. d. L. Rocha, "Cognitive algorithm using fuzzy reasoning for software-defined optical network," *Photonic Network Communications*, vol. 32, no. 2, pp. 281–292, 2016. 26

[52] A. Aamodt and E. Plaza, "Case-based reasoning: Foundational issues, methodological variations, and system approaches," *AI communications*, vol. 7, no. 1, pp. 39–59, 1994. 26, 49, 51

[53] J. L. Kolodner, "An introduction to case-based reasoning," *Artificial Intelligence Review*, vol. 6, no. 1, pp. 3–34, 1992. 26, 49, 60

[54] S. Begum, M. U. Ahmed, P. Funk, N. Xiong, and M. Folke, "Case-based reasoning systems in the health sciences: A survey of recent trends and developments,"

IEEE Transactions on Systems, Man, and Cybernetics, Part C (Applications and Reviews), vol. 41, pp. 421–434, July 2011. 26

[55] S. Montani, L. C. Jain, *et al.*, *Successful case-based reasoning applications*, vol. 305. Springer, 2010. 26

[56] M. Lenz, B. Bartsch-Spörl, H.-D. Burkhard, and S. Wess, *Case-based reasoning technology: from foundations to applications*, vol. 1400. Springer, 2003. 26

[57] S. V. Shokouhi, P. Skalle, and A. Aamodt, "An overview of case-based reasoning applications in drilling engineering," *Artificial Intelligence Review*, vol. 41, no. 3, pp. 317–329, 2014. 26

[58] M. Lee, C. Koo, T. Hong, and H. S. Park, "Framework for the mapping of the monthly average daily solar radiation using an advanced case-based reasoning and a geostatistical technique," *Environmental Science & Technology*, vol. 48, no. 8, pp. 4604–4612, 2014. PMID: 24635702. 26

[59] J. Dou, K.-T. Chang, S. Chen, A. P. Yunus, J.-K. Liu, H. Xia, and Z. Zhu, "Automatic case-based reasoning approach for landslide detection: Integration of object-oriented image analysis and a genetic algorithm," *Remote Sensing*, vol. 7, no. 4, pp. 4318–4342, 2015. 26

[60] A. Sene, B. Kamsu-Foguem, and P. Rumeau, "Telemedicine framework using case-based reasoning with evidences," *Computer methods and programs in biomedicine*, vol. 121, no. 1, pp. 21–35, 2015. 27

[61] R. Platon, V. R. Dehkordi, and J. Martel, "Hourly prediction of a building's electricity consumption using case-based reasoning, artificial neural networks and principal component analysis," *Energy and Buildings*, vol. 92, pp. 10 – 18, 2015. 27

[62] I. L. Chung, C. M. Chou, C. P. Hsu, and D. K. Li, "A programming learning diagnostic system using case-based reasoning method," in *2016 International Conference on System Science and Engineering (ICSSE)*, pp. 1–4, July 2016. 27

[63] L. Rintala, M. Leikola, C. Sauer, J. Aromaa, T. Roth-Berghofer, O. Forsén, and M. Lundstrom, "Designing gold extraction processes: Performance study of a case-based reasoning system," *Minerals Engineering*, vol. 109, pp. 42 – 53, 2017. 27

[64] P. Pesl, P. Herrero, M. Reddy, N. Oliver, D. G. Johnston, C. Toumazou, and P. Georgiou, "Case-based reasoning for insulin bolus advice," *Journal of Diabetes Science and Technology*, vol. 11, no. 1, pp. 37–42, 2017. 27

[65] T. Jiménez, I. de Miguel, J. Aguado, R. Durán, N. Merayo, N. Fernández, D. Sánchez, P. Fernández, N. Atallah, E. Abril, *et al.*, "Case-based reasoning (CBR) to estimate the q-factor in optical networks: An initial approach," in *Networks and Optical Communications (NOC), 2011 16th European Conference on*, pp. 181–184, IEEE, 2011. 27

[66] T. Jiménez, J. C. Aguado, I. de Miguel, R. J. Durán, N. Fernandez, M. Angelou, D. Sánchez, N. Merayo, P. Fernández, N. Atallah, *et al.*, "A cognitive system for fast quality of transmission estimation in core optical networks," in *Optical Fiber Communication Conference*, pp. OW3A–5, Optical Society of America, 2012. 27

[67] T. Jiménez, J. C. Aguado, I. De Miguel, R. J. Durán, N. Fernández, M. Angelou, D. Sánchez, N. Merayo, P. Fernández, N. Atallah, *et al.*, "Enhancing optical networks with cognition: Case-based reasoning to estimate the quality of transmission," in *Cognitive Methods in Situation Awareness and Decision Support (CogSIMA), 2012 IEEE International Multi-Disciplinary Conference on*, pp. 166–169, IEEE, 2012. 27

[68] A. Caballero, J. C. Aguado, R. Borkowski, S. Saldaña, T. Jiménez, I. de Miguel, V. Arlunno, R. J. Durán, D. Zibar, J. B. Jensen, *et al.*, "Experimental demonstration of a cognitive quality of transmission estimator for optical communication systems," *Optics express*, vol. 20, no. 26, pp. B64–B70, 2012. 27

[69] T. Jiménez, J. C. Aguado, I. de Miguel, R. J. Durán, M. Angelou, N. Merayo, P. Fernández, R. M. Lorenzo, I. Tomkos, and E. J. Abril, "A cognitive quality of transmission estimator for core optical networks," *Journal of Lightwave Technology*, vol. 31, no. 6, pp. 942–951, 2013. 27

[70] A. Caballero, R. Borkowski, D. Zibar, and I. T. Monroy, "Performance monitoring techniques supporting cognitive optical networking," in *Transparent Optical Networks (ICTON), 2013 15th International Conference on*, pp. 1–4, IEEE, 2013. 27

[71] Z. Chen, S. Wang, H. Zhang, Y. Liu, and Y. Peng, "Cognitive routing and wavelength assignment algorithm for dynamic optical networks," in *2014 12th International Conference on Optical Internet 2014 (COIN)*, pp. 1–3, Aug 2014. 27

[72] S. Wang, Z. Chen, Y. Liu, Y. Peng, and H. Zhang, "Cognitive approaches for physical impairment-aware routing and wavelength assignment in dynamic optical networks," in *Multimedia Technology IV: Proceedings of the 4th International Conference on Multimedia Technology, Sydney, Australia, 28-30 March 2015*, p. 15, CRC Press, 2015. 27

[73] D. Semrau, T. Xu, N. A. Shevchenko, M. Paskov, A. Alvarado, R. I. Killey, and P. Bayvel, "Achievable information rates estimates in optically amplified transmission systems using nonlinearity compensation and probabilistic shaping," *Opt. Lett.*, vol. 42, pp. 121–124, Jan 2017. 27

[74] D. Aguiar, G. Grasso, A. Righetti, and F. Meli, "EDFA with continuous amplification of c and l bands for submarine applications," in *2015 SBMO/IEEE MTT-S International Microwave and Optoelectronics Conference (IMOC)*, pp. 1–4, Nov 2015. 27

[75] S. V. Firstov, V. F. Khopin, S. V. Alyshev, K. E. Riumkin, M. A. Melkumov, A. N. Guryanov, and E. M. Dianov, "Bismuth-doped optical fiber amplifier and watt-level CW laser for the spectral region 1600 - 1800 nm," p. M3D.6, Optical Society of America, 2016. 27

[76] S. V. Firstov, V. F. Khopin, K. E. Riumkin, S. V. Alyshev, M. A. Melkumov, A. N. Guryanov, and E. M. Dianov, "Bi/er co-doped fibers as an active medium for optical amplifiers for the c-, l- and u- telecommunication bands," in *ECOC 2016; 42nd European Conference on Optical Communication*, pp. 1–3, Sept 2016. 27

[77] Y. Jung, Z. Li, N. Simakov, J. M. O. Daniel, D. Jain, P. C. Shardlow, A. M. Heidt, J. K. Sahu, A. Hemming, W. A. Clarkson, S. U. Alam, and D. J. Richardson, "Silica-based thulium doped fiber amplifiers for wavelengths beyond the l-band," in *2016 Optical Fiber Communications Conference and Exhibition (OFC)*, pp. 1–3, March 2016. 28

[78] Y. Sun, J.-X. Cai, hongbin zhang, H. Batshon, O. Sinkin, C. Davidson, D. Foursa, and A. Pilipetskii, "Optimum design of hybrid Raman-EDFA system to maximize aggregate capacity," p. AS3F.1, Optical Society of America, 2015. 28

[79] J. R. F. de Oliveira, U. C. de Moura, G. E. R. de Paiva, A. P. de Freitas, L. H. H. de Carvalho, V. E. Parahyba, J. C. R. F. de Oliveira, and M. A. Romero, "Hybrid EDFA/raman amplification topology for repeaterless 4.48 tb/s (40 x 112 Gb/s DP-QPSK) transmission over 302 km of g.652 standard single mode fiber," *Journal of Lightwave Technology*, vol. 31, pp. 2799–2808, Aug 2013. 28

[80] M. M. J. Martini, C. E. S. Castellani, M. J. Pontes, M. R. N. Ribeiro, and H. J. Kalinowski, "Performance comparison for raman+EDFA and EDFA+raman hybrid amplifiers using recycled multiple pump lasers for WDM systems," in *2015 SBMO/IEEE MTT-S International Microwave and Optoelectronics Conference (IMOC)*, pp. 1–5, Nov 2015. 28

[81] W. Forysiak, D. S. Govan, I. McClean, B. K. Nayar, O. A. Olubodun, and N. J. Doran, "Analysis of extended range variable gain hybrid Raman-EDFAs in systems using Nyquist-WDM 100/200G PM-QPSK/16QAM," in *OFC 2014*, pp. 1–3, March 2014. 28

[82] Y. Tsuchida, K. Maeda, K. Watanabe, K. Takeshima, T. Sasa, T. Saito, S. Takasaka, Y. Kawaguchi, T. Tsuritani, and R. Sugizaki, "Cladding pumped seven-core EDFA using an absorption-enhanced erbium doped fibre," in *ECOC 2016; 42nd European Conference on Optical Communication*, pp. 1–3, Sept 2016. 28

[83] Y. Wakayama, K. Igarashi, D. Soma, H. Taga, and T. Tsuritani, "Novel 6-mode fibre amplifier with large erbium-doped area for differential modal gain minimization," in *ECOC 2016; 42nd European Conference on Optical Communication*, pp. 1–3, Sept 2016. 28

[84] M. Wada, T. Sakamoto, S. Aozasa, T. Mori, T. Yamamoto, and K. Nakajima, "Core-pumped 10-mode EDFA with cascaded EDF configuration," in *ECOC 2016; 42nd European Conference on Optical Communication*, pp. 1–3, Sept 2016. 28

[85] S. LaRochelle, C. Jin, and Y. Messaddeq, "Design and characterization of multi-core erbium-doped fibers," in *ECOC 2016; 42nd European Conference on Optical Communication*, pp. 1–3, Sept 2016. 28

[86] J. Li, J. Du, L. Ma, M.-J. Li, and Z. He, "Second-order few-mode distributed raman amplifier for mode-division multiplexing transmission," p. Th4A.3, Optical Society of America, 2017. 28

[87] R. Ramaswami, K. Sivarajan, and G. Sasaki, *Optical networks: a practical perspective.* Morgan Kaufmann, 2010. 30, 32, 33, 34, 37, 38, 39, 40, 41, 42, 44

[88] G. P. Agrawal, *Lightwave technology: telecommunication systems.* John Wiley & Sons, New York, 2005. 31, 32, 34, 37, 38, 40

[89] T. S. El-Bawab, *Optical switching.* Springer, 2006. 31, 32

[90] S. Azodolmolky, M. Klinkowski, E. Marin, D. Careglio, J. S. Pareta, and I. Tomkos, "A survey on physical layer impairments aware routing and wavelength assignment algorithms in optical networks," *Computer Networks*, vol. 53, no. 7, pp. 926 – 944, 2009. 33, 34

[91] R. Bellman, "On a routing problem," *Quarterly of applied mathematics*, vol. 16, no. 1, pp. 87–90, 1958. 33

[92] E. W. Dijkstra, "A note on two problems in connexion with graphs," *Numerische Mathematik*, vol. 1, no. 1, pp. 269–271, 1959. 33

[93] B. Mukherjee, *Optical WDM networks.* Springer Science & Business Media, 2006. 34

[94] P. M. Becker, A. A. Olsson, and J. R. Simpson, *Erbium-doped fiber amplifiers: fundamentals and technology.* Academic press, 1999. 35, 40, 41, 45,

[95] J. Zyskind and A. Srivastava, *Optically amplified WDM networks.* Academic press, 2011. 35, 36

[96] E. Desurvire, J. R. Simpson, and P. C. Becker, "High-gain erbium-doped traveling-wave fiber amplifier," *Opt. Lett.*, vol. 12, pp. 888–890, Nov 1987. 36

[97] A. Einstein, "Strahlungs-emission und absorption nach der quantentheorie," *Deutsche Physikalische Gesellschaft*, vol. 18, 1916. 37

[98] G. Keiser, *Optical Fiber Communications.* John Wiley & Sons, Inc., 2003. 37, 41, 42, 43

[99] C. Headley and G. Agrawal, *Raman amplification in fiber optical communication systems.* Academic press, 2005. 42, 44, 45

[100] U. C. Moura, J. R. Oliveira, R. L. Amgarten, G. E. Paiva, and J. C. F. Oliveira, "Caracterizador automatizado de máscara de potência de amplificadores ópticos para redes WDM reconfiguráveis," in *XXX Brazilian Symposium on Telecommunication, Brasilia, Brazil*, 2012. *In portuguese.* 45

[101] Lumentum, *Multichannel Erbium-Doped Fiber Amplifier (EDFA)*, 2015. 45

[102] U. C. d. Moura, "Metodologia de controle adaptativo de ganho para amplificadores ópticos em redes WDM dinâmicas." Master degree dissertation, 2014. *In portuguese.* 48

[103] J. R. Oliveira, A. Caballero, E. Magalhães, U. Moura, R. Borkowski, G. Curiel, A. Hirata, L. Hecker, E. Porto, D. Zibar, *et al.*, "Demonstration of EDFA cognitive gain control via GMPLS for mixed modulation formats in heterogeneous optical networks," in *Optical Fiber Communication Conference*, pp. OW1H–2, Optical Society of America, 2013. 47

[104] J. C. R. F. de Oliveira, *Amplificadores ópticos com controle automático de ganho para aplicação em redes ópticas reconfiguráveis.* PhD thesis, Unicamp, 2007. *In portuguese.* 48, 49

[105] J. T. Ahn and K. H. Kim, "All-optical gain-clamped erbium-doped fiber amplifier with improved noise figure and freedom from relaxation oscillation," *IEEE Photonics Technology Letters*, vol. 16, pp. 84–86, Jan 2004. 48

[106] B.-H. Choi and C.-B. Kim, "An application of a smart optical amplifier to the bidirectional transmission," in *2006 8th International Conference Advanced Communication Technology*, vol. 2, pp. 6 pp.–1079, Feb 2006. 48

[107] C. H. Kim, H. Yoon, S. B. Lee, C. H. Lee, and Y. C. Chung, "All-optical gain-controlled bidirectional add-drop amplifier using fiber bragg gratings," *IEEE Photonics Technology Letters*, vol. 12, pp. 894–896, July 2000. 48

[108] K. Kitamura, K. Udagawa, and H. Masuda, "All-optical dynamic gain control of remotely pumped erbium-doped fiber amplifier," in *2016 21st OptoElectronics and Communications Conference (OECC) held jointly with 2016 International Conference on Photonics in Switching (PS)*, pp. 1–3, July 2016. 48

[109] E. Desurvire, M. Zirngibl, H. M. Presby, and D. DiGiovanni, "Dynamic gain compensation in saturated erbium-doped fiber amplifiers," *IEEE Photonics Technology Letters*, vol. 3, pp. 453–455, May 1991. 48

[110] A. Bianciotto, A. Carena, V. Ferrero, and R. Gaudino, "EDFA gain transients: experimental demonstration of a low cost electronic control," *IEEE Photonics Technology Letters*, vol. 15, pp. 1351–1353, Oct 2003. 48

[111] K. Jones, B. Flintham, J. Drake, and H. Lebreton, "Gain control and transient suppression in long wavelength band EDFA modules," in *ECOC 1999; 25nd European Conference on Optical Communication*, vol. 99, pp. 152–153, 1999. 48

[112] N. E. Jolley, F. Davis, and J. Mun, "Out-of-band electronic gain clamping for a variable gain and output power EDFA with low dynamic gain tilt," in *Proceedings of Optical Fiber Communication Conference*, pp. 134–135, Feb 1997. 48

[113] K. Okamura, E. Otani, T. Yoshikawa, T. Uchino, M. Fukushima, and N. Kagi, "Optical burst amplification using EDFA with fast feedback control," p. OTuN2, Optical Society of America, 2005. 48

[114] A. Lieu, C. Tian, and T. Naito, "Transmission and interactions of WDM burst signals in cascaded EDFAs," p. OTuD5, Optical Society of America, 2006. 48

[115] L. Pavel, "Control design for transient power and spectral control in optical communication networks," in *Proceedings of 2003 IEEE Conference on Control Applications, 2003. CCA 2003.*, vol. 1, pp. 415–422 vol.1, June 2003. 48

[116] H. S. Carvalho, I. J. G. Cassimiro, F. H. C. S. Filho, J. R. F. de Oliveira, and A. C. Bordonalli, "AGC EDFA transient suppression algorithm assisted by cognitive neural network," in *2014 International Telecommunications Symposium (ITS)*, pp. 1–5, Aug 2014. 48

[117] M. Fukutoku and M. Jinno, "Pump power reduction of optical feedback controlled EDFA using electrical feedforward control," in *Optical Amplifiers and Their Applications*, p. AA6, Optical Society of America, 1998. 49

[118] S. Sergeyev, E. Vanin, and G. Jacobsen, "Gain-clamped dynamics in EDFA with combined electronic feed-forward-optical feedback control," in *Optical Fiber Communication Conference and Exhibit*, pp. 518–519, Mar 2002. 49

[119] Y. Jung, Q. Kang, J. K. Sahu, B. Corbett, J. O'Callagham, F. Poletti, S. U. Alam, and D. J. Richardson, "Reconfigurable modal gain control of a few-mode EDFA supporting six spatial modes," *IEEE Photonics Technology Letters*, vol. 26, pp. 1100–1103, June 2014. 49

[120] K. Kitamura, H. Masuda, K. Tayama, T. Tanaka, and K. Ohnishi, "Novel all-optical feedforward automatic gain control scheme for multicore erbium-doped fiber amplifiers," in *2014 OptoElectronics and Communication Conference and Australian Conference on Optical Fibre Technology*, pp. 310–311, July 2014. 49

[121] U. Ghera, A. Shlifer, D. Berger, M. Zaacks, and D. Menashe, "Automatic measurement and gain control of distributed raman amplifiers," 2014. US Patent 8,643,941. 49

[122] J. R. F. Oliveira, U. C. Moura, J. C. R. F. Oliveira, and M. A. Romero, "Hybrid distributed raman/EDFA amplifier with hybrid automatic gain control for reconfigurable WDM optical networks," *Journal of Microwaves, Optoelectronics and Electromagnetic Applications*, vol. 12, pp. 602 – 616, 12 2013. 49

[123] S. Kim, J. KIM, S. Yoon, M. CHOI, and W. CHAE, "Self-automatic gain control distributed raman fiber amplifier and automatic gain control method," 2016. US Patent App. 14/854,918. 49

[124] M. Pantic, "Lecture notes introduction to machine learning and case-based reasoning," 2016. 49

[125] R. Lopez De Mantaras, D. McSherry, D. Bridge, D. Leake, B. Smyth, S. Craw, B. Faltings, M. L. Maher, M. T. Cox, K. Forbus, *et al.*, "Retrieval, reuse, revision and retention in case-based reasoning," *The Knowledge Engineering Review*, vol. 20, no. 03, pp. 215–240, 2005. 50, 51, 61, 107

[126] U. C. d. Moura, M. Garrich, A. C. Cesar, E. d. S. Rosa, J. Oliveira, and E. Conforti, "Execution time improvement for optical amplifier cognitive methodology in dynamic WDM networks," in *Microwave & Optoelectronics Conference (IMOC), 2017 SBMO/IEEE MTT-S International*, pp. 1–5, IEEE, 2017. 55, 60, 62, 90, 91, 92, 93, 94

[127] M. Črepinšek, S.-H. Liu, and M. Mernik, "Exploration and exploitation in evolutionary algorithms: a survey," *ACM Computing Surveys (CSUR)*, vol. 45, no. 3, p. 35, 2013. 57

[128] C. Stanfill and D. Waltz, "Toward memory-based reasoning," *Commun. ACM*, vol. 29, pp. 1213–1228, dec 1986. 61

[129] S. Wess, K.-D. Althoff, and G. Derwand, *Using k-d trees to improve the retrieval step in case-based reasoning*, pp. 167–181. Berlin, Heidelberg: Springer Berlin Heidelberg, 1994. 61

[130] C. Stanfill and D. L. Waltz, "Statistical methods, artificial intelligence, and information retrieval," *Text-based intelligent systems: Current research and practice in information extraction and retrieval*, pp. 215–225, 1992. 61

[131] U. C. d. Moura, M. Garrich, A. C. Cesar, J. D. Reis, J. Oliveira, and E. Conforti, "Optical amplifier cognitive gain adjustment methodology for dynamic and realistic networks," in *Cognitive Technologies*, pp. 1–37, Springer, 2017. 61, 85, 86, 87, 88, 93

[132] M. Garrich, A. Bravalheri, M. Magalhães, H. Carvalho, J. Assine, H. Rusa, H. Yamamura, F. Hooft, U. Moura, J. Januário, M. Nascimento, L. Mariote, and J. Oliveira, "Pioneering hardware modeling and software design for optical infrastructure in the

autonomous network project," in *2016 International Conference on Optical Network Design and Modeling (ONDM)*, pp. 1–6, May 2016. 65, 66, 67

[133] U. Moura, M. Garrich, H. Carvalho, M. Svolenski, A. Andrade, F. Margarido, A. C. César, E. Conforti, and J. Oliveira, "SDN-enabled EDFA gain adjustment cognitive methodology for dynamic optical networks," in *2015 European Conference on Optical Communication (ECOC)*, pp. 1–3, 2015. 65, 71, 73

[134] B. Hoppe, "Webwhompers," 2009. 65

[135] X. Wang, Y. Fei, M. Razo, A. Fumagalli, M. Garrich, A. D. Andrade, M. S. Svolenski, and H. S. Carvalho, "Effects of signal power control strategies and wavelength assignment algorithms on circuit OSNR in WDM networks," *Photonic Network Communications*, vol. 31, no. 3, pp. 404–417, 2016. 66

[136] M. Garrich, A. Bravalheri, M. Magalhães, M. Svolenski, X. Wang, Y. Fei, A. Fumagalli, D. Careglio, J. Solé-Pareta, and J. Oliveira, "Demonstration of dynamic traffic allocation in an SDN-enabled metropolitan optical network test-bed," in *2016 International Conference on Optical Network Design and Modeling (ONDM)*, pp. 1–6, May 2016. 66

[137] H. Carvalho, E. Magalhães, M. Garrich, N. Gonzalez, M. Nascimento, F. Margarido, L. Mariote, A. Bordonalli, and J. Oliveira, "SDN dual-optimization application for EDFAs and WSS-based ROADMs," in *2015 Optical Fiber Communications Conference and Exhibition (OFC)*, pp. 1–3, March 2015. 66

[138] J. ao Januario, M. G. Alabarce, B. Sarti, N. G. Gonzalez, and J. R. Oliveira, "Experimental demonstration of overshoot suppression for cascaded WSS-based ROADMs," in *Optical Fiber Communication Conference*, p. Tu3H.5, Optical Society of America, 2015. 66

[139] H. Carvalho, M. Svolenski, M. Garrich, M. Nascimento, F. Margarido, F. Cabelo, L. Mariote, A. C. Bordonalli, and J. Oliveira, "WSS/EDFA-based optimization strategies for software defined optical networks," in *2015 SBMO/IEEE MTT-S International Microwave and Optoelectronics Conference (IMOC)*, pp. 1–5, Nov 2015. 66

[140] X. Wang, Y. Fei, M. Razo, A. Fumagalli, and M. Garrich, "Network-wide signal power control strategies in WDM networks," in *2015 International Conference on Optical Network Design and Modeling (ONDM)*, pp. 218–221, May 2015. 66

[141] M. Garrich, E. Magalhães, H. Carvalho, N. G. Gonzalez, G. Zervas, D. Simeonidou, and J. R. F. Oliveira, "Experimental demonstration of function programmable add/drop architecture for ROADMs [invited]," *J. Opt. Commun. Netw.*, vol. 7, pp. A335–A343, Feb 2015. 66

[142] J. Januário, M. Garrich, A. Bravalheri, and J. Oliveira, "Modeling and analysis of transient response for cascaded WSS-based ROADMs," in *2015 SBMO/IEEE MTT-S International Microwave and Optoelectronics Conference (IMOC)*, pp. 1–5, Nov 2015. 66

[143] J. Oliveira, J. Oliveira, E. Magalhães, J. ao Januário, M. Siqueira, R. Scaraficci, M. Salvador, L. Mariote, N. Guerrero, L. Carvalho, F. van't Hooft, G. Santos, and M. Garrich, "Toward terabit autonomic optical networks based on a software defined adaptive/cognitive approach [invited]," *J. Opt. Commun. Netw.*, vol. 7, pp. A421–A431, Mar 2015. 66

[144] E. Magalhães, M. Garrich, H. Carvalho, M. Magalhães, N. González, J. Oliveira, A. Bordonalli, and J. Oliveira, "Global WSS-based equalization strategies for SDN metropolitan mesh optical networks," in *2014 The European Conference on Optical Communication (ECOC)*, pp. 1–3, Sept 2014. 66

[145] E. Magalhães, J. Oliveira, H. Carvalho, M. Magalhães, M. G. Alabarce, M. Siqueira, A. Bordonalli, and J. Oliveira, "Global ROADM-Based spectrum equalizer in SDN architecture for QoT optimization at DWDM networks," in *Optical Fiber Communication Conference*, p. W2A.35, Optical Society of America, 2014. 66

[146] E. Magalhães, M. Garrich, U. Moura, L. Nascimento, J. Oliveira, and A. Bordonalli, "Experimental-based subsystem models for simulation of heterogeneous optical networks," *Journal of Microwaves, Optoelectronics and Electromagnetic Applications*, vol. 13, pp. 197 – 213, 12 2014. 66

[147] M. Garrich, E. Magalhães, H. Carvalho, A. Bianco, P. Giaccone, G. Zervas, D. Simeonidou, N. G. González, J. Oliveira, and J. Oliveira, "Experimental demonstration

of backplane architectures for programmable optical nodes," in *2014 The European Conference on Optical Communication (ECOC)*, pp. 1–3, Sept 2014. 66

[148] V. E. S. Parahyba, *Análise de Métodos de Compensação de Efeitos Não Lineares em Sistemas de Transmissão Óptica de Alta Capacidade*. PhD thesis, Unicamp, 2016. *In portuguese.* 69

[149] T. U. of Adelaide, "The internet topology zoo," 2013. 78, 85

[150] P. Poggiolini, A. Carena, V. Curri, G. Bosco, and F. Forghieri, "Analytical modeling of nonlinear propagation in uncompensated optical transmission links," *IEEE Photonics technology letters*, vol. 23, no. 11, pp. 742–744, 2011. 107

[151] G. S. Pavani, *Otimização por colônia de formigas e sua aplicação em redes ópticas.* PhD thesis, Unicamp, 2006. *In portuguese.*

[152] "Terms and definitions of traffic engineering." ITU-T G.600 (03/1993), March 1993. ITU-T Recommendations.

[153] E. M. G. d. Queiroz, *Redes ópticas multidomínio: métodos de escolha de nós de borda e algoritmo de roteamento de tráfego.* PhD thesis, EESC-USP, 2012. *In portuguese.*

Appendices

Appendix A

OSNR calculation

In this work, the networks present links composed of optical amplifiers, fiber spans and ROADM nodes. Thus, for the signal point of view, each link is a black box with an equivalent noise figure and gain, as shown in Figure A.1.

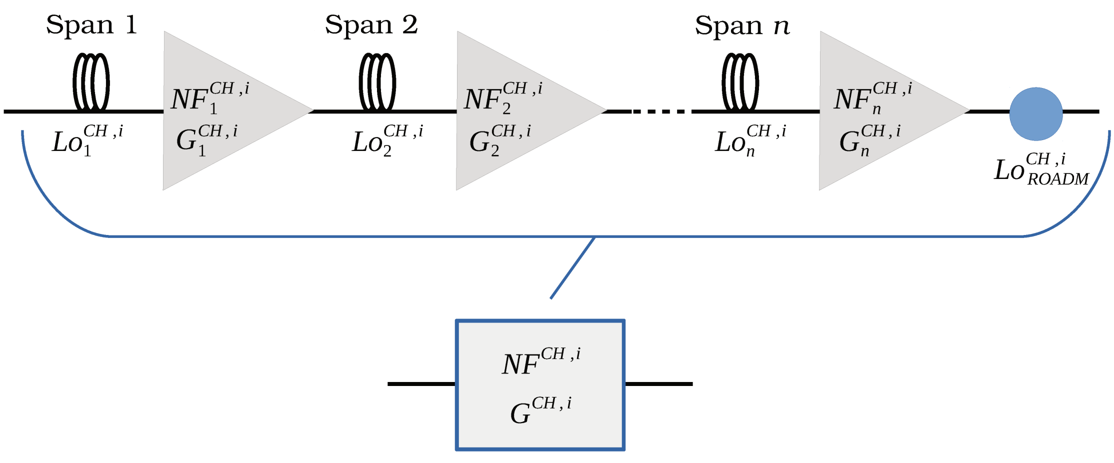

Figure A.1: Optical amplifier chain in a link.

The equivalent noise figure for the *i-th* link and channel CH, denoted by $NF^{CH,i}$, can be calculated considering an association of optical amplifiers and fiber spans in chain, also illustrated in Figure A.1, which leads to [94]:

$$NF^{CH,i} = \frac{NF_1^{CH,i}}{Lo_1^{CH,i}} + \frac{NF_2^{CH,i}}{Lo_1^{CH,i} G_1^{CH,i} Lo_2^{CH,i}} + ... + \frac{NF_n^{CH,i}}{Lo_1^{CH,i} G_1^{CH,i} Lo_2^{CH,i} G_2^{CH,i} ... Lo_n^{CH,i}} \quad (A.1)$$

in which $NF_k^{CH,i}$ and $G_k^{CH,i}$ are the noise figure and the gain of *k-th* amplifier for channel *CH*, and $Lo_k^{CH,i}$ is the fiber loss of the *k-th* span for channel *CH*. All these values are dimensionless. The amplifier noise figure and gain are obtained in the characterization process, described in Section 2.3.3. They also consider the devices' modeling described in Sections 4.1.2,5.1.1 and 5.2.1 [7].

In this work, the first fiber span (span 1) is not used. Thus, Equation A.1 becomes:

$$NF^{CH,i} = NF_1^{CH,i} + \frac{NF_2^{CH,i}}{G_1^{CH,i} Lo_2^{CH,i}} + ... + \frac{NF_n^{CH,i}}{G_1^{CH,i} Lo_2^{CH,i} ... G_{n-1}^{CH,i} Lo_n^{CH,i}} \quad (A.2)$$

The total gain of the channel *CH* at the link i is calculated according to:

$$G^{CH,i} = G_1^{CH,i} L_2^{CH,i} G_2^{CH,i} ... L_n^{CH,i} G_n^{CH,i} Lo_{ROADM}^{CH,i} \quad (A.3)$$

where $Lo_{ROADM}^{CH,i}$ is the ROADM loss for channel *CH* at the end of the *i-th* link.

As a lightpath (LP) is composed of a cascade of links, as illustrated in Figure A.2, it is possible to estimate the LP noise figure for channel *CH* ($NF^{CH,LP}$) by [94]:

$$NF^{CH,LP} = NF^{CH,1} + \frac{NF^{CH,2}}{G^{CH,1}} + ... + \frac{NF^{CH,m}}{G^{CH,1} ... G^{CH,m-1}} \quad (A.4)$$

for a LP with m links and $NF^{CH,i}$ and $G^{CH,i}$ the noise figure and gain for the *i-th* link and channel *CH*, obtained by Equations A.2 and A.3, respectively.

Note that Equation A.2 does not consider the ROADM loss to calculate the noise figure of the link. It is because the ROADM is placed at the end of the link, not contributing to noise addition or reducing the power level at the input of any amplifier inside the link. However, it is considered to calculate the equivalent noise figure of the LP in Equation A.4 by using $G^{CH,i}$, since it reduces the input power in the first amplifier on the next link [7].

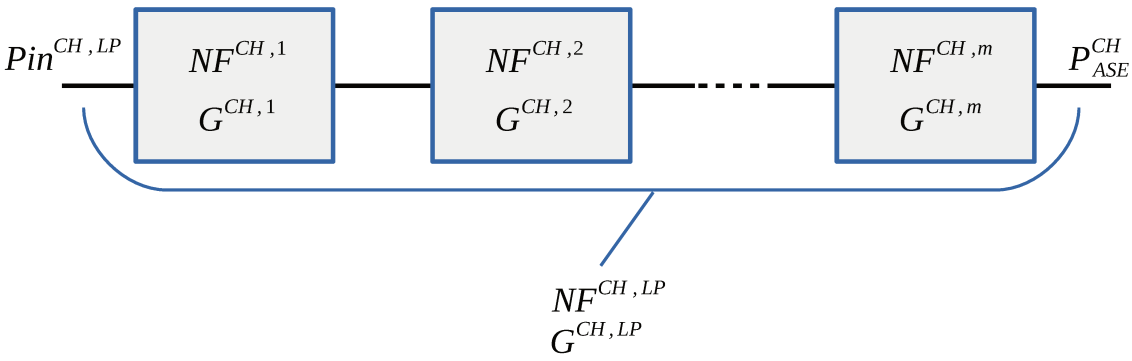

Figure A.2: Lightpath (LP) illustration as a cascade of links.

On the other hand, the total LP gain for channel CH is given by:

$$G^{CH,LP} = G^{CH,1}G^{CH,2}...G^{CH,m} \tag{A.5}$$

Finally, the channel OSNR at the end of the LP can be estimated by considering Equation 2.4 [94], used in Section 2.3.3 and following rewritten:

$$NF^{CH,LP} = \frac{P_{ASE}^{CH}}{h\nu^{CH}\Delta\nu^{CH}G^{CH,LP}} + \frac{1}{G^{CH,LP}} \tag{A.6}$$

where P_{ASE}^{CH} is the channel noise power (in W) at the end of the LP (illustrated in Figure A.2), h is the Planck's constant (in m^2kg/s); ν^{CH} is the channel frequency; $\Delta\nu^{CH}$ is the channel band in which signal and noise were measured (both in Hz) and $G^{CH,LP}$ is the channel gain along the LP. Equation A.6 is used when the system input power is free of noise [94].

Substituting $NF^{CH,LP}$ by Equation A.4, G^{CH} by Equation A.5 and P_{ASE}^{CH} by $OSNR^{CH}G^{CH,LP}Pin^{CH,LP}$ (where $Pin^{CH,LP}$ is the channel input power, illustrated in Figure A.2), in Equation A.6, it yields to:

$$OSNR^{CH} = \frac{G^{CH,LP}Pin^{CH,LP}}{(G^{CH,LP}NF^{CH,LP} - 1)h\nu^{CH}\Delta\nu^{CH}} \tag{A.7}$$

in which $G^{CH,LP}$ and $NF^{CH,LP}$ must be dimensionless values, $Pin^{CH,LP}$ must be in W, and, as Equation A.7 is derived from A.6, $Pin^{CH,LP}$ must be free of noise [7].

Appendix B

Traffic modeling

The most typical model for a traffic generation in telecommunication networks is considering a Poisson distribution. This is the same model used on the traditional telephone networks, in which the connections are independent, the time interval between connections (t_g) and their duration (C_d) are modeled by exponential distributions [151]:

$$t_g = \frac{-log(1-\omega)}{l} \tag{B.1}$$

$$c_d = \frac{-log(1-f)}{m} \tag{B.2}$$

in which ω and f are random variables in a uniform distribution inside [0,1], m is the service rate, l is the connections arrival rate defined as $l = Er/T$, with Er being the traffic load in erlang[1], and T is the connections duration mean, given by $T = 1/m$.

Figure B.1 helps to understand the traffic generation, illustrating how simultaneous connections are distributed along the time. It presents the time interval between connections (t_g) obtained by Equation B.1, and the connections' duration (C_d), obtained by Equation B.2. Note that the resources, such as channel slot and bandwidth, are al-

[1]The unit usually used for traffic intensity according to the ITU-T [152].

located at the beginning of the connections and deallocated at the end, to make them available for future connections [153].

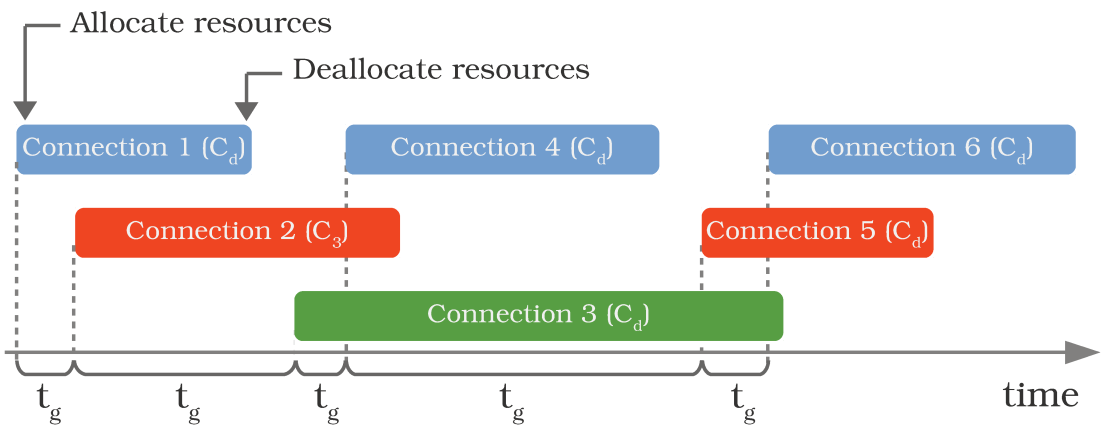

Figure B.1: Traffic generation. Adapted from [153].